

An extended catalog of galaxy-galaxy strong gravitational lenses discovered in DES using convolutional neural networks

C. JACOBS,^{1,2} T. COLLETT,³ K. GLAZEBROOK,^{1,2} E. BUCKLEY-GEER,⁴ H. T. DIEHL,⁴ H. LIN,⁴ C. McCARTHY,⁵
 A. K. QIN,⁵ C. ODDEN,^{4,6} M. CASO ESCUDERO,^{4,6} P. DIAL,^{4,6} V. J. YUNG,^{4,6} S. GAITSCH,⁴ A. PELLICO,⁴
 K. A. LINDGREN,⁴ T. M. C. ABBOTT,⁷ J. ANNIS,⁸ S. AVILA,⁹ D. BROOKS,¹⁰ D. L. BURKE,^{11,12} A. CARNERO ROSELL,^{13,14}
 M. CARRASCO KIND,^{15,16} J. CARRETERO,¹⁷ L. N. DA COSTA,^{14,18} J. DE VICENTE,¹³ P. FOSALBA,^{19,20} J. FRIEMAN,^{8,21}
 J. GARCÍA-BELLIDO,⁹ E. GAZTANAGA,^{19,20} D. A. GOLDSTEIN,²² D. GRUEN,^{23,11,12} R. A. GRUENDL,^{15,16} J. GSCHWEND,^{14,18}
 D. L. HOLLOWOOD,²⁴ K. HONScheid,^{25,26} B. HOYLE,^{27,28} D. J. JAMES,²⁹ E. KRAUSE,³⁰ N. KUROPATKIN,⁸ O. LAHAV,¹⁰
 M. LIMA,^{31,14} M. A. G. MAIA,^{14,18} J. L. MARSHALL,³² R. MIQUEL,^{33,17} A. A. PLAZAS,³⁴ A. RODMAN,^{11,12} E. SANCHEZ,¹³
 V. SCARPINE,⁸ S. SERRANO,^{19,20} I. SEVILLA-NOARBE,¹³ M. SMITH,³⁵ F. SOBREIRA,^{36,14} E. SUCHYTA,³⁷
 M. E. C. SWANSON,¹⁶ G. TARLE,³⁸ V. VIKRAM,³⁹ A. R. WALKER,⁷ AND Y. ZHANG⁸
 (DES COLLABORATION)

¹Centre for Astrophysics and Supercomputing, Swinburne University of Technology, P.O. Box 218, Hawthorn, VIC 3122, Australia

²ARC Centre of Excellence for All Sky Astrophysics in 3 Dimensions (ASTRO 3D), Swinburne University of Technology, Hawthorn, VIC 3122, Australia

³Institute of Cosmology & Gravitation, University of Portsmouth, Portsmouth, po1 3fx, UK

⁴Fermi National Accelerator Laboratory, P. O. Box 500, Batavia, IL 60510, USA

⁵School of Software and Electrical Engineering, Swinburne University of Technology, P.O. Box 218, Hawthorn, VIC 3122, Australia

⁶Phillips Academy, Andover, MA 01810

⁷Cerro Tololo Inter-American Observatory, National Optical Astronomy Observatory, Casilla 603, La Serena, Chile

⁸Fermi National Accelerator Laboratory, P. O. Box 500, Batavia, IL 60510, USA

⁹Instituto de Física Teórica UAM/CSIC, Universidad Autónoma de Madrid, 28049 Madrid, Spain

¹⁰Department of Physics & Astronomy, University College London, Gower Street, London, WC1E 6BT, UK

¹¹Kavli Institute for Particle Astrophysics & Cosmology, P. O. Box 2450, Stanford University, Stanford, CA 94305, USA

¹²SLAC National Accelerator Laboratory, Menlo Park, CA 94025, USA

¹³Centro de Investigaciones Energéticas, Medioambientales y Tecnológicas (CIEMAT), Madrid, Spain

¹⁴Laboratório Interinstitucional de e-Astronomia - LIneA, Rua Gal. José Cristino 77, Rio de Janeiro, RJ - 20921-400, Brazil

¹⁵Department of Astronomy, University of Illinois at Urbana-Champaign, 1002 W. Green Street, Urbana, IL 61801, USA

¹⁶National Center for Supercomputing Applications, 1205 West Clark St., Urbana, IL 61801, USA

¹⁷Institut de Física d'Altes Energies (IFAE), The Barcelona Institute of Science and Technology, Campus UAB, 08193 Bellaterra (Barcelona) Spain

¹⁸Observatório Nacional, Rua Gal. José Cristino 77, Rio de Janeiro, RJ - 20921-400, Brazil

¹⁹Institut d'Estudis Espacials de Catalunya (IEEC), 08034 Barcelona, Spain

²⁰Institute of Space Sciences (ICE, CSIC), Campus UAB, Carrer de Can Magrans, s/n, 08193 Barcelona, Spain

²¹Kavli Institute for Cosmological Physics, University of Chicago, Chicago, IL 60637, USA

²²California Institute of Technology, 1200 East California Blvd, MC 249-17, Pasadena, CA 91125, USA

²³Department of Physics, Stanford University, 382 Via Pueblo Mall, Stanford, CA 94305, USA

²⁴Santa Cruz Institute for Particle Physics, Santa Cruz, CA 95064, USA

²⁵Center for Cosmology and Astro-Particle Physics, The Ohio State University, Columbus, OH 43210, USA

²⁶Department of Physics, The Ohio State University, Columbus, OH 43210, USA

²⁷Max Planck Institute for Extraterrestrial Physics, Giessenbachstrasse, 85748 Garching, Germany

²⁸Universitäts-Sternwarte, Fakultät für Physik, Ludwig-Maximilians Universität München, Scheinerstr. 1, 81679 München, Germany

²⁹Harvard-Smithsonian Center for Astrophysics, Cambridge, MA 02138, USA

³⁰Department of Astronomy/Steward Observatory, University of Arizona, 933 North Cherry Avenue, Tucson, AZ 85721-0065, USA

³¹Departamento de Física Matemática, Instituto de Física, Universidade de São Paulo, CP 66318, São Paulo, SP, 05314-970, Brazil

³²George P. and Cynthia Woods Mitchell Institute for Fundamental Physics and Astronomy, and Department of Physics and Astronomy, Texas A&M University, College Station, TX 77843, USA

³³Institució Catalana de Recerca i Estudis Avançats, E-08010 Barcelona, Spain

³⁴Department of Astrophysical Sciences, Princeton University, Peyton Hall, Princeton, NJ 08544, USA

³⁵School of Physics and Astronomy, University of Southampton, Southampton, SO17 1BJ, UK

³⁶Instituto de Física Gleb Wataghin, Universidade Estadual de Campinas, 13083-859, Campinas, SP, Brazil

³⁷Computer Science and Mathematics Division, Oak Ridge National Laboratory, Oak Ridge, TN 37831

³⁸Department of Physics, University of Michigan, Ann Arbor, MI 48109, USA

³⁹Argonne National Laboratory, 9700 South Cass Avenue, Lemont, IL 60439, USA

Submitted to ApJ

ABSTRACT

We search Dark Energy Survey (DES) Year 3 imaging for galaxy-galaxy strong gravitational lenses using convolutional neural networks, extending previous work with new training sets and covering a wider range of redshifts and colors. We train two neural networks using images of simulated lenses, then use them to score postage stamp images of 7.9 million sources from the Dark Energy Survey chosen to have plausible lens colors based on simulations. We examine 1175 of the highest-scored candidates and identify 152 probable or definite lenses. Examining an additional 20,000 images with lower scores, we identify a further 247 probable or definite candidates. After including 86 candidates discovered in earlier searches using neural networks and 26 candidates discovered through visual inspection of blue-near-red objects in the DES catalog, we present a catalog of 511 lens candidates.

Keywords: gravitational lensing:strong — methods: data analysis, statistical — surveys

1. INTRODUCTION

Gravitational lensing is a phenomenon arising from the relativistic curvature of spacetime around massive objects (Einstein 1936; Zwicky 1937, see Treu (2010) for an overview). When strong gravitational lensing occurs, we sometimes observe multiple magnified images of distant sources that lie behind the lensing mass. When the lens is a massive galaxy, group or cluster, strong lensing can be detectable across cosmological distances. Lensing observables such as the Einstein radius are sensitive to the mass of the lens as well as to cosmological parameters, lending strong lensing analysis to many applications across astrophysics and cosmology.

One of strong lensing’s applications is as a precise probe of lens mass, dark and baryonic, out to redshift 1 and beyond. Early Type Galaxies (ETGs) contain much of the local universe’s stellar mass (Renzini 2006), and are the majority of known galaxy lenses due to their high surface mass densities. By measuring the evolution of the total-mass density slopes of ETGs (i.e. constrain the exponent γ , where $\rho(r) \propto r^\gamma$), we can test the two-phase model of galaxy assembly predicted by theorists. Simulations predict that at early times, gas-rich assembly from filaments and gas-rich mergers lead to *in situ* star formation, concentrating baryons in galaxy centres and steepening the density profile. At later times, mass assembly is dominated by dry minor mergers, depositing mass on the outskirts of galaxies and thus increasing size, decreasing γ (Wellons et al. 2015; Bellstedt et al. 2018). Observations have so far failed to confirm this prediction, with a weak steepening over time of γ observed instead (Sonnenfeld et al. 2013; Remus et al. 2017). At non-local redshifts, galaxy-scale strong lensing remains the only feasible method for measuring these

density slopes. However, the current lens sample is not large enough to conclusively resolve this tension between simulations and the existing observations. More galaxy-scale strong lenses are needed, and at higher redshifts.

The statistics of strong lenses may also prove important in ruling in or out particular models of dark matter. Strong lensing can produce bright arcs, and in some cases near-perfect Einstein rings. These rings and arcs are perturbed if they intersect sub-structure within the lens’s dark matter halo, producing detectable ‘kinks’ in the ring. The strong lens system SDSS J120602.09+514229.5 described in Vegetti et al. (2010) contains a visible dwarf that lies on the Einstein ring and introduces a visible distortion in the ring; the same effect will be detectable for dark subhaloes. Exploiting this effect using a large sample of bright arcs and rings will allow us to constrain the subhalo mass function (Koopmans 2005; Vegetti & Koopmans 2009), a technique demonstrated by Vegetti et al. (2014) on 11 strong lensing systems resulting in a single detection. Li et al. (2016) use simulations to calculate that as few as 100 bright arcs, with sufficient image resolution to detect subhaloes down to $10^7 h^{-1} M_\odot$ (consistent with future observations) would tightly constrain the subhalo cutoff mass. Such analysis may confirm the Λ CDM paradigm by providing direct evidence for the low-mass subhalos predicted by theory; conversely, a detection of low-mass subhaloes could provide strong evidence for a warm dark matter candidate such as a keV-mass sterile neutrino. Despali et al. (2018) have also demonstrated a method to constrain the subhalo mass function using lensing and line-of-sight substructure.

Double-source plane lenses, where two strongly-lensed sources at different redshifts are detectable, can func-

tion as unique cosmological probes. The ratio of the Einstein radii of the two lenses, β , is independent of the Hubble parameter but sensitive to the dark energy equation of state, w and to both Ω_M and Ω_k . Collett & Auger (2014) used a model of double-source plane lens SDSSJ0946+1006 to constrain w with 30 per cent greater precision than *Planck* alone. Only a few examples of such lenses have been discovered so far (Gavazzi et al. 2008; Tanaka et al. 2016; Diehl et al. 2017).

Artificial Neural Networks (ANNs) are the key machine learning technique that underpins recent advances in so-called ‘Deep Learning’. An overview of ANNs and deep learning can be found in Schmidhuber (2015). Convolutional Neural Networks (CNNs; LeCun et al. 1989) are a type of ANN optimised for problems involving image data. For standard computer vision tasks such as image classification and object detection, CNNs have proven highly successful and now routinely exceed human performance. CNNs have already found many successful applications in astronomy, for instance galaxy morphology classification (Dieleman et al. 2015; Dai & Tong 2018); star-galaxy separation (Kim & Brunner 2017; Cabayol et al. 2019); or identifying quasars from spectra (Busca & Balland 2018).

Here we are concerned with finding and exploiting strong lenses on the galaxy and group scales. Several hundred examples of galaxy-galaxy strong lenses are currently known¹. Simulations, such as Collett (2015) predict that several thousand lenses should be discoverable in current-generation surveys such as the Dark Energy Survey (DES; Dark Energy Survey Collaboration et al. 2016), Kilo Degree Survey (KiDS; de Jong et al. 2015), and Subaru Hyper-Suprime Cam (Miyazaki et al. 2018). Although in decades past most strong lenses were discovered serendipitously or through visual inspection of an entire survey, the scale of modern surveys means a more targeted approach is required. Previous strategies have included searching catalogs for multiple blue sources near red ETGs (Diehl et al. 2017), modeling all sources as strong lenses and testing for goodness of fit (Marshall et al. 2009; Chan et al. 2015); or recruiting citizen scientists to examine images in quantity (Marshall et al. 2016; More et al. 2016). Recently, many efforts have employed modern computer vision and machine learning techniques. Neural nets have been shown to be effective at distinguishing between simulated lenses and non-lenses (Lanusse et al. 2018; Avestruz et al. 2017; Hezaveh et al. 2017). Applied to imaging surveys, Ja-

cobs et al. (2017, hereafter Paper 1) used CNNs to recover several hundred known lenses and 17 new candidates in an hour of inspection time, and Petrillo et al (2019; 2017) used neural networks to discover over 300 candidate lenses in KiDS.

In Jacobs et al. 2019 (hereafter Paper 2) we presented 84 candidate lenses at redshifts 0.8 and above discovered in the Dark Energy Survey Year 3 imaging using convolutional neural networks.

In the present paper we present the results of a wider search of the DES images. We apply the technique developed in Paper 1 and Paper 2 to the DES Year 3 coadd images² (Abbott et al. 2018; Morganson et al. 2018), using newly trained networks and searching for lenses from a wider range of redshifts, morphologies and colors. In section 2 we outline the method used to train the networks and score candidates. In section 3 we present the results of the search and discuss the likely completeness of the search. In section 4 we offer concluding remarks.

2. METHOD

The lenses in the catalog presented in this paper were discovered using the methodology presented in Paper 1 and Paper 2. Here we summarize the method and describe refinements made since the earlier searches. The catalog presented in this work includes candidates discovered in searches using variations on the color cuts, network architectures and simulation parameters employed in previous work. The search described in Paper 2 used simulations to target strong lenses in a constrained redshift range; here we refine the simulations and expand the search, targeting discoverable lenses across all redshifts, morphologies and colors, aiming for a larger and purer candidate set. We note variations from the earlier search in the text and in Table 3 where appropriate. The method described below describes the parameters of the latest and most comprehensive search.

2.1. Creating simulated lenses

In order to train a convolutional neural network to distinguish between lenses and non-lenses, we require a training set of labeled examples. To train a network with tens of millions of trainable weights, of the size required for reliably processing image data, we require a training set of order tens or hundreds of thousands of labeled examples (e.g. Krizhevsky et al. 2012). Since this exceeds the number of known lenses by orders of magnitude, we must instead use simulations to create training sets.

¹ L.A. Moustakas & J. Brownstein, priv. comm. Database of confirmed and probable lenses from all sources, curated by the University of Utah. <http://admin.masterlens.org>

² Now available publicly as Data Release 1 at <https://des.ncsa.illinois.edu/releases/dr1/>

To generate simulations we use the LENSPOP code described in Collett (2015). LENSPOP generates a population of synthetic elliptical galaxies as lenses, with singular isothermal ellipsoid mass profiles, using masses, ellipticities and redshifts drawn from realistic distributions. The lenses are simulated with an elliptical De Vaucouleurs profile, and lensed sources are modelled as exponential disks with properties drawn from the COSMOS sample (Ilbert et al. 2009). Lens images are created using the GRAVELENS ray-tracing code (Keeton 2001), with simulated seeing and shot noise appropriate for DES imaging (see Paper 2). The simulations produced by LENSPOP follow a realistic distribution of lensing parameters such as Einstein radius and magnification; for the purposes of training the networks we want clear, bright examples of strong lensing, so we both discard undetectable lenses and make simulated sources brighter by one magnitude. The thresholds used for detectability are: signal-to-noise > 20 , magnification > 5 and Einstein radius $> 2''$. Simulated lens and source images are combined with random patches of DES imaging to create postage stamps with realistic sky noise, foreground objects, artifacts and other contaminants.

In addition to the simulations described above and in Paper 2, we create a further set of simulated lenses using the redMaGiC catalog (Rozo et al. 2016) of luminous red galaxies (LRGs). For each of the 88,307 galaxies in the catalog, we use the supplied photometric redshift of the galaxy and a nominal velocity dispersion value, calculated using the Hyde & Bernardi (2009) fundamental plane of SDSS ellipticals to convert between rest frame r -band absolute magnitude and velocity dispersion (assuming a Λ CDM cosmology, $h = 0.7$). We used the redMaGiC photometric redshifts and assumed a 10 Gyr old passive SED to convert the observed i -band magnitude into the rest frame r -band absolute magnitude. We then sample 3 simulated sources at different positions in the source plane, and produce images via raytracing for each of the lensed sources. These are then combined with the actual DES imaging for the galaxy to create simulated lens images.

Figure 1 depicts simulations, with and without synthetic lenses, used for training.

2.2. Training neural networks

We use the simulations to create training sets for the neural networks. For the positive examples we use the simulated lenses described in section 2.1. For the negative examples, we use a combination of simulated non-lenses and real sources from the field. For the former, we use simulations without any flux from a lensed source added, depicting only the simulated ETG. For the sec-

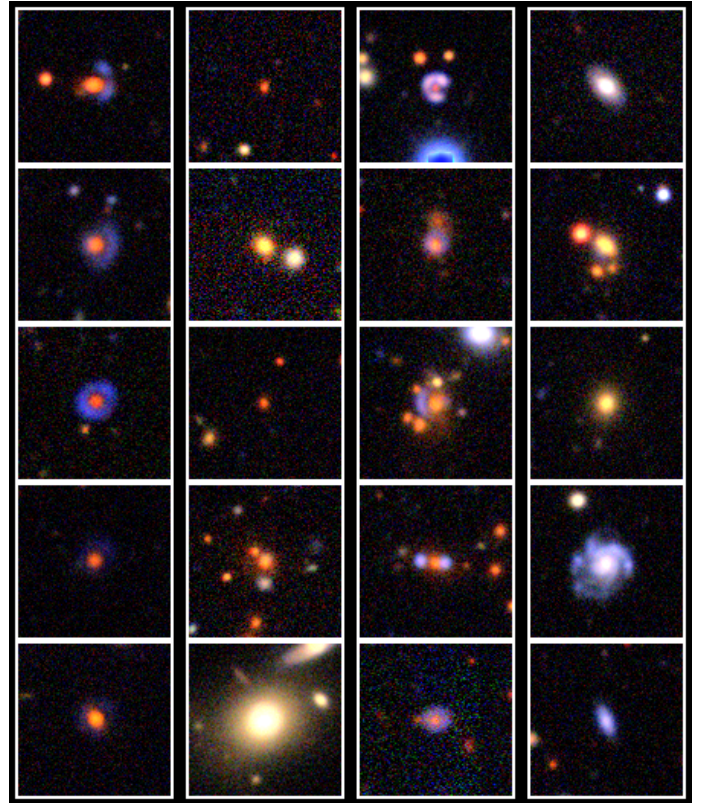


Figure 1. Images used in training the neural networks. Left column: Simulated lenses and lensed sources. Second from left: Simulated ETGs without a lensed source. Third from left: redMaGiC galaxies and simulated lensed sources. Right column: Field galaxies, used as negative examples.

ond, we take postage stamps of galaxies randomly selected from the target search catalog (section 2.3). Since strong lenses are rare - as few as one in 100,000 galaxies - a random sample of sources from the survey catalog is unlikely to contain any contamination with strong lenses. (We are expecting to find a few hundred lenses in our search catalog of 7.9 million galaxies.)

We use two types of negative examples for the following reasons. Firstly, we use simulated ETGs with and without a lensed source. This way, the network learns that the presence of a lensed background source is the significant feature, and that the presence of the elliptical lens is not in itself indicative of lensing. Even if the simulated ellipticals are unrealistic in some way, such as color, the networks should learn to ignore them as they are present in both positive and negative examples and are therefore not discriminatory in arriving at the correct class. The second type of training set, incorporating real galaxies as negative examples, exposes the networks to spiral galaxies, mergers, and other sources that represent non-lenses and will be present in the images to be tested. In this way the network learns that an elliptical

galaxy with lensing is the target, and that potentially confusing objects such as spiral arms and tidal tails are to be ignored.

We normalise the training data so that in each band, the mean value of the supplied image data is zero and the standard deviation is one; this aids in quicker convergence of the neural network training process.

We create training sets of up to 200,000 images, consisting of equal numbers of positive and negative examples. We construct a neural network with the following architecture: Four convolutional layers, with kernel sizes 11, 5, 3, and 3 and ReLU³ activations; 2x2 max pooling⁴ after each convolutional layer; and two fully-connected layers of 1024 neurons each, with an output layer of two neurons. The network architecture of CN1 and CN2 is described in detail in Appendix A.

The process of training, which employs the backpropagation algorithm, is described in Paper 1, Paper 2 and LeCun et al. (1989). Briefly: For each training example, the algorithm determines a correction to each of the weights in the network that would decrease a loss function L , where $L = 0$ if all classifications are correct and increases as accuracy decreases. With each iteration, each of the weights of the network are updated with the mean optimal adjustment calculated over a batch of 128 training images. By this process, the network learns key features of the images and converges on higher classification accuracy. During training we measure the loss and accuracy on a validation set, consisting of images not shown to the network during the training steps. This allows us to determine whether the improvements are due to an over-fitting to the training set or will generalise well to new examples.

We train until the validation loss (the loss on the validation set) does not improve by more than 10^{-4} over six epochs (where an epoch is a run through the entire training set).

In addition to the networks described in Paper 2, we train four new CNNs using these training sets, as described in Table 1.

2.3. Selecting a catalog to search

Even a highly accurate classifier will produce false positives, especially if it is likely to see irregular objects at classification time that were not represented in training, which will be the case for some proportion of sources in any imaging survey. We can minimise false positives by

³ Rectified Linear Unit: $f(x) = \max(0, x)$.

⁴ Reduces the spatial extent of the input, such that for each 2x2 pixel area in the input, the output is a single value, the maximum of the four values.

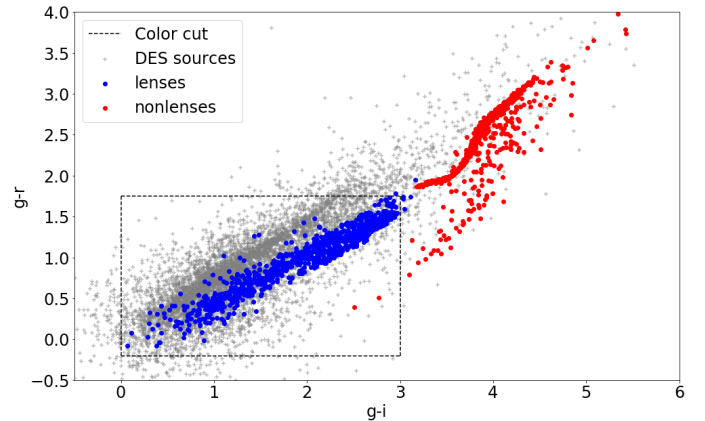


Figure 2. Integrated colors of simulated ETGs (blue), simulated strong lenses (red), and a sample of 5000 sources selected at random from the DES catalog (grey). The color cuts used to assemble our search catalog are shown in green. Note that Some simulated galaxies lie at the edge of the DES g -band magnitude limit, resulting in large magnitude errors and consequent scatter along the diagonal.

minimising the number of objects we classify, if we can do so without discarding any true positives. We restrict our search to only objects that have the colors of plausible lenses. Although the color of likely lensing ETGs is well known, the color of combined lens and lensed source systems in the aperture photometry of the survey catalog is not known *a priori*. We again turn to simulations as a guide. Figure 2 depicts the combined $g - r$, $g - i$ colors of a sample of 10,000 simulated lenses.

In Paper 2 we searched 1.4 million sources with colors $2 < g - i < 5$, $0.6 < g - r < 3$, or $1.8 < g - i < 2$, $0.8 < g - r < 1.2$, based on simulated lenses at redshifts 0.8 and above. Here we search for lenses across all redshifts. Using cuts of $0 < g - i < 3$, $-0.2 < g - r < 1.75$, which encompasses 98.7% of our simulations, we assemble a catalog of 7.9 million sources from the 300 million objects in the DES catalog for scoring by the neural networks.

2.4. Scoring and examining candidates

We score 100x100 pixel postage stamp images in $griz$ bands⁵ with CNNs trained using the two training sets, RM1 and RM2, described in section 2.1. Each network produces a score in the interval $(0, 1)$ for each image. We choose thresholds for the CNN scores, producing lists of candidates with scores greater than those thresholds. Adjusting this parameter produces candidate sets of varying size, with different (and unknown) purity and

⁵ Previous searches used simulations and survey data in gri bands only.

Table 1. A summary of training sets used to train neural networks to search DES imaging. redMaGiC sims use real galaxies for the simulated deflector, LensPop simulates both deflector and lensed source. Networks TS1 and TS2 are described in Paper 2.

Network	Positive examples	Negative examples	Training set size
RM1	redMaGiC sims	redMaGiC galaxies	160,000
RM2	redMaGiC sims	catalog galaxies	200,000
CN1	LensPop sims	LensPop sims	200,000
CN2	LensPop sims	catalog galaxies	200,000
TS1	LensPop high-z sims	LensPop sims	250,000
TS2	LensPop high-z sims	Real galaxies	150,000

completeness. The thresholds are initially chosen to produce a candidate set of a few thousand, a convenient size to inspect. We then determine the purity of the sample, lower the threshold and inspect further candidates with lower scores. We repeat this process until the purity has dropped to the point where diminishing returns (less than one quality lens candidate per thousand inspections) make further inspection unworkable.

We inspect RGB images of these candidates using software, LensRater⁶ developed for that purpose, which displays PNG images made with *gri* imaging using three different scaling parameters. We assign each source a grade from 0-3, where 0 = not a lens, 1 = “possibly a lens”, 2 = “probably a lens”, and 3 = “definitely a lens”. The grades used throughout the paper represent the mean grade assigned by authors CJ, TC, EBG and KG.

2.5. Blue-near-red and rich cluster search

In addition to candidates discovered with the CNN search, for completeness we include in our catalog 26 candidates discovered through two visual searches. A search was performed on 53,000 candidates selected from the DES Y3A1 catalog using a methodology similar to that described in Diehl et al. (2017), extended to an extra 3500 square degrees of sky (covering the entire DES footprint in line with the CNN-based search). Then, excluding sources examined in Diehl et al. (2017), blue-near-red sources were selected from the DES Y3A1 catalog as follows:

- Select luminous red galaxies (LRGs) with *i*-band magnitude < 22 , with redshift $0.22 < z < 0.70$;
- Count blue-colored sources ($-1 \leq g - r < 1, -1 \leq r - i < 1$) within $10''$;
- Examine sources where two blue sources were found near LRGs brighter than 21st magnitude

in *r*, and three or more were found near LRGs brighter than 22nd magnitude.

We also examined 759 sources from the redMaPPer galaxy cluster catalog (Rykoff et al. 2014) that matched with high-flux sources detected by the Chandra X-ray Observatory (Weisskopf et al. 1996).

After visual inspection, and systematic grading according to the prescription above, 40 candidates were graded as “likely” or “definite” lenses, of which 14 were also discovered in the CNN search; 13 are previously known; five were both rediscovered by the CNN search and previously known; and 26 were new. These candidates are indicated in Table 3.

3. RESULTS AND DISCUSSION

3.1. Training the network and scoring sources

The networks described in section 2.2 required approximately five hours each to train on an NVidia Tesla P90 GPU. Training converged on accuracies of between 99% and 99.9% on the validation sets (images not used in the training process) as shown in Figure 3. A typical Receiver Operating Characteristic (ROC) curve, depicting the trade-off between false positives and false negatives on our training sets, can be found in Paper 2.

Including the overheads of loading images into memory, scoring the 8 million images in our catalog took a total of 20 hours using a Tesla P90 GPU; scoring an individual object required of order $1\mu s$. scores assigned by the networks are shown in Table 2.

3.2. Selecting candidates

We choose candidates to examine by selecting a CNN score threshold and examining the candidates with a score greater than this number. We seek a candidate set that is as complete as possible in detectable lenses included but is of a tractable size and as high a purity (lowest fraction of false positives) as possible. If the networks are working, i.e. the score adds significant information, then we should find fewer good candidates at lower score values. We first examine a smaller candidate

⁶ <https://github.com/coljac/lensrater>

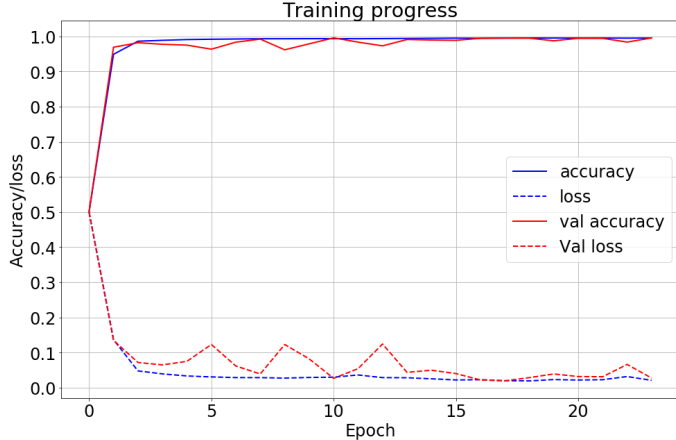


Figure 3. Training a neural network on simulated lenses and non-lenses. Blue dashed line: The loss value, optimized by the training process, decreasing over time. Red dashed line: The loss evaluated on a validation set not used for training. Blue solid line: Accuracy in classification on the training set. Red solid line: Accuracy measured on the validation set.

Table 2. How the convolutional neural networks scored the catalog of 7.9 million DES sources. The number of sources scored 1.0 by both RM1 and RM2 was 1175; by CN1 and CN2, 164.

Network	scores = 0	scores > .5	scores = 1
RM1	6248566	64525	3708
RM2	3295227	1840383	330069
CN1	7869097	2799	1000
CN2	2090100	1868791	228776

set, with a high score threshold, and grade the candidates; then we examine further candidates with lower scores, until diminishing returns suggest further searching is not feasible. The scores, subsequent candidate set sizes, and results are summarized in Table 2.

After examining 1175 images with scores of 1.0 by both RM1 and RM2, we grade 152 with grade ≥ 2 and a further 148 ≥ 1 . We then test for diminishing returns by examining further, lower-scored sources. We lower the thresholds and examine further candidates. Using a score threshold of > 0.5 for both networks, we examine a further 15,172 images and grade them as 247 ≥ 2 , 401 ≥ 1 .

Finally, we include candidates from other searches. This includes networks and catalogs prepared for the search in Paper 2, and accounts for approximately 20,000 further image inspections. We identify a further 86 candidates with grade ≥ 2 and 188 with grade ≥ 1 not identified in the other inspections. Including 26 candidates from the rich cluster and blue-near-red searches,

we assemble a total catalog of 511 “probable” and “definite” lenses. These candidates are presented in Table 3. Postage-stamp images of these candidates are presented in Figure 6, which also depicts their CNN scores and human grades. The 742 candidates with grades ≥ 1 are presented in Appendix B, for reference in future lens searches.

3.3. Purity and completeness of the candidate catalog

Previous lens searches have uncovered of order a few hundred potential lenses in DES. Diehl et al (2017) conducted a search of DES science verification (SV) and Year 1 (Y1) imaging and identified 374 candidate strong lens systems, approximately half of which were graded as “probable” or “definite” lenses. The candidates were selected using the survey catalog, searching for blue-near-red objects and examining a known catalog of ETGs. Assembling this catalog involved inspection of approximately 400,000 cutout images. Nord et al (2016) searched DES SV and Y1 data for group and cluster-scale strong lenses, identifying 99 candidates of which 21 were confirmed spectroscopically.

On simulated data the CNNs are able to achieve accuracies above 99% for a score threshold of 0.5 - in other words, if we consider each candidate with a score above this value to be a lens. At this rate, we would expect up to 80,000 false positives from our search catalog in the best case that the networks were as accurate on real data as on simulations.

Collett’s (2015) simulations suggest ~ 1300 lenses should be findable in DES imaging, using detectability criteria of a signal-to-noise in $g > 20$, an Einstein radius > 2 times seeing, and a magnification of at least 3. However, blind tests on simulated images of lenses (see Paper 2) indicate that these detectability criteria may be overly optimistic by a factor of up to five at estimating what an astronomer can confidently pick from RGB images. Ideally, we could also examine lens-subtracted images, however this requires accurate PSF modelling which is complicated for the DES coadd imaging. Poor PSFs lead to ring-like artifacts in the resultant imaging, making the discovery of genuine Einstein rings difficult.

LENSPOP suggests that ~ 1300 lenses should be detectable; if only one-fifth of these can be confirmed by human experts, we expect that ~ 300 lenses should be detectable with confidence. We therefore conclude that our sample is mostly complete for the survey imaging. As noted below in Section 3.5, 41 previously identified high-quality candidates were not recovered in the CNN search. This indicates that improvements to the networks would yield further candidates.

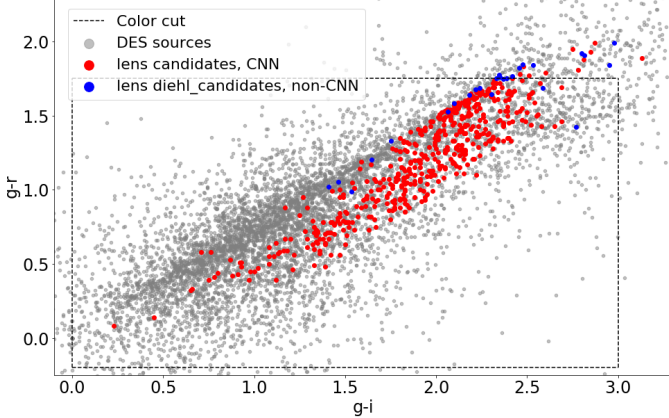


Figure 4. Colors of the CNN lens candidates (red), non-CNN lens candidates (blue), and source catalog (grey).

If subsequent improvements can be made in visualisation and grading of DES images, it is possible the detectability threshold could be lowered and new lenses would become findable.

3.4. Suitability of the search catalog

The area of $g-i$, $g-r$ color space encompassed by our search catalog contained 98.5% of our simulated lenses. Figure 4 depicts the location of our candidate lenses in this space. The density of candidates with $g-i < 1$ is low, indicating that the search is likely complete at the blue end of our sample. At the red end, the density of candidates with $g-i > 2.5$ also diminishes. Only 27.5% of our search catalog lies below this value, but 79% of our candidates are in this region. If we had restricted our search to sources bluer than $g-i$ of 2.5, we would have recovered three-quarters of our best candidates but tested only a quarter as many (~ 2 million) sources. This would have yielded a purer sample for human inspection, at the cost of some completeness. Of the Diehl et al (2017) candidates, 16 high-quality candidates lay outside (redward) of our color cuts by up to 0.25 magnitudes, an indication that future searches would benefit from relaxing the criteria.

More candidates lie in the redder end ($g-r > 1$), suggesting that searching further into the red may be worthwhile. However, fewer sources overall lie in this region of the color space ($\sim 5\%$ of the DES catalog are redder than our cuts), and so we expect diminishing returns to be evident in this area as well.

When we examine the location in this space of candidates with grades of 1 compared to those with a grade of 3, no particular trend is apparent. More ambiguous candidates in our sample have colors similar to higher-quality ones.

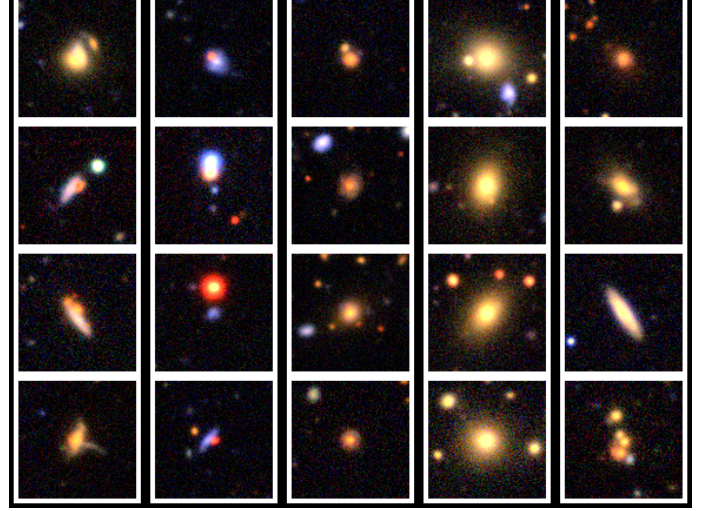


Figure 5. False positives scored as definite lenses (score = 1) by a CNN. Left: False arcs. Second from left: Blue-near-red objects. Middle: Low signal-to-noise. Second from right: Bright ETGs. Right: No clear pattern.

3.5. Comparison with blue-near-red and rich cluster search

The blue-near-red (BNR) search, using the methodology described in Section 2.5 and Diehl et al. (2017), was able to discover several high-quality lens candidates, but was less efficient than the CNN search. Visual inspection of over 50,000 sources yielded 40 probable or definite lenses, a rate of one in 1250; the CNN-based search required the inspection of approximately 30,000 candidates and yielded 485 probable or definite lenses, a rate of one in 62 (as high as one in five in the purest sample).

Of the 26 lenses discovered only in the BNR search, four are of galaxy-galaxy scale; the remainder are groups and clusters. Since our training set did not simulate group- and cluster-scale lenses, we do not expect the CNN to discover these lenses, many of which have Einstein radii larger than the postage stamp images scored with the CNNs.

The blue-near-red search methodology was also employed in the Diehl et al (2017) bright arcs survey. 41 high-quality candidates from that search which satisfied our color cuts were not recovered in this CNN search (they received scores below the thresholds we used by at least one of our networks). Conversely, of our 485 CNN-selected candidates, 48 were found by that search. Identifying those candidates involved visual inspection of over 400,000 images.

3.6. False positives

The purest candidate sample inspected yielded 255 quality candidates from a sample of 1175, about one in five. Figure 5 depicts some examples of false positives, which fall into four loose categories:

- False arcs: Arc-like features in the image appear to have confused the networks. (5%)
- Blue-near-red: A chance alignment of blue and red sources may have confused the network. (24%)
- Low signal-to-noise: Could be a lens but the image is not deep enough to be sure. (10%)
- Unknown: No clear reason (61%; however, 33% are bright ETGs which could have lensed sources obscured by the lens in the RGB imaging inspected by us.)

The rate of one-in-five represents a significant improvement from previous searches, but the fact that a human astronomer would reject the majority of the CNN-selected candidates clearly implies there is further room for improvement of the method.

3.7. Improvements for future searches

Our networks produced a candidate set of 1175 candidates with a purity of $\sim 13\%$, defined as the proportion of probable or definite lenses; this figure is greater than 20% if we include possible lenses. Although this represents high accuracy given the number and variety of sources scored by the networks, with a false positive rate of 1 in 8,000, it suggests that the network could be improved to be more aggressive in rejecting certain types of candidates that a human would classify as unlikely. Retraining networks with highly-scored false positives classified by human inspectors may drop the false positive rate without significantly impacting the false negative rate. Reducing the false positive rate would also make wider searches, for instance the entire survey catalog, more feasible.

The use of transfer learning (Bengio 2012; Vilalta 2018), where a network trained on one particular problem domain or training set can be applied to a different problem domain with minimal need for retraining, could assist future searches. The use of transfer learning for a network with an understanding of galaxy morphology was demonstrated on SDSS and DES data in Sánchez et al. (2019). Retraining networks trained to find lenses in another survey or with larger training sets of known lenses could improve networks used in future searches of DES or other surveys.

An improvement in the quality of simulations used for training is also likely to result in improved accuracy. The

use of the redMaGiC simulations resulted in a noticeable improvement in the quality of candidates, indicating that there was some property of the simulations that the networks relied on too heavily in scoring. A greater diversity in synthetic stellar populations, redshifts and morphology may lead to an improvement in completeness. Our simulations use a PSF drawn from a distribution consistent with DES Year 1 SV data, which may not be optimal for the Y3 coadd imaging we searched. This may bias the networks to images with seeing closer to the simulated distribution. This could also be tested with more varied simulations.

Finally, if the quality of the simulations is not the limiting factor in performance, then deeper networks may also lead to an improvement. In theory, larger (more trainable weights) or deeper (more layers) networks would have the ability to extract more relevant information from the training sets, but can also prove more difficult to train. Further work exploring this balance is warranted.

4. CONCLUSION

In this paper we present a catalog of 485 strong gravitational lens candidates discovered in the Dark Energy Survey Y3A1 coadd images using convolutional neural networks. We used simulated lenses to determine color cuts, which we applied to the 300 million sources in the DES survey catalog, yielding 7.9 million sources to search. We scored each image with several neural networks trained with simulated lenses and real galaxies, and combined the scores to produce small sub-sets of our search catalog that were examined by human inspectors and graded for quality. Examining one set of 1175 images (0.01% of the search catalog) resulted in 152 high-quality (probable or definite lenses). Experimenting with networks of different architectures and training sets, a further approximately 20,000 images were inspected bringing the total catalog of high-quality candidates to 399. To this we add 86 candidates found in previous CNN searches and 26 new candidates discovered in other visual searches, examining rich clusters and blue-near-red sources. The 511 candidates we discovered in DES with a grade ≥ 2 (“probably a lens”) are presented in Table 3.

For reference by future lens searches, in Appendix B we include 742 lenses with grades < 2 , i.e. possible lenses. If a significant proportion of these are confirmed in future, it may indicate that the CNNs are able to distinguish lensing features that are difficult for a human astronomer to confidently identify.

Future searches will seek to improve the purity of the samples by retraining networks using discovered lenses

and false positives graded by human experts including citizen scientist volunteers.

5. ACKNOWLEDGEMENTS

This paper has gone through internal review by the DES collaboration.

This research was supported by the Australian Research Council Centre of Excellence for All Sky Astrophysics in 3 Dimensions (ASTRO 3D), through project number CE170100013.

TEC is supported by a Dennis Sciama Fellowship from the University of Portsmouth.

Funding for the DES Projects has been provided by the U.S. Department of Energy, the U.S. National Science Foundation, the Ministry of Science and Education of Spain, the Science and Technology Facilities Council of the United Kingdom, the Higher Education Funding Council for England, the National Center for Supercomputing Applications at the University of Illinois at Urbana-Champaign, the Kavli Institute of Cosmological Physics at the University of Chicago, the Center for Cosmology and Astro-Particle Physics at the Ohio State University, the Mitchell Institute for Fundamental Physics and Astronomy at Texas A&M University, Financiadora de Estudos e Projetos, Fundação Carlos Chagas Filho de Amparo Pesquisa do Estado do Rio de Janeiro, Conselho Nacional de Desenvolvimento Científico e Tecnológico and the Ministério da Ciência, Tecnologia e Inovação, the Deutsche Forschungsgemeinschaft and the Collaborating Institutions in the Dark Energy Survey.

The Collaborating Institutions are Argonne National Laboratory, the University of California at Santa Cruz, the University of Cambridge, Centro de Investigaciones Energéticas, Medioambientales y Tecnológicas-Madrid, the University of Chicago, University College London, the DES-Brazil Consortium, the University of Edinburgh, the Eidgenössische Technische Hochschule (ETH) Zürich, Fermi National Accelerator Laboratory, the University of Illinois at Urbana-Champaign, the Institut de Ciències de l'Espai (IEEC/CSIC), the Institut de Física d'Altes Energies, Lawrence Berkeley National Laboratory, the Ludwig-Maximilians Universität München and the associated Excellence Cluster Universe, the University of Michigan, the National Optical Astronomy Observatory, the University of Nottingham, The Ohio State University, the University of

Pennsylvania, the University of Portsmouth, SLAC National Accelerator Laboratory, Stanford University, the University of Sussex, Texas A&M University, and the OzDES Membership Consortium.

Based in part on observations at Cerro Tololo Inter-American Observatory, National Optical Astronomy Observatory, which is operated by the Association of Universities for Research in Astronomy (AURA) under a cooperative agreement with the National Science Foundation.

The DES data management system is supported by the National Science Foundation under Grant Numbers AST-1138766 and AST-1536171. The DES participants from Spanish institutions are partially supported by MINECO under grants AYA2015-71825, ESP2015-66861, FPA2015-68048, SEV-2016-0588, SEV-2016-0597, and MDM-2015-0509, some of which include ERDF funds from the European Union. IFAE is partially funded by the CERCA program of the Generalitat de Catalunya. Research leading to these results has received funding from the European Research Council under the European Union's Seventh Framework Program (FP7/2007-2013) including ERC grant agreements 240672, 291329, and 306478. We acknowledge support from the Australian Research Council Centre of Excellence for All-sky Astrophysics (CAASTRO), through project number CE110001020, and the Brazilian Instituto Nacional de Ciência e Tecnologia (INCT) e-Universe (CNPq grant 465376/2014-2).

This manuscript has been authored by Fermi Research Alliance, LLC under Contract No. DE-AC02-07CH11359 with the U.S. Department of Energy, Office of Science, Office of High Energy Physics. The United States Government retains and the publisher, by accepting the article for publication, acknowledges that the United States Government retains a non-exclusive, paid-up, irrevocable, world-wide license to publish or reproduce the published form of this manuscript, or allow others to do so, for United States Government purposes.

This research has made use of the NASA/IPAC Extragalactic Database (NED), which is operated by the Jet Propulsion Laboratory, California Institute of Technology, under contract with the National Aeronautics and Space Administration.

CWJ acknowledges travel support for this work provided by the Astronomical Society of Australia.

Table 3. Strong lens candidates from visual inspection of the neural network-selected sources, sorted by grade. Redshifts are BPZ⁸ photometric redshifts except where indicated with ^ where spectroscopic redshifts are substituted. imag is the *i*-band magnitude from the DES Y3A1 catalog aperture photometry. Notes: a) previously known (74 candidates); b) discovered through blue-near-red and rich cluster search described in Section 2.5; c) found in both searches; d) found in previous CNN-based search. REFERENCES. ¹ Diehl et al. (2017), ² Bleem et al. (2015b), ³ Furlanetto et al. (2013), ⁴ Stark et al. (2013), ⁵ More et al. (2012), ⁶ More et al. (2016), ⁷ Cabanac et al. (2007), ⁸ Gavazzi et al. (2014), ⁹ Hammer (1991), ¹⁰ Postman et al. (2012), ¹¹ Bayliss (2012), ¹² Lin et al. (2017), ¹³ Bayliss et al. (2016), ¹⁴ Menanteau et al. (2010), ¹⁵ Bleem et al. (2015a), ¹⁶ Abell et al. (1989), ¹⁷ Nord et al. (2016), ¹⁸ Buckley-Geer et al. (2011), ¹⁹ Sonnenfeld et al. (2018), ²⁰ Kostrzewska-Rutkowska et al. (2014)

Candidate	objectid	RA	dec	grade	photoz	imag	notes
DESJ0002-3507	139741252	0.59845	-35.12122	2.3	0.51	19.2	
DESJ0003-3348	139823797	0.81825	-33.80120	2.7	0.68	19.3	
DESJ0006-4429	142775105	1.68592	-44.49735	2.0	0.53	18.6	a ¹
DESJ0007-4434	142779522	1.87201	-44.57949	3.0	0.52	18.1	a ¹
DESJ0010-4315	182452355	2.62678	-43.25413	2.3	0.84	19.9	d
DESJ0011-4614	182003535	2.97135	-46.23942	3.0	0.60	18.5	a ^{1,2} d
DESJ0013+0040	179698697	3.29016	0.66767	2.3	0.75	20.0	
DESJ0013-0335	180799530	3.29224	-3.59597	2.3	0.53	19.1	
DESJ0013-4239	184282860	3.38649	-42.65808	2.0	0.89	20.0	
DESJ0014+0041	179696961	3.60116	0.69596	2.0	0.59	19.4	
DESJ0015-0230	181705322	3.96725	-2.51252	2.0	0.77	20.1	
DESJ0015-4636	190717082	3.92831	-46.60305	2.3	0.44	18.4	
DESJ0017+0158	189671458	4.32556	1.97183	2.0	0.75	18.8	
DESJ0018-4549	191052533	4.50945	-45.82622	2.3	0.51	18.9	
DESJ0019-4136	189506468	4.81803	-41.61405	2.0	0.49	18.5	
DESJ0021-4040	195762492	5.39182	-40.66717	2.0	0.56	18.6	a ¹
DESJ0024-3400	204184446	6.23732	-34.01479	2.7	0.69	19.5	
DESJ0025-3139	199018206	6.29223	-31.65755	2.7	0.45	19.4	
DESJ0026-5504	204588321	6.52789	-55.07581	2.0	0.40	17.2	
DESJ0027-0413	202591480	6.75025	-4.22321	3.0	0.57	18.0	
DESJ0028-5108	147213612	7.19578	-51.14695	2.3	0.60	19.1	
DESJ0031-6420	150263838	7.83200	-64.34380	2.3	0.64	20.1	
DESJ0034-2405	208995017	8.52670	-24.09052	2.3	0.50	19.8	
DESJ0035-2526	210368868	8.78153	-25.44932	2.7	0.74	19.5	
DESJ0037-4131	154676430	9.36280	-41.53054	3.0	0.67	19.8	a ¹
DESJ0038-2936	157799078	9.69256	-29.60189	2.7	0.73	20.4	d
DESJ0040-3732	157101125	10.16456	-37.54704	2.7	0.71	20.0	
DESJ0041-0043	157857664	10.28753	-0.73025	2.7	0.53	19.0	a ³ d
DESJ0042-3718	272459491	10.73881	-37.31623	2.7	0.77	20.2	
DESJ0046+0127	273530428	11.74831	1.46004	2.0	0.55	19.4	
DESJ0046-0156	274369747	11.50837	-1.94118	2.0	0.64	18.7	
DESJ0046-5741	273462967	11.55797	-57.69931	2.3	0.41	16.7	d
DESJ0047-2905	274128225	11.75654	-29.08823	2.0	0.35	17.5	
DESJ0048+0311	275754958	12.11340	3.18808	2.7	0.39	18.0	
DESJ0050-1720	276477563	12.73017	-17.34235	2.3	0.59	19.4	
DESJ0050-4651	278178553	12.55113	-46.86210	2.7	0.73	20.1	
DESJ0052-4650	278177446	13.05359	-46.84080	2.7	0.52	18.3	a ¹
DESJ0053-0502	280210635	13.41314	-5.03359	2.0	0.54	19.0	
DESJ0056-4117	284471622	14.21105	-41.29355	2.3	0.74	20.0	
DESJ0057-5905	287581455	14.39678	-59.08847	2.3	0.65	19.8	
DESJ0058-2317	284406080	14.52023	-23.28713	2.0	0.83	19.9	

Table 3 continued

Table 3 (*continued*)

Candidate	objectid	RA	dec	grade	photoz	imag	notes
DESJ0058-5201	283879328	14.64465	-52.03323	2.7	0.66	19.1	
DESJ0101-2126	289119426	15.49817	-21.44871	2.7	0.47	17.6	c
DESJ0101-3343	290880302	15.36604	-33.72201	3.0	0.63	18.7	
DESJ0101-4917	290048397	15.49182	-49.29394	3.0	0.77	19.7	
DESJ0102+0158	289961235	15.65959	1.98243	3.0	0.81	19.7	
DESJ0102-1500	289516803	15.51229	-15.00786	2.0	0.45	17.6	
DESJ0102-2911	291358790	15.73954	-29.18939	2.7	0.41	16.9	c d
DESJ0103-4322	289419858	15.77502	-43.38144	2.3	0.62	19.9	
DESJ0105+0144	291983478	16.33185	1.74904	3.0	0.44	17.8	a ⁴
DESJ0105-2952	293813558	16.37624	-29.88030	2.3	0.73	19.5	
DESJ0105-3725	300793100	16.45017	-37.42846	2.0	0.52	18.9	
DESJ0105-3939	293220440	16.41856	-39.65728	2.0	0.43	17.8	
DESJ0106-4432	293872042	16.74639	-44.53373	3.0	0.51	19.3	
DESJ0106-6258	293662059	16.71496	-62.97051	2.3	0.75	19.5	
DESJ0109-0455	295037190	17.29452	-4.91948	2.0	0.70	19.4	d
DESJ0109-3335	301649992	17.46945	-33.59256	2.2	0.61	17.8	b
DESJ0112-0434	297291474	18.07535	-4.58298	2.0	0.55	19.2	
DESJ0112-1902	297683272	18.17142	-19.04563	2.0	0.63	18.8	
DESJ0112-5509	298183415	18.17438	-55.16470	2.3	0.79	20.1	
DESJ0113-2924	298513392	18.48794	-29.41090	2.7	0.62	20.1	
DESJ0114-3613	304672421	18.53489	-36.22043	2.7	0.53	19.0	
DESJ0115-3520	299965546	18.92008	-35.33872	2.7	0.55	18.7	
DESJ0116-2437	303683708	19.19494	-24.61724	2.3	0.49	18.9	
DESJ0116-2812	306051370	19.03047	-28.20691	2.3	0.57	19.4	
DESJ0117-0527	306602282	19.49477	-5.45492	3.0	0.57	19.4	
DESJ0117-2428	305408672	19.48697	-24.47351	2.3	0.60	19.6	
DESJ0118-6156	356474720	19.67740	-61.93700	2.7	0.36	17.9	d
DESJ0120-1524	352509235	20.21765	-15.40024	2.7	0.14	19.8	
DESJ0120-1820	354176405	20.10736	-18.33381	2.7	0.56	19.7	
DESJ0120-5143	356634575	20.17597	-51.73141	3.0	0.53	18.9	a ¹
DESJ0121-2430	350999635	20.28930	-24.51592	2.3	0.46	18.6	
DESJ0122-3654	217857957	20.61365	-36.90738	2.0	0.46	18.2	
DESJ0122-5837	217795122	20.50437	-58.62184	2.3	0.50	19.4	a ¹
DESJ0124-0157	221584166	21.17193	-1.95944	2.0	0.82	20.5	
DESJ0124-1443	223066247	21.22109	-14.71738	2.7	0.46	18.6	
DESJ0124-2401	217262328	21.08599	-24.02993	2.7	0.65	19.0	
DESJ0124-2918	222540376	21.11886	-29.31561	2.0	0.52	19.1	
DESJ0124-5207	219528181	21.13009	-52.11745	3.0	0.89	20.7	
DESJ0125-3645	266734513	21.26461	-36.76638	2.7	0.77	19.5	
DESJ0125-4142	224929412	21.38994	-41.70499	2.7	0.58	19.7	a ¹
DESJ0126-1316	223750447	21.54952	-13.27835	2.7	0.71	20.0	
DESJ0127-4532	226005640	21.97158	-45.54274	3.0	0.54	19.2	
DESJ0129-1142	223226715	22.38341	-11.70389	2.0	0.40	18.7	
DESJ0130-1520	226417019	22.61039	-15.33691	2.7	0.63	18.9	
DESJ0130-1600	226454845	22.71060	-16.00237	2.3	0.67	19.3	
DESJ0130-3744	227384193	22.51201	-37.74938	3.0	0.68	18.6	d
DESJ0132-4707	229648634	23.20825	-47.12700	2.0	0.65	19.2	
DESJ0133-1252	229855710	23.34212	-12.86700	3.0	0.71	19.9	
DESJ0133-3137	231118197	23.36279	-31.61788	2.0	0.64	20.0	
DESJ0133-6434	231207919	23.47773	-64.57028	3.0	0.39	17.3	
DESJ0134-2007	231379862	23.51597	-20.11916	2.3	0.82	20.1	
DESJ0134-2910	233143229	23.56563	-29.17774	2.3	0.48	19.5	
DESJ0135-1724	232664847	23.81460	-17.40428	2.0	0.59	20.1	d
DESJ0135-2033	234710389	23.92831	-20.55986	3.0	0.60	18.6	

Table 3 continued

Table 3 (*continued*)

Candidate	objectid	RA	dec	grade	photoz	imag	notes
DESJ0135-4232	233214974	23.84512	-42.53987	3.0	0.41	18.3	a ¹
DESJ0136+0008	232681341	24.16310	0.13836	2.0	0.39	17.3	
DESJ0136-1946	234789337	24.17633	-19.76814	2.0	0.56	20.0	d
DESJ0136-2200	233940448	24.21191	-22.00758	2.3	0.65	19.4	
DESJ0137-0830	232424091	24.32850	-8.51552	2.3	0.51	19.2	
DESJ0138-2844	235536548	24.59567	-28.73555	3.0	0.44	18.6	d
DESJ0141-1713	250156458	25.27558	-17.22326	2.7	0.61	19.0	
DESJ0141-4040	249306554	25.39168	-40.67592	3.0	0.73	19.5	
DESJ0142-1648	250131070	25.64570	-16.80487	3.0	0.60	19.5	
DESJ0142-1831	266036534	25.72030	-18.52105	3.0	0.69	19.0	
DESJ0143-0850	266637953	25.86222	-8.83925	3.0	0.68	19.6	
DESJ0143-5010	252503033	25.80483	-50.17021	2.0	0.83	20.2	
DESJ0144-0007	250028514	26.01673	-0.12953	2.0	0.55	19.0	
DESJ0144-1142	266563942	26.13855	-11.70328	2.7	0.20	20.5	c
DESJ0145+0402	266307302	26.48478	4.04139	2.7	0.66	19.8	
DESJ0145-0455	266806536	26.26791	-4.93084	2.7	0.60	19.0	a ²⁰
DESJ0145-3541	269158080	26.44493	-35.69093	3.0	0.49	18.8	
DESJ0146-0929	267163838	26.73342	-9.49779	3.0	0.46	17.4	b
DESJ0147-1206	268993332	26.80800	-12.11332	2.3	0.64	20.2	d
DESJ0147-4726	258039666	26.92084	-47.44452	2.3	0.47	18.8	a ¹ d
DESJ0148-2251	254368847	27.13131	-22.85774	2.3	0.62	19.2	d
DESJ0149-1306	258360663	27.47387	-13.10269	2.7	0.78	20.1	
DESJ0149-1349	257546600	27.32835	-13.81795	2.7	0.84	20.3	
DESJ0149-1658	256687047	27.27158	-16.98188	2.3	0.63	18.6	d
DESJ0149-3137	257110637	27.28328	-31.62730	2.7	0.71	19.1	
DESJ0149-3806	254428301	27.43714	-38.11493	2.3	0.54	18.6	
DESJ0149-3825	255329067	27.35922	-38.42540	2.7	0.40	17.9	
DESJ0150-0242	258491830	27.67649	-2.70180	2.0	0.62	19.6	
DESJ0150-0304	253888373	27.53794	-3.07730	3.0	0.68	20.4	d
DESJ0150-2216	255897453	27.70849	-22.27092	2.7	0.41	18.2	d
DESJ0151-3237	257318192	27.95172	-32.62105	2.3	0.44	17.3	b
DESJ0152-5838	263627869	28.06807	-58.64509	2.3	0.48	19.0	
DESJ0153-1351	260170996	28.33026	-13.85861	2.3	0.41	19.9	
DESJ0154-4828	258225641	28.71909	-48.48199	2.3	0.40	17.6	
DESJ0156-1011	151384552	29.17803	-10.18339	2.3	0.76	19.7	
DESJ0156-6417	270068234	29.01120	-64.29168	2.0	0.70	19.6	
DESJ0157-5311	262725875	29.46787	-53.19866	2.3	0.78	19.1	
DESJ0158-0039	62581880	29.60320	-0.66649	2.7	0.60	19.1	
DESJ0158-1301	61814814	29.68192	-13.02580	2.0	0.50	18.6	
DESJ0158-2912	61748499	29.56390	-29.20502	2.7	0.65	18.6	d
DESJ0159-1856	63651238	29.78989	-18.94999	2.3	0.40	18.0	d
DESJ0159-3413	65150639	29.76662	-34.21786	2.5	0.47	17.4	b
DESJ0159-4317	64583005	29.87848	-43.29910	2.0	0.45	18.4	
DESJ0159-4818	67328558	29.94591	-48.30353	2.3	0.71	19.8	
DESJ0201-1551	63636548	30.28319	-15.85473	2.7	0.49	18.6	d
DESJ0201-2739	66305304	30.43611	-27.66177	3.0	0.88	20.6	
DESJ0202-2156	66995978	30.64198	-21.93967	2.0	0.41	18.2	b
DESJ0202-2445	69413913	30.52770	-24.75106	2.3	0.71	19.4	
DESJ0202-4105	68398953	30.62112	-41.08867	2.0	0.78	19.2	
DESJ0203-2338	67920213	30.76671	-23.63405	3.0	0.62	18.9	c
DESJ0205-0123	69436305	31.32083	-1.38902	2.7	0.69	19.6	
DESJ0205-0208	70123404	31.48689	-2.14297	2.0	0.59	19.2	a ¹⁹
DESJ0205-3539	68181311	31.35872	-35.66317	2.7	0.45	17.7	
DESJ0205-4038	75249343	31.27043	-40.64118	2.0	0.58	19.3	a ¹

Table 3 continued

Table 3 (*continued*)

Candidate	objectid	RA	dec	grade	photoz	imag	notes
DESJ0206-0114	69428156	31.55611	-1.23817	2.3	0.77	19.2	
DESJ0206-1807	74397517	31.71314	-18.12256	2.3	0.75	20.2	
DESJ0206-2054	78494330	31.59147	-20.90561	2.3	0.62	19.4	
DESJ0207-2726	79306856	31.77773	-27.44577	2.7	0.42	17.3	c
DESJ0209-0643	77958138	32.37218	-6.71994	2.0	0.42	18.3	a ⁵
DESJ0210-0119	87141292	32.70906	-1.31827	2.0	0.67	20.0	d
DESJ0210-5351	87591843	32.65344	-53.86460	2.7	0.51	19.7	
DESJ0212-0852	90442652	33.10507	-8.86967	2.7	0.69	19.5	a ⁶
DESJ0214-0206	92012386	33.53333	-2.10789	2.0	0.67	19.3	
DESJ0215-2909	152641072	33.80953	-29.15711	2.7	0.70	19.9	
DESJ0216-2920	100388067	34.12915	-29.33520	2.0	0.55	19.9	
DESJ0217-0513	101828110	34.40483	-5.22483	2.7	0.55	19.7	a ^{7,8,22} d
DESJ0220-3833	111920425	35.24032	-38.55092	3.0	0.42	17.6	c
DESJ0220-4530	113247709	35.17619	-45.50086	2.3	0.86	20.1	
DESJ0220-5335	109454820	35.05973	-53.58636	2.3	0.79	20.1	
DESJ0221-0210	112068778	35.41721	-2.17230	2.3	0.57	19.6	a ¹⁹
DESJ0225-0737	118955435	36.44218	-7.62732	2.3	0.58	18.6	a ⁷ d
DESJ0225-1505	116423633	36.44888	-15.09220	2.3	0.67	19.3	
DESJ0226+0206	117170717	36.62452	2.11304	2.0	0.60	20.2	d
DESJ0227-4718	118887468	36.78734	-47.31550	3.0	0.68	18.6	
DESJ0228-5547	131561232	37.18616	-55.79889	2.0	0.47	18.0	d
DESJ0229-0338	121270216	37.37707	-3.64339	2.0	0.64	19.4	a ¹⁹
DESJ0229-2908	128509254	37.37911	-29.13786	3.0	0.87	20.0	
DESJ0230-3122	133666062	37.56991	-31.36689	2.3	0.48	19.2	
DESJ0232+0013	129621911	38.04683	0.22756	2.3	0.81	20.0	d
DESJ0232-0323	130346208	38.20774	-3.39054	3.0	0.47	18.0	ac ^{1,4}
DESJ0233-0438	306380750	38.27943	-4.64393	2.0	0.58	19.6	a ^{8,22}
DESJ0234-6222	308603002	38.64655	-62.38180	2.3	0.64	19.5	
DESJ0235-4510	311169228	38.77465	-45.18173	2.0	0.69	19.9	
DESJ0235-4818	308226924	38.86317	-48.30583	2.0	0.47	19.6	
DESJ0236+0321	311007100	39.20024	3.35832	2.0	0.41	19.2	
DESJ0236-5121	358035059	39.00938	-51.36216	2.3	0.84	19.4	a ¹ d
DESJ0237-0913	310489076	39.36384	-9.21903	2.7	0.82	20.2	
DESJ0237-1801	311649867	39.43907	-18.01724	2.7	0.71	20.0	
DESJ0239-0134	313249545	39.97131	-1.58221	3.0	0.44	17.4	ac ⁹
DESJ0239-2047	314286307	39.77696	-20.78834	2.7	0.64	19.0	
DESJ0239-3211	312045408	39.87360	-32.19155	3.0	0.43	18.8	
DESJ0239-4620	315501070	39.93357	-46.34466	2.7	0.40	17.2	
DESJ0241-4115	316978966	40.27731	-41.25195	3.0	0.77	20.4	
DESJ0241-5949	315606461	40.37339	-59.82580	2.0	0.58	19.9	
DESJ0242-0207	317586407	40.56738	-2.13037	2.7	0.57	19.8	
DESJ0242-2943	315970445	40.62048	-29.71815	2.7	0.47	18.6	
DESJ0242-4811	318896675	40.68463	-48.19355	2.3	0.48	19.1	
DESJ0243-0006	316036876	40.76267	-0.10005	2.7	0.45	17.7	c
DESJ0243-2142	316505122	40.86666	-21.70053	2.3	0.59	19.4	
DESJ0244-0008	322334792	41.17054	-0.14366	2.3	0.52	19.4	
DESJ0244-3019	318630744	41.20595	-30.32132	2.7	0.67	19.5	
DESJ0245-5129	322546320	41.46421	-51.49750	2.7	0.68	18.8	a ¹ d
DESJ0245-5301	320239802	41.35337	-53.02927	2.7	0.39	17.2	
DESJ0247-3750	320382487	41.80879	-37.83504	2.3	0.39	17.9	d
DESJ0247-4432	320576771	41.75052	-44.53640	2.0	0.74	18.7	
DESJ0247-5917	323527567	41.77716	-59.29213	2.7	0.41	17.5	a ¹ d
DESJ0248-0331	323148175	42.01411	-3.52913	3.0	0.38	15.6	b
DESJ0248-3955	320189990	42.03972	-39.93008	3.0	0.66	19.1	c

Table 3 continued

Table 3 (*continued*)

Candidate	objectid	RA	dec	grade	photoz	imag	notes
DESJ0248-6054	322703225	42.24005	-60.90097	2.7	0.56	19.2	
DESJ0249-5056	324524229	42.49448	-50.94399	2.3	0.60	19.9	
DESJ0250-1610	324211306	42.71571	-16.16883	2.3	0.40	17.7	
DESJ0250-1811	323759326	42.61404	-18.19468	2.0	0.67	19.9	
DESJ0250-2545	325876415	42.58849	-25.75382	2.3	0.65	19.6	
DESJ0250-5524	331348861	42.71781	-55.40325	3.0	0.75	19.6	
DESJ0251-0613	324179816	42.93427	-6.22482	2.7	0.42	17.4	
DESJ0251-1220	325171876	42.89705	-12.33367	3.0	0.46	18.1	d
DESJ0252-2145	325350854	43.18031	-21.75937	2.3	0.45	18.7	
DESJ0252-4732	325184579	43.08284	-47.54382	2.3	0.49	18.4	a ¹ d
DESJ0253-1239	332638388	43.37844	-12.65088	2.7	0.68	19.8	
DESJ0253-2050	326901259	43.41658	-20.83750	2.0	0.58	18.8	
DESJ0253-3547	328771437	43.39711	-35.79207	2.7	0.66	19.8	
DESJ0256-1215	350492611	44.01502	-12.25496	2.7	0.49	18.1	
DESJ0256-2707	333129437	44.09736	-27.12183	3.0	0.76	20.1	
DESJ0259-0804	332519880	44.95084	-8.07945	2.3	0.57	19.0	
DESJ0259-1521	335268116	44.80894	-15.36354	2.7	0.44	18.0	
DESJ0259-5206	337550755	44.85811	-52.11193	2.3	0.57	17.8	d
DESJ0300-5001	335766992	45.09019	-50.02469	3.0	0.53	18.4	a ¹
DESJ0300-5144	337527643	45.13631	-51.74562	3.0	0.61	18.4	a ¹
DESJ0301-4426	337812631	45.46380	-44.44055	2.3	0.76	20.2	
DESJ0302-2137	336668432	45.59119	-21.63207	2.7	0.48	18.7	
DESJ0303-4626	341691067	45.95070	-46.44066	2.7	1.37	20.7	a ¹
DESJ0303-5023	338494005	45.96811	-50.39776	2.0	0.64	19.7	
DESJ0304-4921	341631765	46.06729	-49.35725	3.0	0.34	17.5	b ^{1,2}
DESJ0304-5846	341516834	46.15722	-58.77995	2.3	0.73	19.9	
DESJ0305-1024	341195944	46.27306	-10.40325	2.0	0.75	20.1	d
DESJ0305-1636	337847674	46.31967	-16.60365	2.3	0.60	18.9	d
DESJ0306-2304	342445367	46.69704	-23.07635	2.3	0.52	19.0	
DESJ0307-1811	342297166	46.93881	-18.18558	2.0	0.26	20.9	
DESJ0307-5042	344560939	46.96054	-50.70122	2.3	0.59	18.4	b ^{1,2}
DESJ0307-6241	341257301	46.87411	-62.68482	2.0	0.48	18.1	
DESJ0308-2106	343364859	47.20000	-21.10386	3.0	0.76	20.2	d
DESJ0309-1332	342860023	47.33215	-13.53674	2.0	0.59	19.8	d
DESJ0309-1437	343011680	47.43782	-14.62114	2.7	0.79	20.2	a ¹¹
DESJ0309-3805	343290165	47.33576	-38.09604	2.7	0.62	18.9	
DESJ0309-6239	328377991	47.32498	-62.66179	2.3	0.44	18.7	
DESJ0310-0903	342955143	47.52242	-9.05404	2.0	0.61	19.4	
DESJ0310-4647	345606854	47.63526	-46.78398	2.7	0.71	19.1	b ^{1,2}
DESJ0311-2601	329906936	47.77324	-26.01778	2.7	0.94	20.5	
DESJ0311-4232	340768337	47.86322	-42.53863	2.7	0.37	17.5	
DESJ0313-2006	327373298	48.29103	-20.10875	2.3	0.80	19.8	
DESJ0313-3610	382872932	48.40598	-36.17775	3.0	0.40	20.5	d
DESJ0314-2127	382406538	48.64811	-21.46665	2.3	0.45	17.8	d
DESJ0314-2841	339342483	48.57753	-28.69899	2.3	0.54	19.1	
DESJ0315-6220	348227502	48.93026	-62.34321	2.0	0.51	19.1	
DESJ0316-2236	346057868	49.16179	-22.60925	3.0	0.79	19.6	
DESJ0317-2118	347820479	49.42391	-21.30499	2.7	0.48	18.1	d
DESJ0317-2625	349590200	49.29261	-26.42107	2.0	0.76	20.3	
DESJ0318-1942	348794656	49.62499	-19.70766	2.0	0.64	19.4	
DESJ0319-1734	351516752	49.92199	-17.56790	3.0	0.68	20.1	
DESJ0319-4759	354488458	49.99213	-47.98763	2.0	0.48	19.3	
DESJ0319-5318	348242739	49.75905	-53.30547	2.0	0.43	17.7	a ¹
DESJ0319-5751	354864135	49.90701	-57.85219	2.7	0.54	19.2	

Table 3 continued

Table 3 (*continued*)

Candidate	objectid	RA	dec	grade	photoz	imag	notes
DESJ0320-1624	352008867	50.15414	-16.40618	3.0	0.59	19.6	
DESJ0320-3119	355312277	50.06689	-31.32149	2.0	0.75	19.5	
DESJ0320-4159	349979646	50.11682	-41.98881	2.7	0.66	19.1	
DESJ0321-1530	353748149	50.35660	-15.50098	2.7	0.62	19.5	
DESJ0322-2339	355712108	50.67685	-23.66524	2.3	0.54	19.4	
DESJ0322-3946	358893159	50.71632	-39.76936	2.7	0.85	20.3	
DESJ0322-4224	358251063	50.59429	-42.40605	2.3	0.57	19.3	
DESJ0322-5234	359440586	50.56837	-52.57790	3.0	0.46	18.0	a ¹
DESJ0324-3556	359347789	51.02925	-35.93638	2.0	0.38	17.6	
DESJ0326-4812	362343856	51.51215	-48.20995	2.0	0.43	17.7	d
DESJ0326-5645	361461421	51.62299	-56.76170	2.7	0.68	20.2	a ¹
DESJ0327-1326	360253469	51.86318	-13.43961	3.0	0.56	19.0	b
DESJ0327-3246	361760653	51.79729	-32.77616	2.7	0.65	19.0	
DESJ0328-2140	362669813	52.05660	-21.67208	2.3	0.59	18.2	b
DESJ0328-3833	361724422	52.24989	-38.55273	2.3	0.41	18.3	
DESJ0328-4029	363968737	52.00516	-40.49922	2.0	0.51	19.2	
DESJ0329-5656	361472987	52.26624	-56.94944	2.7	0.40	17.3	
DESJ0330-2127	362656939	52.62838	-21.45315	2.0	0.72	20.0	d
DESJ0330-5228	368913139	52.73718	-52.47028	2.5	0.46	17.7	b ^{1,2}
DESJ0332-1325	365125003	53.01064	-13.41950	2.3	0.64	20.2	d
DESJ0333-1440	366164591	53.48320	-14.66914	2.2	0.53	18.5	b
DESJ0333-1837	366216886	53.41061	-18.61902	2.0	0.26	20.2	
DESJ0334-1838	366217976	53.74324	-18.64403	2.7	0.51	19.1	
DESJ0334-2634	367701604	53.74703	-26.57546	2.0	0.44	17.7	d
DESJ0334-4817	367248708	53.54557	-48.28704	2.0	0.50	18.3	a ¹
DESJ0334-4940	368398173	53.58416	-49.67789	2.0	0.66	19.1	
DESJ0334-6034	368841941	53.74437	-60.58056	2.3	0.58	18.3	
DESJ0336-2021	367624957	54.17408	-20.35310	2.0	0.65	19.6	b
DESJ0336-3812	368270048	54.11897	-38.20245	2.0	0.45	18.6	
DESJ0337-3152	370414914	54.32183	-31.87043	3.0	0.47	18.6	
DESJ0338-1619	371619216	54.69029	-16.32305	2.7	0.70	19.7	
DESJ0339-5830	370944473	54.77706	-58.50469	2.3	0.36	17.2	
DESJ0340-2533	374318639	55.08904	-25.55837	2.7	0.67	19.5	d
DESJ0341-5130	374811766	55.37833	-51.51241	2.7	0.42	19.0	a ¹
DESJ0342-5355	374878192	55.51920	-53.92059	3.0	0.63	18.4	a ¹ d
DESJ0344-4447	378734502	56.14624	-44.79555	3.0	0.81	20.1	
DESJ0345-2459	378104707	56.36640	-24.98848	3.0	0.47	19.3	
DESJ0347-2454	378100572	56.93556	-24.90874	3.0	0.57	19.2	
DESJ0347-3158	424959030	56.95311	-31.98063	2.3	0.38	17.5	d
DESJ0347-3647	380333963	56.93924	-36.79364	2.3	0.61	19.2	
DESJ0347-4535	379955716	56.80535	-45.58500	3.0	0.66	19.0	a ¹
DESJ0348-1306	379862967	57.14437	-13.11303	2.0	0.59	18.4	d
DESJ0348-2145	379404679	57.00965	-21.75082	3.0	0.43	17.2	
DESJ0348-2655	379292496	57.02437	-26.92048	2.0	0.37	17.6	
DESJ0349-1500	382692058	57.45008	-15.00234	2.3	0.37	17.3	
DESJ0349-4857	380145919	57.33127	-48.95926	3.0	0.65	18.8	a ¹
DESJ0350-4824	381150466	57.70236	-48.40619	2.3	0.78	20.1	
DESJ0352-3825	385542120	58.17670	-38.42915	3.0	0.54	18.4	
DESJ0353-1706	386508843	58.44268	-17.11090	3.0	0.60	19.2	
DESJ0354-1609	386476783	58.57614	-16.16450	2.7	0.63	18.7	
DESJ0354-2420	386408997	58.69798	-24.33749	3.0	0.66	19.5	
DESJ0356-1457	386858139	59.21895	-14.96632	2.3	0.55	19.4	
DESJ0356-2408	386397276	59.20438	-24.14476	3.0	0.48	18.7	
DESJ0356-5607	392535235	59.02600	-56.12484	2.0	0.48	17.6	d

Table 3 continued

Table 3 (*continued*)

Candidate	objectid	RA	dec	grade	photoz	imag	notes
DESJ0357-5810	482065451	59.40346	-58.18149	2.7	0.61	18.5	a ¹
DESJ0357-5951	386543661	59.33565	-59.86512	2.3	0.58	19.3	
DESJ0358-2950	387200923	59.53509	-29.84965	2.0	0.40	18.3	
DESJ0402-2205	484107721	60.52380	-22.09897	3.0	0.49	19.3	d
DESJ0402-5258	482528109	60.73983	-52.97845	2.0	0.87	20.5	a ¹
DESJ0403-1512	486502907	60.80335	-15.21602	2.0	0.65	19.9	
DESJ0403-5432	488465172	60.84466	-54.54363	3.0	0.75	19.7	
DESJ0406-2646	484389531	61.60206	-26.77362	3.0	1.54	20.3	
DESJ0407-5713	389992748	61.81508	-57.21756	2.7	0.40	17.8	d
DESJ0408-5354	488067795	62.09132	-53.90026	2.7	0.04	19.5	a ^{1,12}
DESJ0410-3037	406431056	62.55545	-30.62385	2.0	0.73	19.8	
DESJ0411-2256	398879866	62.78340	-22.94312	2.3	0.57	19.8	
DESJ0411-3144	397635797	62.95688	-31.74853	2.7	0.78	20.3	
DESJ0411-4819	400940211	62.79569	-48.32768	2.7	0.46	17.7	ac ^{1,13}
DESJ0411-5107	403494207	62.92814	-51.12636	2.3	0.48	17.8	
DESJ0412-1954	401080659	63.16191	-19.90303	2.7	0.64	19.5	c
DESJ0412-2646	402142279	63.17877	-26.77565	2.3	0.43	17.1	
DESJ0413-2344	400295190	63.42129	-23.73947	2.0	0.71	19.4	
DESJ0415-4012	398187423	63.91078	-40.20893	2.0	0.55	19.7	
DESJ0415-4143	402556287	63.93554	-41.72949	2.3	0.75	19.2	d
DESJ0416-5525	496377974	64.18671	-55.41675	2.7	0.43	17.6	a ¹ d
DESJ0416-5908	401596916	64.16482	-59.14804	2.3	0.53	19.1	
DESJ0418-5457	406587770	64.54117	-54.95973	2.7	0.53	19.6	a ¹
DESJ0418-6125	496621301	64.60748	-61.42413	2.3	0.38	17.5	
DESJ0419-2959	495663192	64.77709	-29.99383	2.0	0.91	20.3	
DESJ0420-5422	498547848	65.17820	-54.37706	2.0	0.73	19.8	
DESJ0422-2132	496451011	65.57590	-21.54608	3.0	0.64	19.3	
DESJ0422-4031	498968361	65.60553	-40.53217	3.0	0.41	17.9	d
DESJ0424-3317	498603518	66.16119	-33.29491	3.0	0.62	18.2	c
DESJ0428-3218	499443386	67.06771	-32.30001	2.3	0.71	19.4	
DESJ0429-2243	469427390	67.37815	-22.73322	2.3	0.66	19.6	
DESJ0429-2826	505469261	67.28763	-28.43800	2.0	0.47	18.5	
DESJ0429-6011	470193950	67.39444	-60.19064	2.3	1.06	20.2	
DESJ0430-2051	469242961	67.59246	-20.85277	2.0	0.62	19.5	
DESJ0431-4317	505813589	67.92345	-43.29463	2.0	0.55	19.5	
DESJ0431-5422	469937250	67.84590	-54.37902	2.3	0.55	19.3	
DESJ0433-2714	469726289	68.26475	-27.23982	2.7	0.53	19.6	
DESJ0433-4456	470414267	68.45305	-44.93493	2.0	0.60	19.6	
DESJ0437-5136	508636686	69.45059	-51.60777	2.3	0.59	19.6	
DESJ0437-6428	490781756	69.31460	-64.47504	2.3	0.44	17.8	
DESJ0437-6502	497809494	69.48652	-65.03786	2.3	0.63	18.7	
DESJ0438-3228	490038071	69.52573	-32.48116	2.0	0.40	17.3	
DESJ0441-4314	496058773	70.37184	-43.23723	2.7	0.51	19.3	
DESJ0442-2920	495043677	70.62357	-29.34467	2.3	0.57	19.3	
DESJ0442-6257	506943132	70.70370	-62.95143	2.0	0.45	19.7	d
DESJ0443-2026	497282912	70.79929	-20.44658	2.7	0.66	19.2	
DESJ0443-6228	506890546	70.93285	-62.46824	2.3	0.65	19.9	
DESJ0446-2001	503213475	71.56238	-20.02854	2.3	0.43	18.4	d
DESJ0446-2714	503055747	71.66670	-27.24653	2.3	0.63	18.9	
DESJ0448-5807	503582193	72.02201	-58.12258	3.0	0.42	18.3	a ¹
DESJ0449-2918	479366135	72.28966	-29.30456	2.0	0.60	18.6	
DESJ0450-5715	481189495	72.53670	-57.25556	3.0	0.42	17.9	a ¹
DESJ0452-3540	486595893	73.12391	-35.67423	2.0	0.61	19.1	
DESJ0453-5535	487409539	73.38443	-55.59106	2.0	0.36	17.6	

Table 3 continued

Table 3 (*continued*)

Candidate	objectid	RA	dec	grade	photoz	imag	notes
DESJ0454-6234	408367693	73.68189	-62.56679	2.7	0.64	20.0	
DESJ0455-2530	397694347	73.90302	-25.51280	2.7	0.44	17.7	b
DESJ0456-2946	398369563	74.16540	-29.77272	2.7	0.46	18.5	
DESJ0457-3549	394429819	74.39074	-35.83147	2.0	0.69	19.5	d
DESJ0457-4115	394973892	74.42190	-41.25687	2.0	0.50	18.8	d
DESJ0457-4331	399018963	74.46276	-43.52617	2.7	0.78	19.7	
DESJ0458-4045	394868723	74.69941	-40.75106	2.0	0.49	19.1	
DESJ0459-2045	395472372	74.75610	-20.75189	2.7	0.68	19.4	
DESJ0501-5054	397556846	75.27780	-50.91315	2.7	0.53	19.5	
DESJ0502-5828	409607810	75.66420	-58.47481	2.7	0.43	18.6	
DESJ0503-3553	405612468	75.76990	-35.88520	2.7	0.68	19.2	
DESJ0504-3548	405607557	76.07334	-35.80170	2.0	0.73	19.6	
DESJ0505-4611	410418835	76.26967	-46.19931	2.0	0.63	19.4	
DESJ0505-6149	412242213	76.44598	-61.83072	2.3	0.77	20.0	
DESJ0506-2049	412357300	76.50219	-20.81680	2.3	0.61	19.5	
DESJ0506-4220	412598534	76.73095	-42.34575	2.7	0.43	18.0	d
DESJ0507-5348	412809087	76.94602	-53.81148	2.0	0.44	18.2	d
DESJ0508-2144	413900270	77.20527	-21.74187	2.7	0.73	18.9	d
DESJ0508-2746	414408351	77.17749	-27.77706	2.7	0.70	20.1	
DESJ0509-5342	412802769	77.33914	-53.70351	2.5	0.45	18.3	b ^{1,2}
DESJ0510-3232	415264664	77.55331	-32.53492	2.7	0.51	18.5	
DESJ0510-5637	416330172	77.55490	-56.63171	2.7	0.56	19.0	a ¹
DESJ0511-3134	413601266	77.82017	-31.57560	2.3	0.84	19.6	
DESJ0512-5041	414671694	78.00324	-50.68968	2.7	0.80	20.4	
DESJ0513-3847	415684203	78.25092	-38.79534	3.0	0.42	17.2	
DESJ0514-5456	423087260	78.53033	-54.94835	2.0	0.89	20.2	
DESJ0516-2208	421153300	79.01322	-22.14642	2.0	0.74	18.9	
DESJ0516-4416	425110323	79.17349	-44.27903	2.7	0.70	19.9	
DESJ0522-6036	432182051	80.58806	-60.60666	2.7	0.38	17.0	
DESJ0524-2721	495171666	81.09859	-27.35316	2.3	0.38	17.3	
DESJ0525-4424	431878468	81.36681	-44.40375	2.3	0.54	19.2	a ¹
DESJ0528-3811	434441869	82.13907	-38.19495	2.0	0.66	19.8	
DESJ0530-6109	437004264	82.51363	-61.16180	2.0	0.50	19.4	
DESJ0531-3158	435151688	82.92694	-31.98092	2.0	0.56	18.7	
DESJ0533-2536	436520077	83.45553	-25.61511	3.0	0.71	19.8	
DESJ0534-5347	476312399	83.68678	-53.78785	2.7	0.46	18.4	
DESJ0536-5338	441387666	84.02185	-53.64641	2.7	0.75	19.6	a
DESJ0537-4647	440192267	84.35163	-46.78401	2.0	0.41	18.0	
DESJ0537-4711	442349695	84.44091	-47.18897	2.3	0.45	17.4	a ¹
DESJ0538-4735	440626159	84.51923	-47.58715	3.0	0.64	19.5	a ¹
DESJ0542-5949	446496955	85.60111	-59.83305	2.3	0.82	20.0	
DESJ0543-3034	443691408	85.99182	-30.58041	2.3	0.46	18.6	
DESJ0543-3752	443873820	85.75861	-37.87701	2.3	0.54	19.3	d
DESJ0546-2000	445925268	86.52108	-20.00709	2.3	0.68	18.9	
DESJ0546-3329	446691881	86.61455	-33.48964	2.3	0.46	18.5	d
DESJ0553-2853	455705762	88.29686	-28.89357	2.0	0.73	19.8	
DESJ0554-2238	460703862	88.60108	-22.63505	2.0	0.45	20.1	b
DESJ0557-4159	448420913	89.39342	-41.99730	2.7	0.58	19.9	d
DESJ0559-3540	449284676	89.95629	-35.67013	2.0	0.69	19.9	
DESJ0602-4524	454651910	90.69522	-45.41200	3.0	0.53	18.6	a ¹ d
DESJ0612-3920	461287032	93.11443	-39.34343	2.0	0.51	19.1	
DESJ0613-5552	464163629	93.30138	-55.87347	2.7	0.81	20.4	
DESJ0620-5628	467246294	95.07919	-56.48287	2.7	0.61	19.4	
DESJ0624-4709	467288040	96.06586	-47.16168	2.7	0.84	19.9	d

Table 3 continued

Table 3 (*continued*)

Candidate	objectid	RA	dec	grade	photoz	imag	notes
DESJ0625-4526	466018111	96.25055	-45.43576	2.7	0.60	18.9	a ¹
DESJ0626-5730	467900153	96.59632	-57.50837	2.7	0.72	18.8	
DESJ0628-5023	467004961	97.03929	-50.39994	2.0	0.44	18.1	
DESJ2014-5757	166130477	303.58076	-57.95041	3.0	0.80	20.0	d
DESJ2025-4204	166736956	306.32627	-42.08248	2.0	0.71	20.2	b
DESJ2028-5231	170303276	307.23246	-52.52177	3.0	0.66	19.7	
DESJ2039-5459	174184226	309.79778	-54.99594	2.7	0.17	21.0	a ¹
DESJ2045-6344	218602325	311.29752	-63.74792	2.0	0.48	17.9	
DESJ2051-6450	179178262	312.99332	-64.84365	2.0	0.62	20.0	
DESJ2053-5046	242818860	313.28612	-50.78121	2.3	0.70	20.7	d
DESJ2056-4238	186351000	314.06590	-42.64923	2.7	0.71	20.4	
DESJ2101-5629	236804532	315.25851	-56.49656	2.0	0.41	18.7	
DESJ2105-4934	187548006	316.27045	-49.57829	2.0	0.51	18.2	
DESJ2106-4411	188387027	316.52989	-44.19821	2.7	0.46	18.5	d
DESJ2106-5402	184661871	316.64790	-54.04109	2.0	0.42	17.8	d
DESJ2110-5639	185701755	317.52247	-56.65849	2.7	0.59	18.3	a ¹ d
DESJ2112+0009	188723770	318.17974	0.15577	2.7	0.59	18.4	
DESJ2113-0114	192966022	318.48453	-1.24069	2.7	0.53	18.9	a ¹
DESJ2116-5947	193746022	319.11382	-59.78382	3.0	0.48	17.8	
DESJ2117-0056	196646767	319.34830	-0.94774	2.3	0.53	17.8	d
DESJ2118-4317	193632443	319.60728	-43.29433	2.3	0.51	19.2	
DESJ2119-0009	195317995	319.83958	-0.16294	2.3	0.54	20.0	
DESJ2122-4250	196144920	320.55153	-42.84999	2.0	0.62	19.1	
DESJ2124-4128	197645134	321.19662	-41.47104	2.3	0.63	19.0	d
DESJ2125-6504	191159999	321.30012	-65.07408	3.0	0.78	19.4	d
DESJ2126-0058	199596977	321.71310	-0.97425	2.0	0.60	19.6	
DESJ2127-5149	198186510	321.77933	-51.83083	3.0	0.77	19.3	a ¹ d
DESJ2130+0159	198514358	322.69589	1.99907	2.3	0.69	19.6	
DESJ2131-4019	203401336	322.77049	-40.32251	2.2	0.45	17.7	b
DESJ2131-4655	204721418	322.98474	-46.92895	2.0	0.71	19.7	
DESJ2132-4305	200096605	323.07334	-43.09307	2.0	0.50	18.7	
DESJ2137-0129	208765710	324.49176	-1.48996	2.7	0.41	18.2	
DESJ2139-4251A	244329751	324.78020	-42.86152	2.3	0.46	19.5	b
DESJ2140-0149	207661829	325.21674	-1.82716	2.3	0.67	19.2	
DESJ2140-4207	212627230	325.02644	-42.12956	2.7	0.56	19.4	
DESJ2144-4149	242604259	326.22656	-41.83128	2.0	0.37	17.2	
DESJ2145-4306	214625101	326.44328	-43.11370	2.0	0.51	18.9	
DESJ2149-0012	215694905	327.31380	-0.21431	2.0	0.64	18.0	a ¹
DESJ2152-5250	243367339	328.22047	-52.83500	2.3	0.65	19.1	
DESJ2159-4307	245879871	329.77985	-43.12946	2.2	0.39	16.2	b
DESJ2200-4128	247210752	330.18545	-41.47227	2.3	0.56	19.8	a ²
DESJ2201-6047	247165409	330.27719	-60.78407	2.3	0.48	18.1	d
DESJ2203-6408	70905032	330.89934	-64.13907	2.3	0.69	19.4	
DESJ2211-5438	76343894	332.98655	-54.64442	2.3	0.64	19.3	
DESJ2212-4128	75848635	333.02475	-41.47315	2.0	0.37	18.0	
DESJ2215-0138	75042870	333.96727	-1.63723	2.0	0.65	19.0	d
DESJ2216-4419	76102671	334.15922	-44.32216	2.7	0.63	18.2	
DESJ2218-4504	75469120	334.74019	-45.07379	2.3	0.65	18.9	
DESJ2219-4348	80103224	334.80166	-43.80975	3.0	0.71	19.1	
DESJ2219-4504	75469581	334.80513	-45.08072	2.0	0.72	19.5	
DESJ2220-5949	80012526	335.21651	-59.82418	2.0	0.55	19.4	
DESJ2226+0041	82782545	336.53876	0.69504	2.7	0.74	19.4	a ^{1,19}
DESJ2226-4636	84960890	336.62064	-46.60151	2.3	0.48	18.4	
DESJ2228-4650	83291276	337.14677	-46.83995	2.0	0.37	19.9	b

Table 3 continued

Table 3 (*continued*)

Candidate	objectid	RA	dec	grade	photoz	imag	notes
DESJ2232-5959	84477903	338.14086	-59.99810	2.0	0.65	18.5	a ²
DESJ2234-4110	88791681	338.58932	-41.17777	2.7	0.47	18.8	
DESJ2238-4317	96933817	339.71254	-43.29173	2.3	0.65	19.4	
DESJ2245-5017	100785152	341.26572	-50.29037	3.0	0.50	19.8	
DESJ2248-0123	98187103	342.15155	-1.39278	2.3	0.65	18.5	d
DESJ2248-4431	100664389	342.18318	-44.53080	2.7	0.27	16.7	b ^{1,2}
DESJ2254-4055	104947647	343.51270	-40.93031	2.7	0.66	19.2	a ¹
DESJ2255-4123	104511812	343.77631	-41.38895	2.0	0.67	19.2	
DESJ2259-4504	106557886	344.97848	-45.08013	2.0	0.52	19.1	
DESJ2300-4454	106547800	345.01328	-44.90647	2.0	0.50	19.4	
DESJ2301-6501	109542319	345.40177	-65.03269	2.0	0.60	19.8	
DESJ2303-5115	127551471	345.76962	-51.25050	2.7	0.53	18.2	
DESJ2305-0002	112454911	346.34025	-0.03655	3.0	0.51	19.0	a ²²
DESJ2305-4441	112637264	346.36599	-44.69629	2.3	0.59	19.1	d
DESJ2308-0211	113660691	347.09255	-2.19214	2.3	0.42	16.7	b ¹⁶
DESJ2308-0212	113661583	347.10308	-2.20378	2.3	0.43	17.2	b ¹⁶
DESJ2311-4546	124310010	347.79872	-45.78281	2.3	0.59	19.0	
DESJ2312-4754	122895085	348.00185	-47.90321	2.0	0.63	19.7	
DESJ2321-4630	126963595	350.36821	-46.51371	3.0	0.64	18.8	ac ¹
DESJ2322-6409	129115213	350.68261	-64.16565	3.0	0.41	17.5	d
DESJ2323-0030	126557178	350.94191	-0.51056	2.0	0.85	20.4	
DESJ2325-0052	131224001	351.48903	-0.87407	2.3	0.73	20.0	
DESJ2325-4111	130067409	351.29546	-41.19026	2.7	1.43	100.0	b ^{1,2}
DESJ2329-5328	135432654	352.48378	-53.47715	2.0	0.51	19.0	d
DESJ2331+0037	135139282	352.87703	0.62594	2.0	0.52	19.4	a ²² d
DESJ2334-5715	136894134	353.70143	-57.25099	2.0	0.47	18.5	
DESJ2334-6404	136837812	353.74665	-64.06860	3.0	0.72	19.5	
DESJ2335-5152	137085303	353.96636	-51.87161	3.0	0.61	18.8	a ¹
DESJ2336-5352	137565894	354.02969	-53.87662	2.0	0.50	18.1	a ^{1,17}
DESJ2337-4730	137735570	354.39475	-47.50669	2.7	0.52	19.6	d
DESJ2345-4126	158856314	356.25481	-41.43636	2.0	0.65	19.7	
DESJ2349-5113	214800683	357.37523	-51.22751	3.0	0.48	17.5	a ¹
DESJ2351-5452	164741263	357.90859	-54.88168	3.0	0.43	17.3	a ^{1,14,18}
DESJ2355-6136	169555789	358.82982	-61.61029	2.7	0.53	18.9	
DESJ2357-5710	175719968	359.32342	-57.17383	2.3	0.56	19.4	
DESJ2358-5440	283922617	359.52065	-54.67623	2.0	0.44	20.6	
DESJ2358-5638	184225540	359.69297	-56.64720	2.3	0.63	19.6	d
DESJ2359-5538	284516950	359.75900	-55.63496	2.0	0.73	19.9	d

REFERENCES

- Abbott T. M. C., et al., 2018, *ApJS*, 239, 18
- Abell G. O., Corwin Jr. H. G., Olowin R. P., 1989, *ApJS*, 70, 1
- Avestruz C., Li N., Lightman M., Collett T. E., Luo W., 2017, preprint, 1704, arXiv:1704.02322
- Bayliss M. B., 2012, *ApJ*, 744, 156
- Bayliss M. B., et al., 2016, *ApJS*, 227, 3
- Bellstedt S., et al., 2018, *MNRAS*
- Bengio Y., 2012, in Proceedings of ICML Workshop on Unsupervised and Transfer Learning. Bellvue, Washington, USA, pp 17–36
- Bleem L. E., Stalder B., Brodin M., Busha M. T., Gladders M. D., High F. W., Rest A., Wechsler R. H., 2015a, *ApJS*, 216, 20
- Bleem L. E., et al., 2015b, *ApJS*, 216, 27
- Buckley-Geer E. J., et al., 2011, *ApJ*, 742, 48
- Busca N., Balland C., 2018, arXiv:1808.09955 [astro-ph]
- Cabanac R. A., et al., 2007, *A&A*, 461, 813
- Cabayol L., et al., 2019, *MNRAS*, 483, 529
- Chan J. H. H., Suyu S. H., Chiueh T., More A., Marshall P. J., Coupon J., Oguri M., Price P., 2015, *ApJ*, 807
- Collett T. E., 2015, *ApJ*, 811, 20

- Collett T. E., Auger M. W., 2014, *MNRAS*, 443, 969
- Dai J.-M., Tong J., 2018, arXiv:1807.10406 [astro-ph]
- Dark Energy Survey Collaboration et al., 2016, *MNRAS*, 460, 1270
- Despali G., Vegetti S., White S. D. M., Giocoli C., Bosch V. D., C F., 2018, *MNRAS*, 475, 5424
- Diehl H. T., et al., 2017, *ApJS*, 232, 15
- Dieleman S., Willett K. W., Dambre J., 2015, *MNRAS*, 450, 1441
- Einstein A., 1936, *Science*, 84, 506
- Furlanetto C., et al., 2013, *MNRAS*, 432, 73
- Gavazzi R., Treu T., Koopmans L. V. E., Bolton A. S., Moustakas L. A., Scott Burles Marshall P. J., 2008, *ApJ*, 677, 1046
- Gavazzi R., Marshall P. J., Treu T., Sonnenfeld A., 2014, *ApJ*, 785, 144
- Hammer F., 1991, *ApJ*, 383, 66
- Hezaveh Y. D., Levasseur L. P., Marshall P. J., 2017
- Hyde J. B., Bernardi M., 2009, *MNRAS*, 396, 1171
- Ilbert O., et al., 2009, *ApJ*, 690, 1236
- Jacobs C., Glazebrook K., Collett T., More A., McCarthy C., 2017, *MNRAS*, 471, 167
- Jacobs C., et al., 2019, *Mon Not R Astron Soc*, 484, 5330
- Keeton C. R., 2001, arXiv:astro-ph/0102340
- Kim E. J., Brunner R. J., 2017, *MNRAS*, 464, 4463
- Koopmans L. V. E., 2005, *Mon Not R Astron Soc*, 363, 1136
- Kostrzewa-Rutkowska Z., Wyrzykowski Ł., Auger M. W., Collett T. E., Belokurov V., 2014, *MNRAS*, 441, 3238
- Krizhevsky A., Sutskever I., Hinton G. E., 2012, in Pereira F., Burges C. J. C., Bottou L., Weinberger K. Q., eds., , Advances in Neural Information Processing Systems 25. Curran Associates, Inc., pp 1097–1105
- Lanusse F., Ma Q., Li N., Collett T. E., Li C.-L., Ravanbakhsh S., Mandelbaum R., Póczos B., 2018, *MNRAS*, 473, 3895
- LeCun Y., Boser B., Denker J. S., Henderson D., Howard R. E., Hubbard W., Jackel L. D., 1989, *Neural Comput.*, 1, 541
- Li R., Frenk C. S., Cole S., Gao L., Bose S., Hellwing W. A., 2016, *MNRAS*, 460
- Lin H., et al., 2017, *ApJL*, 838, L15
- Marshall P. J., Hogg D. W., Moustakas L. A., Fassnacht C. D., Bradač M., Tim Schrabback Blandford R. D., 2009, *ApJ*, 694, 924
- Marshall P. J., et al., 2016, *MNRAS*, 455
- Menanteau F., et al., 2010, *ApJS*, 191, 340
- Miyazaki S., et al., 2018, *Publ Astron Soc Jpn Nihon Tenmon Gakkai*, 70
- More A., Cabanac R., More S., Alard C., Limousin M., Kneib J.-P., Gavazzi R., Motta V., 2012, *ApJ*, 749, 38
- More A., et al., 2016, *MNRAS*, 455
- Morganson E., et al., 2018, *Publications of the Astronomical Society of the Pacific*, 130, 074501
- Nord B., et al., 2016, *ApJ*, 827, 51
- Petrillo C. E., et al., 2017, *MNRAS*, 472, 1129
- Petrillo C. E., et al., 2019, *MNRAS*, 484, 3879
- Postman M., et al., 2012, *ApJS*, 199, 25
- Remus R.-S., Dolag K., Naab T., Burkert A., Hirschmann M., Hoffmann T. L., Johansson P. H., 2017, *MNRAS*, 464, 3742
- Renzini A., 2006, *ARA&A*, 44, 141
- Rozo E., et al., 2016, *MNRAS*, 461, 1431
- Rykoff E. S., et al., 2014, *ApJ*, 785, 104
- Sánchez H. D., et al., 2019, *Monthly Notices of the Royal Astronomical Society*, 484, 93
- Schmidhuber J., 2015, *Neural Networks*, 61, 85
- Sonnenfeld A., Treu T., Gavazzi R., Suyu S. H., Marshall P. J., Auger M. W., Nipoti C., 2013, *ApJ*, 777, 98
- Sonnenfeld A., et al., 2018, *Publications of the Astronomical Society of Japan*, 70, S29
- Stark D. P., et al., 2013, *MNRAS*, 436, 1040
- Tanaka M., et al., 2016, *ApJ Letters*, 826, L19
- Treu T., 2010, *ARA&A*, 48, 87
- Vegetti S., Koopmans L. V. E., 2009, *MNRAS*, 400
- Vegetti S., Czoske O., Koopmans L. V. E., 2010, *MNRAS*, 407, 225
- Vegetti S., Koopmans L. V. E., Auger M. W., Treu T., Bolton A. S., 2014, *Mon Not R Astron Soc*, 442, 2017
- Vilalta R., 2018, arXiv:1812.10403 [astro-ph]
- Weisskopf M. C., O'dell S. L., van Speybroeck L. P., 1996, in Multilayer and Grazing Incidence X-Ray/EUV Optics III. pp 2–7, doi:10.1117/12.245079
- Wellons S., et al., 2015, *Mon Not R Astron Soc*, 449, 361
- Wong K. C., et al., 2018, *ApJ*, 867, 107
- Zwicky F., 1937, *Phys. Rev.*, 51, 290
- de Jong J. T. A., et al., 2015, *A&A*, 582, A62

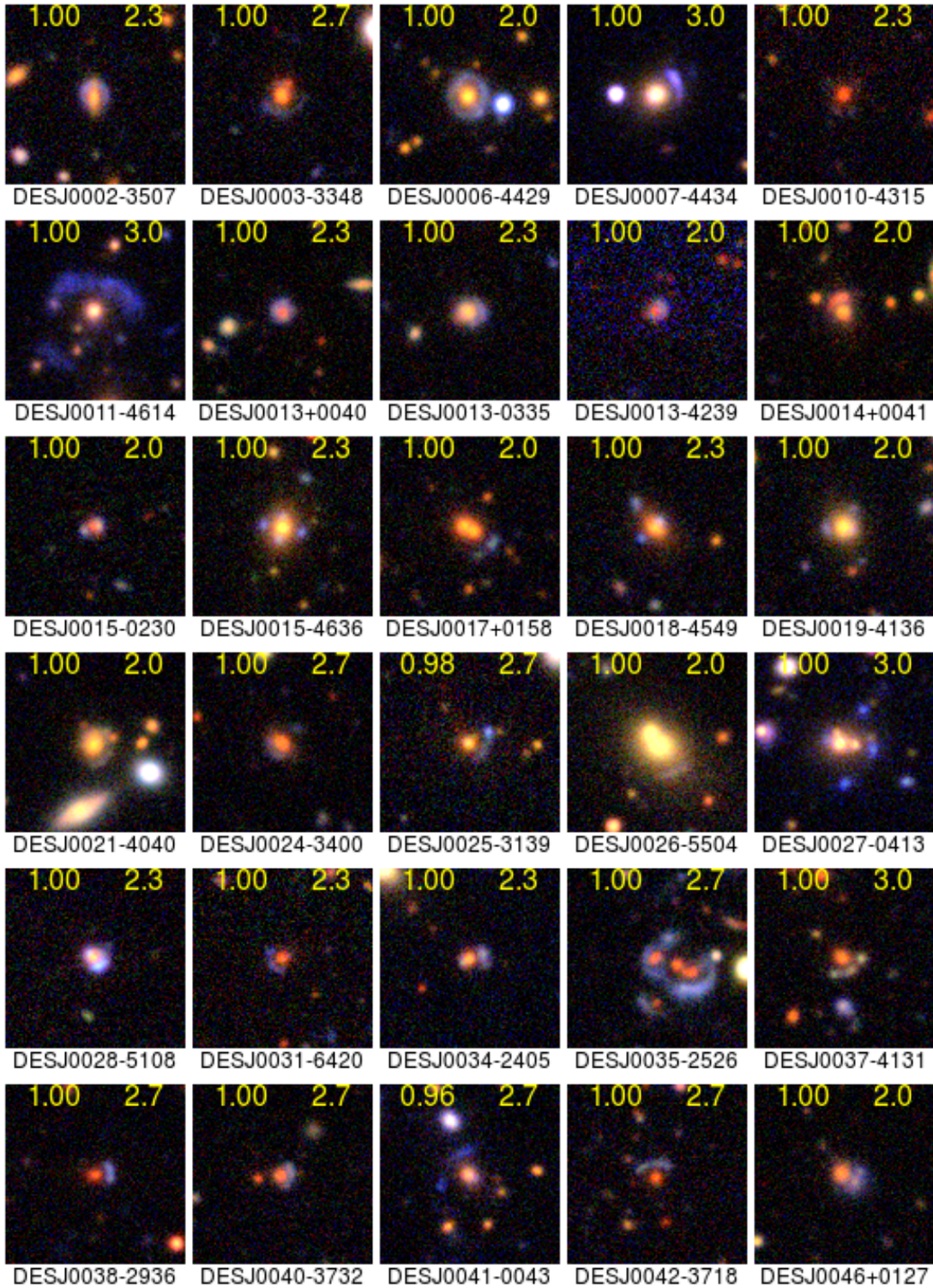


Figure 6. Candidate lenses found in DES using CNNs. In yellow, left: best CNN score, right: human grade.

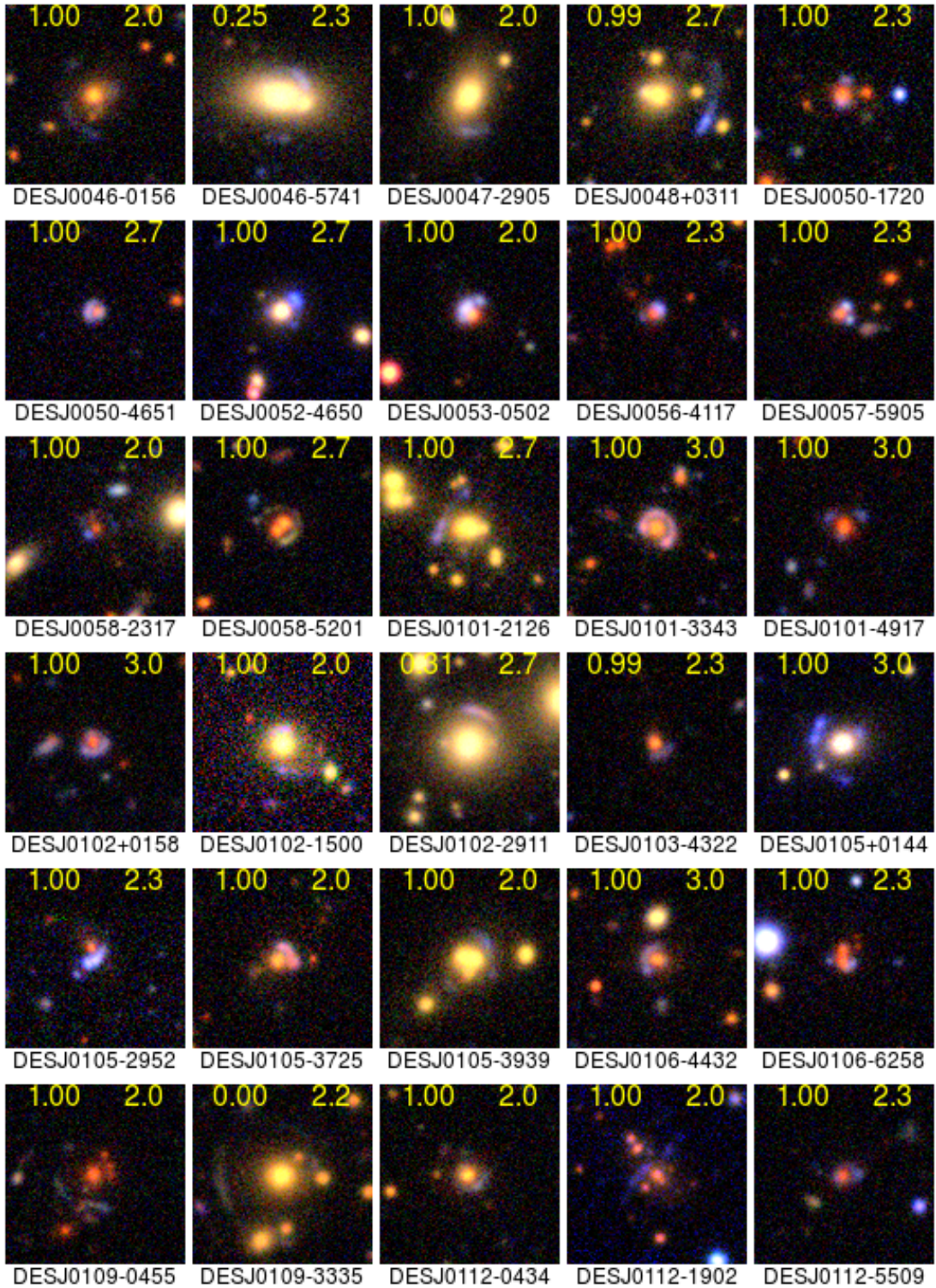


Figure 7. Candidate lenses found in DES using CNNs. In yellow, left: best CNN score, right: human grade.

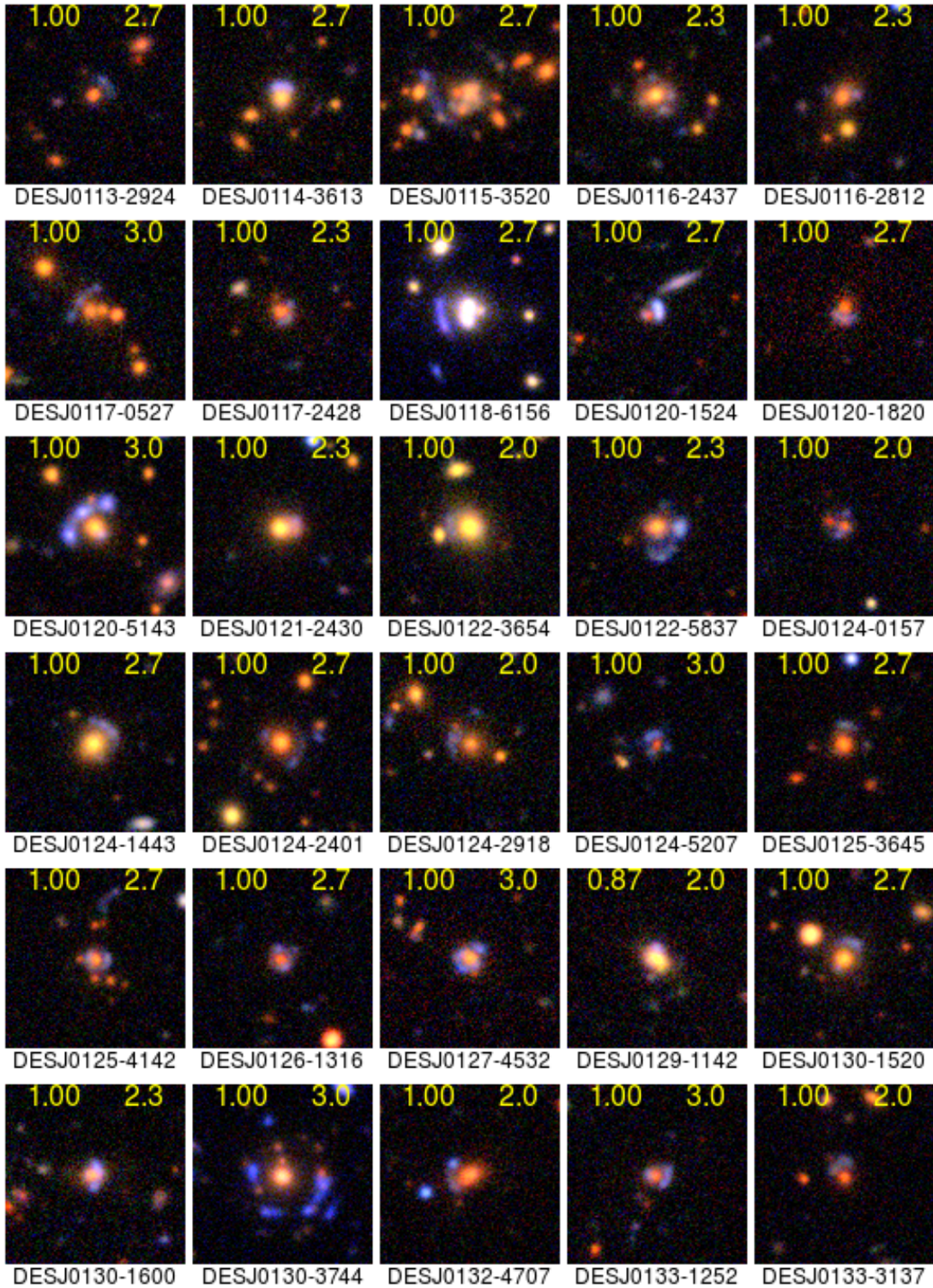


Figure 8. Candidate lenses found in DES using CNNs. In yellow, left: best CNN score, right: human grade.

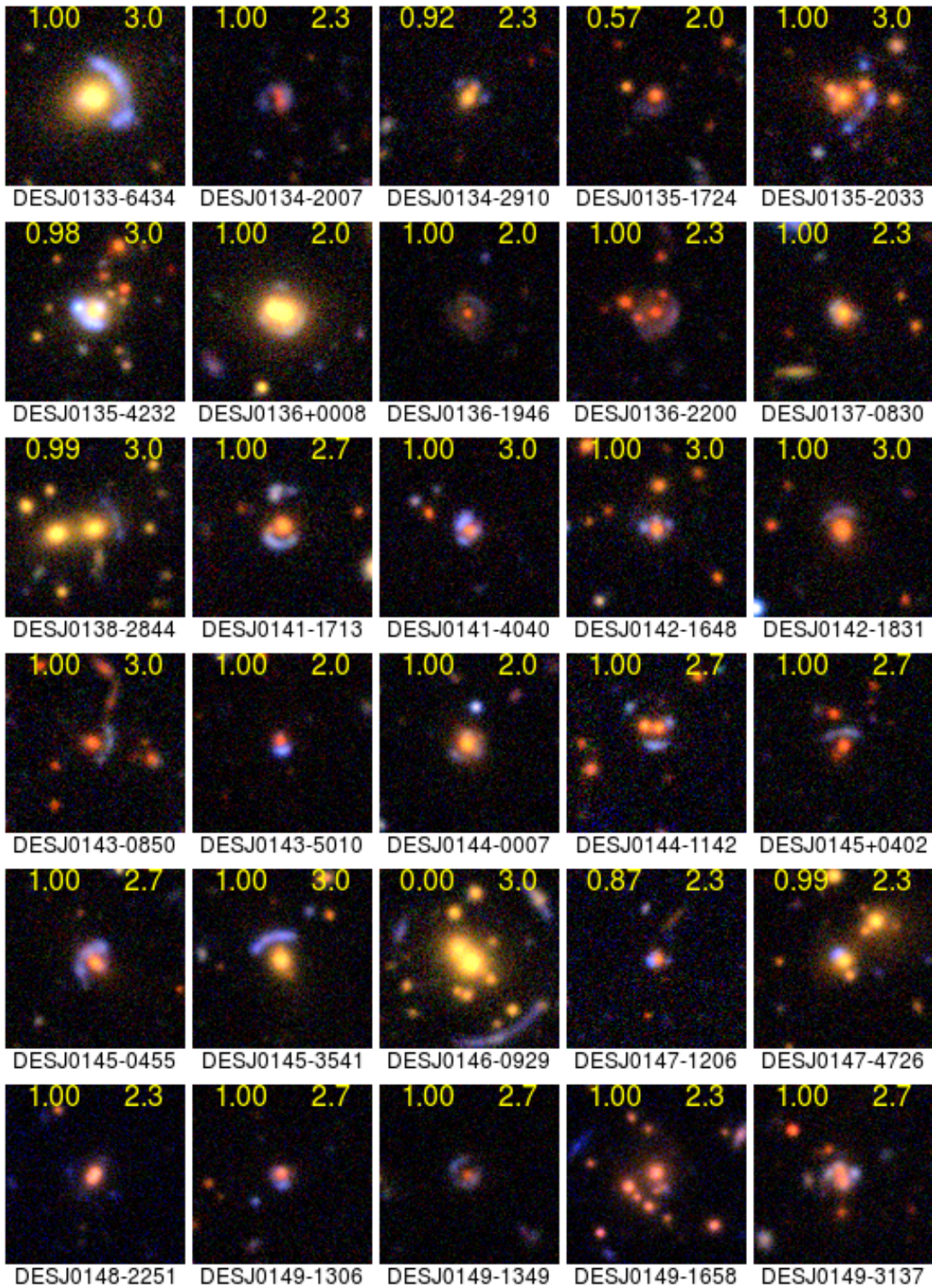


Figure 9. Candidate lenses found in DES using CNNs. In yellow, left: best CNN score, right: human grade.

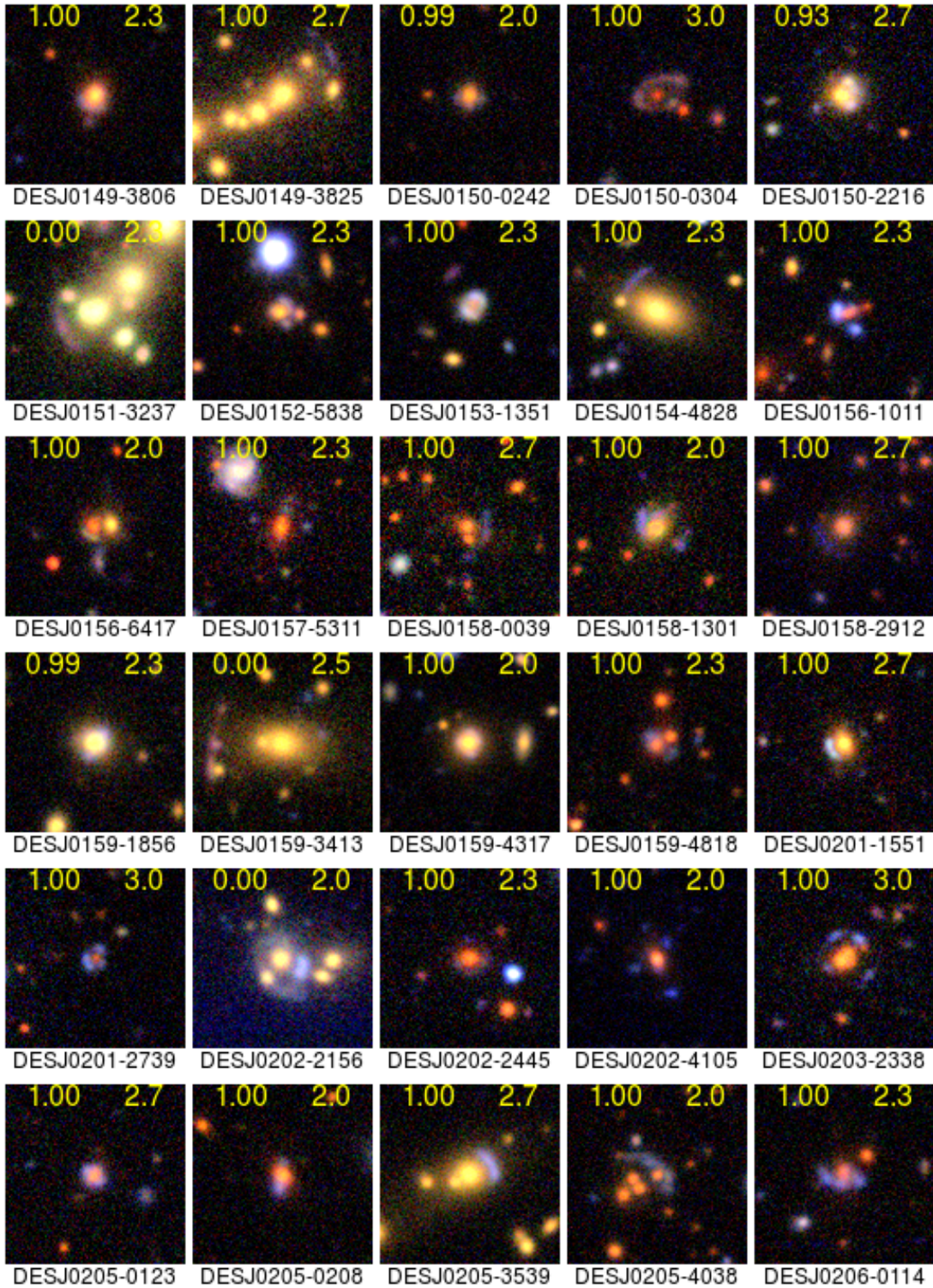


Figure 10. Candidate lenses found in DES using CNNs. In yellow, left: best CNN score, right: human grade.

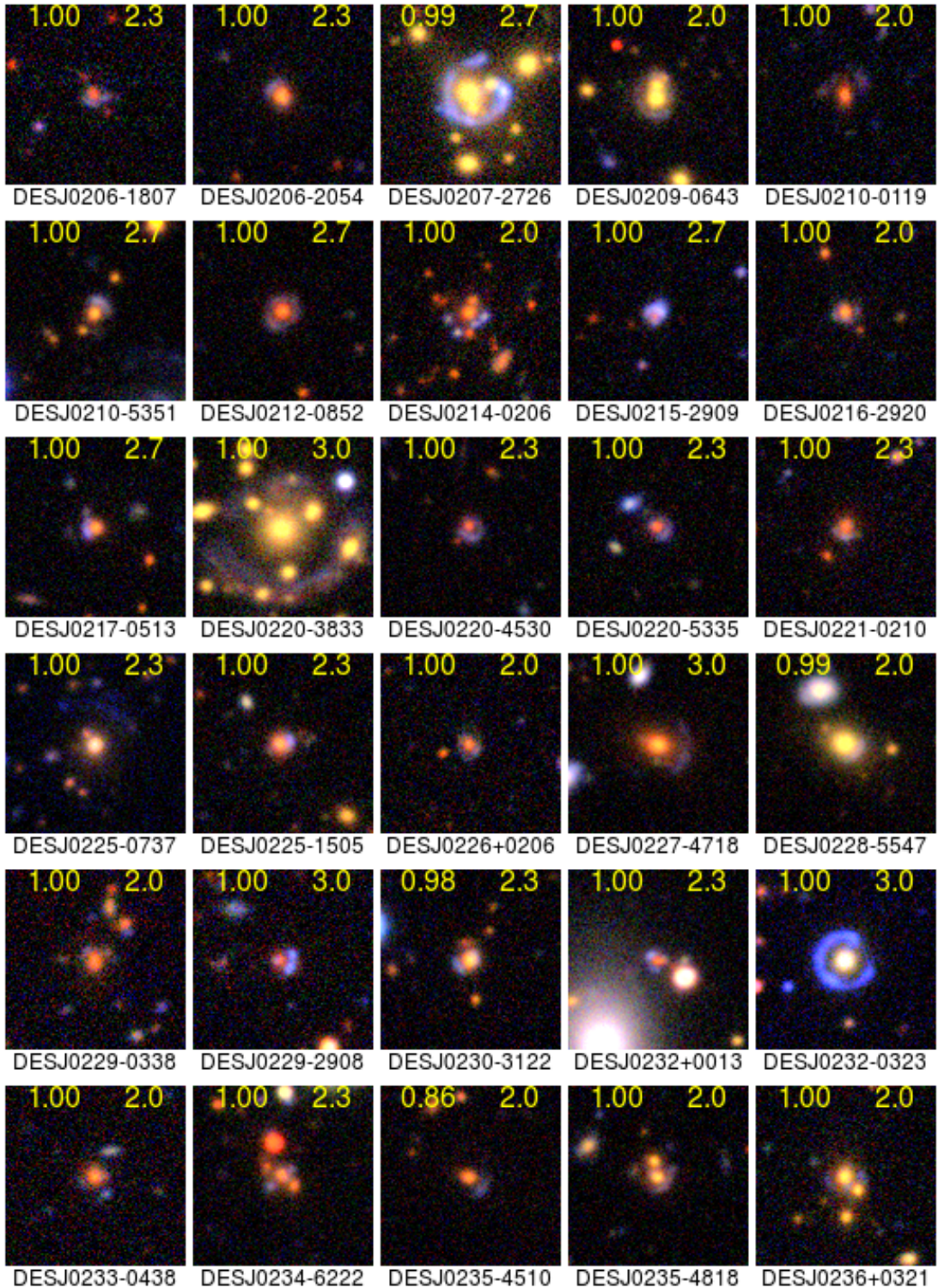


Figure 11. Candidate lenses found in DES using CNNs. In yellow, left: best CNN score, right: human grade.

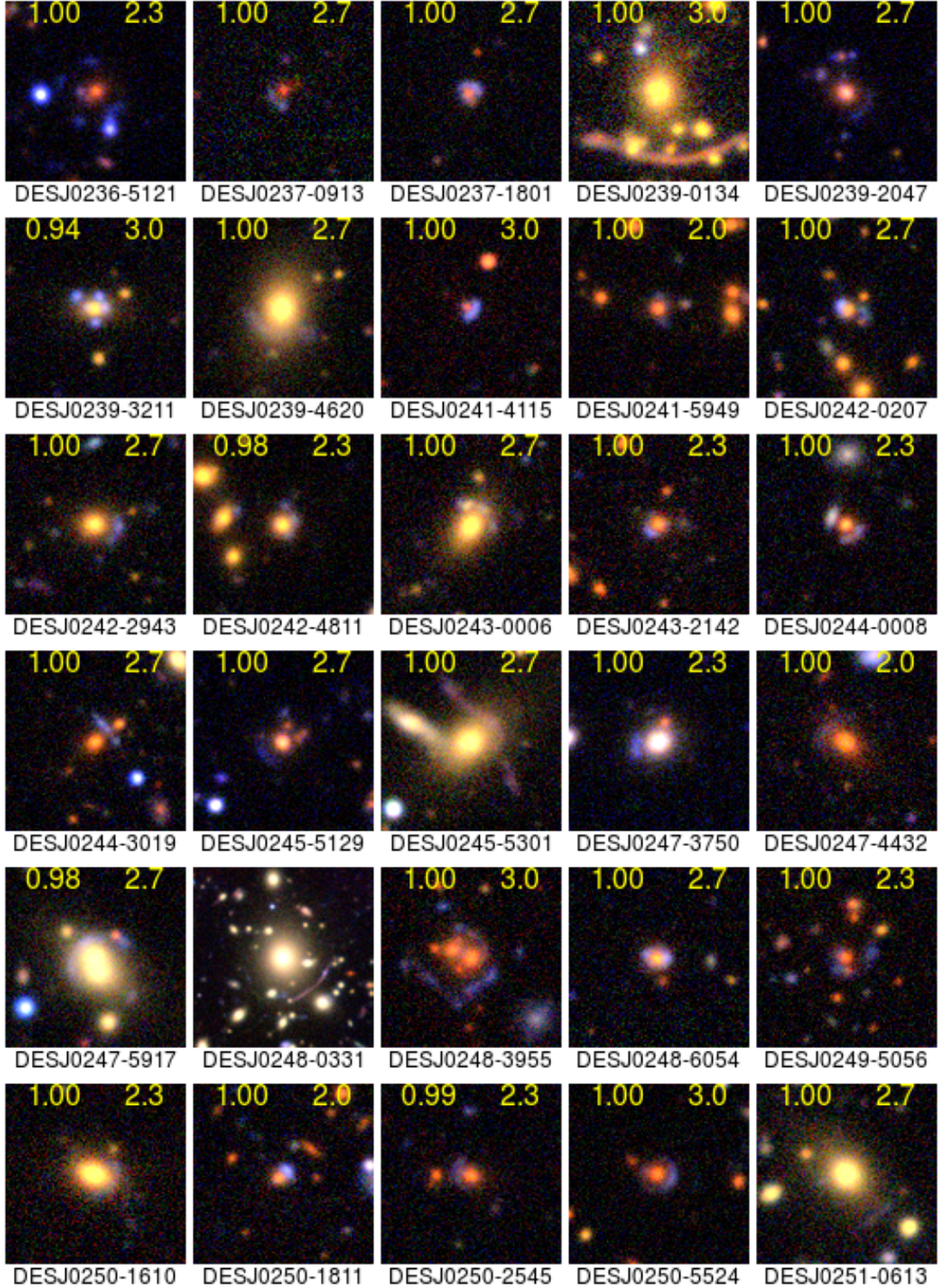


Figure 12. Candidate lenses found in DES using CNNs. In yellow, left: best CNN score, right: human grade.

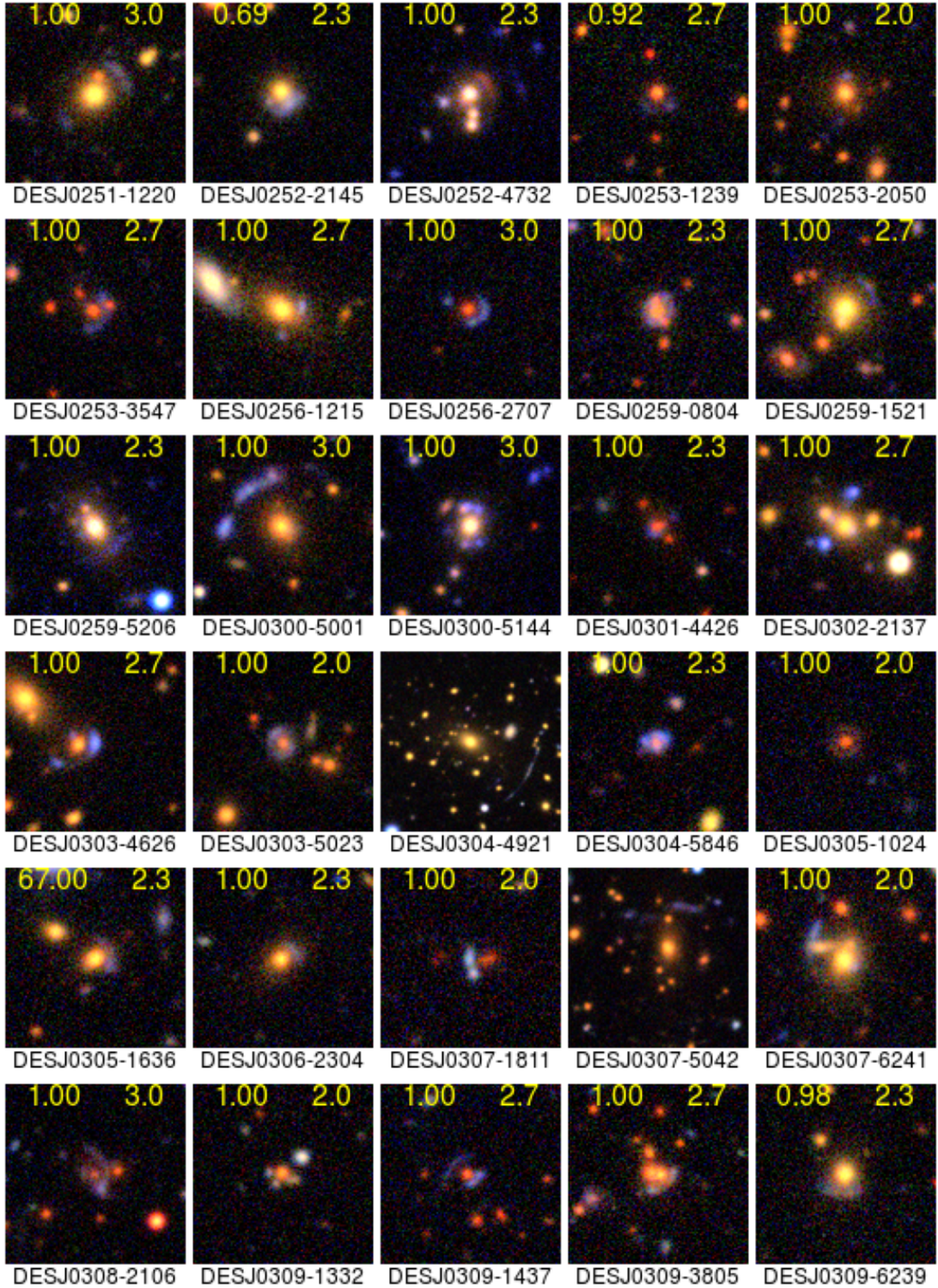


Figure 13. Candidate lenses found in DES using CNNs. In yellow, left: best CNN score, right: human grade.

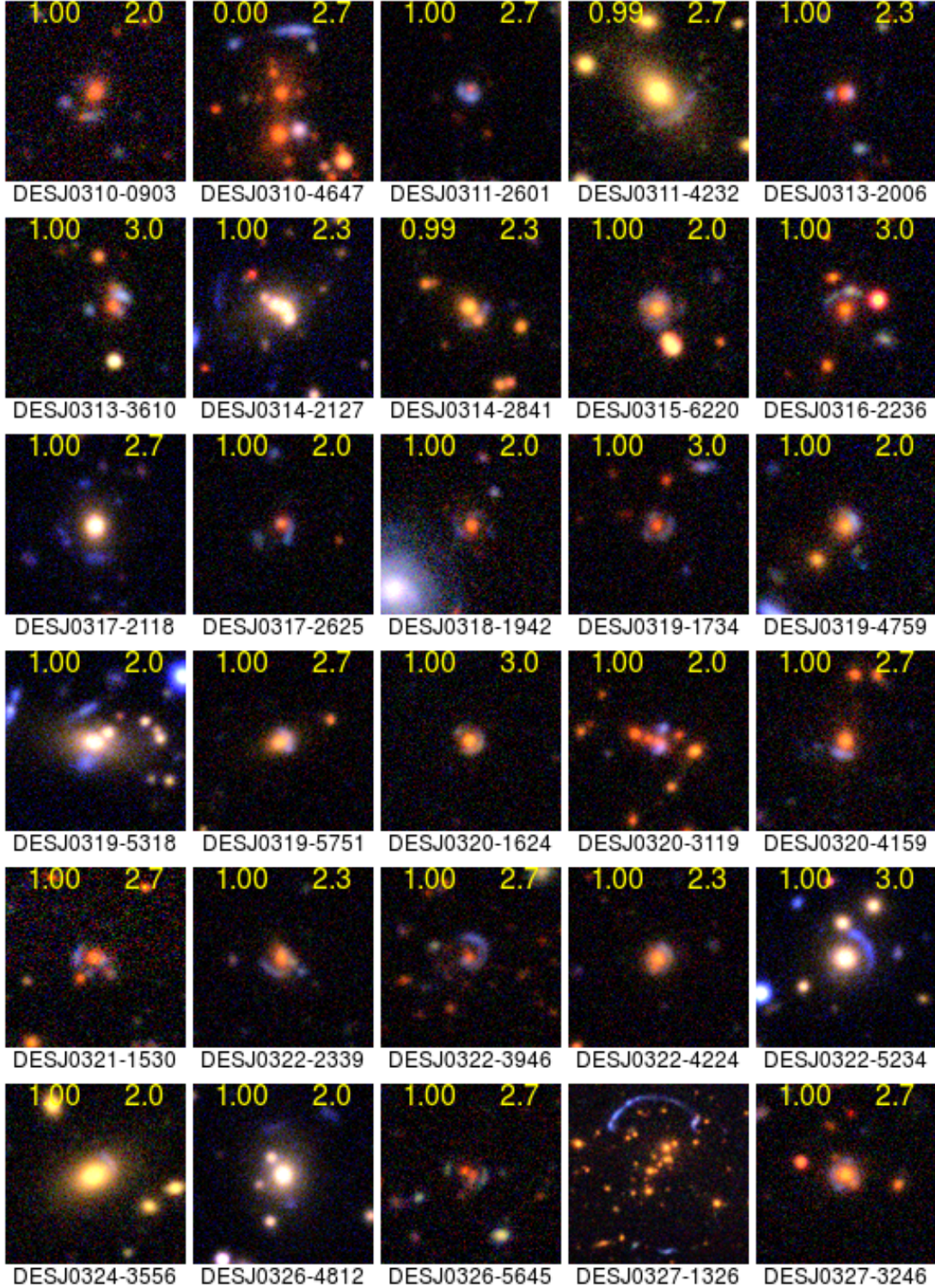


Figure 14. Candidate lenses found in DES using CNNs. In yellow, left: best CNN score, right: human grade.

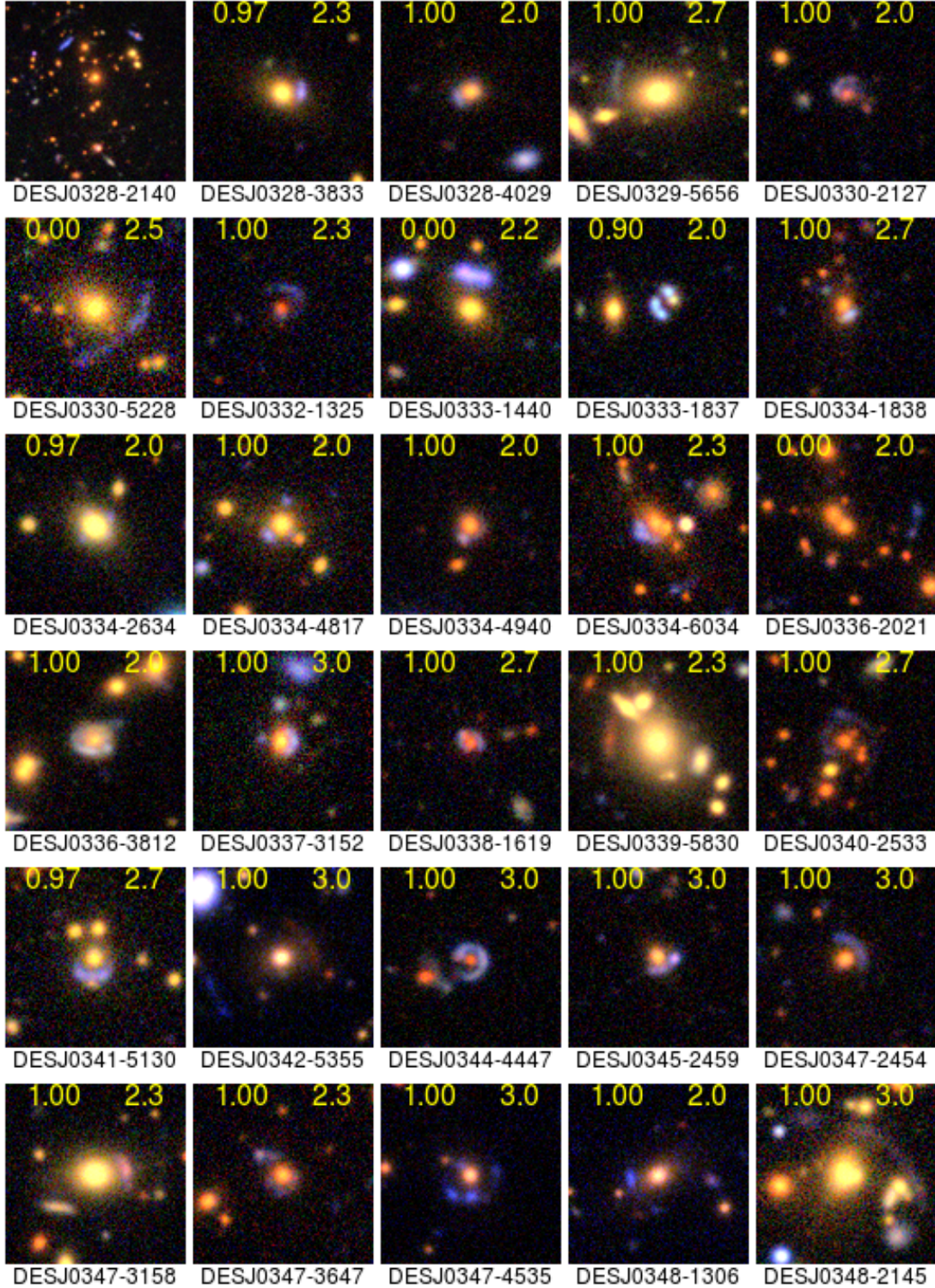


Figure 15. Candidate lenses found in DES using CNNs. In yellow, left: best CNN score, right: human grade.

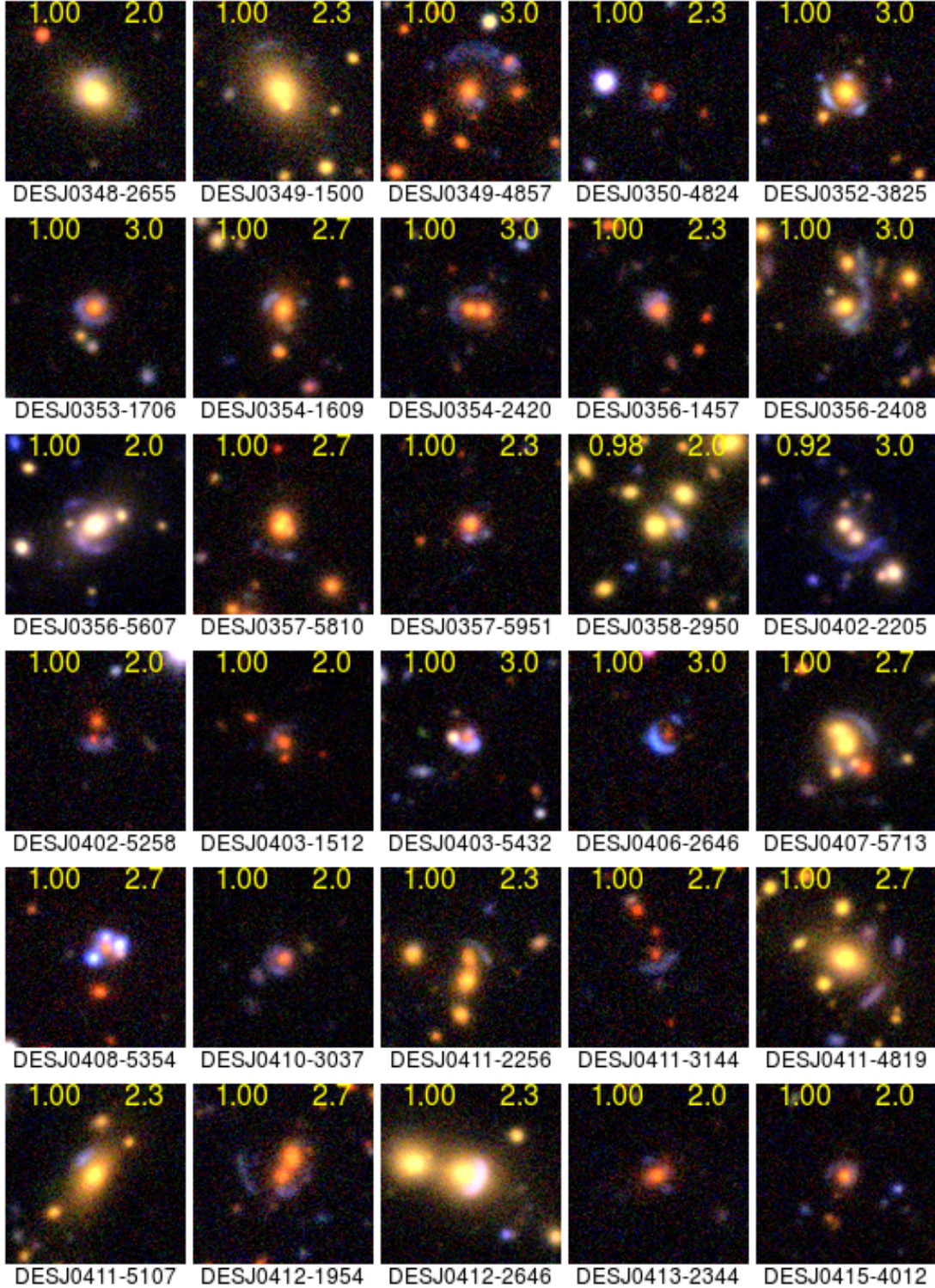


Figure 16. Candidate lenses found in DES using CNNs. In yellow, left: best CNN score, right: human grade.

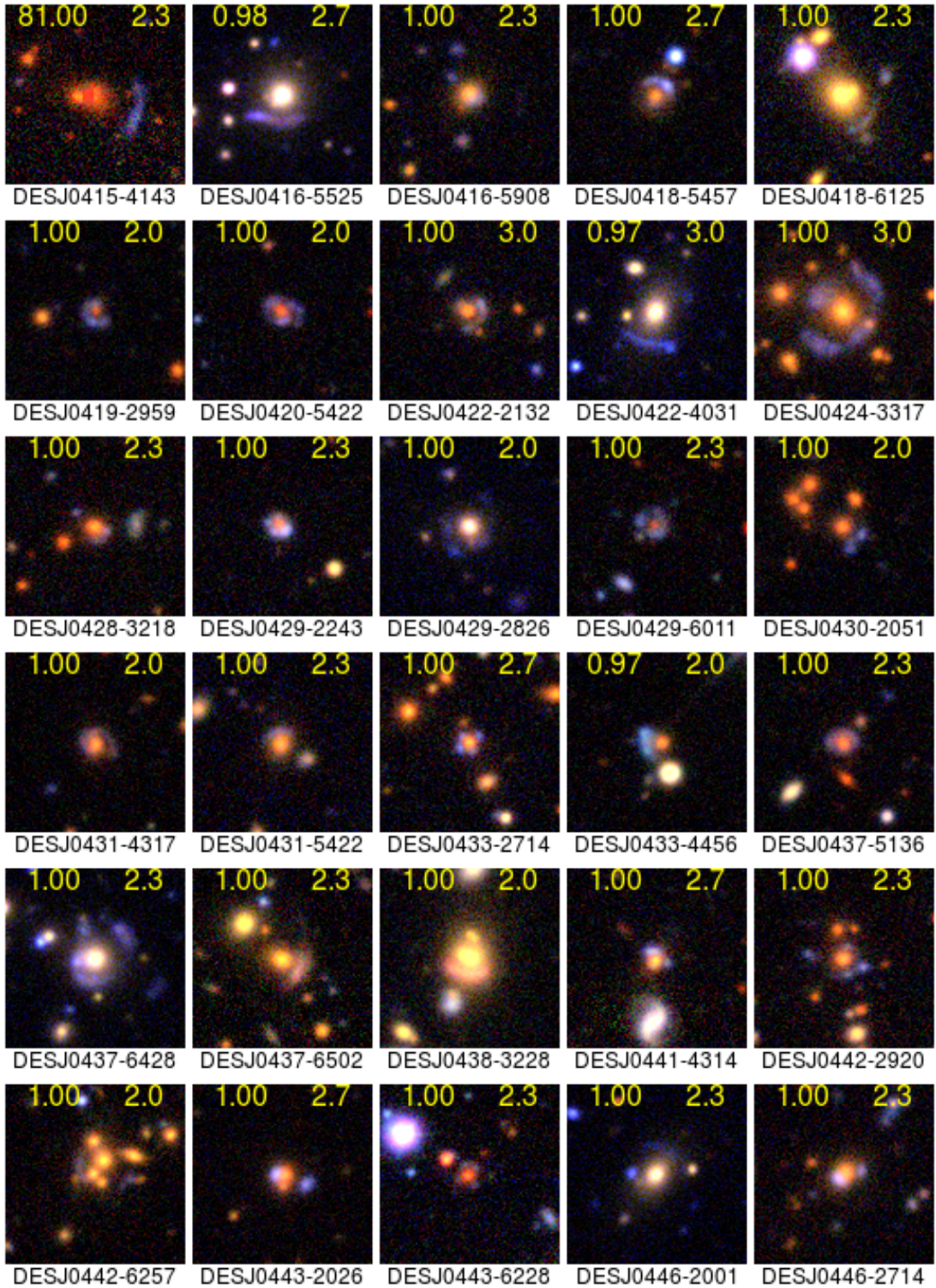


Figure 17. Candidate lenses found in DES using CNNs. In yellow, left: best CNN score, right: human grade.

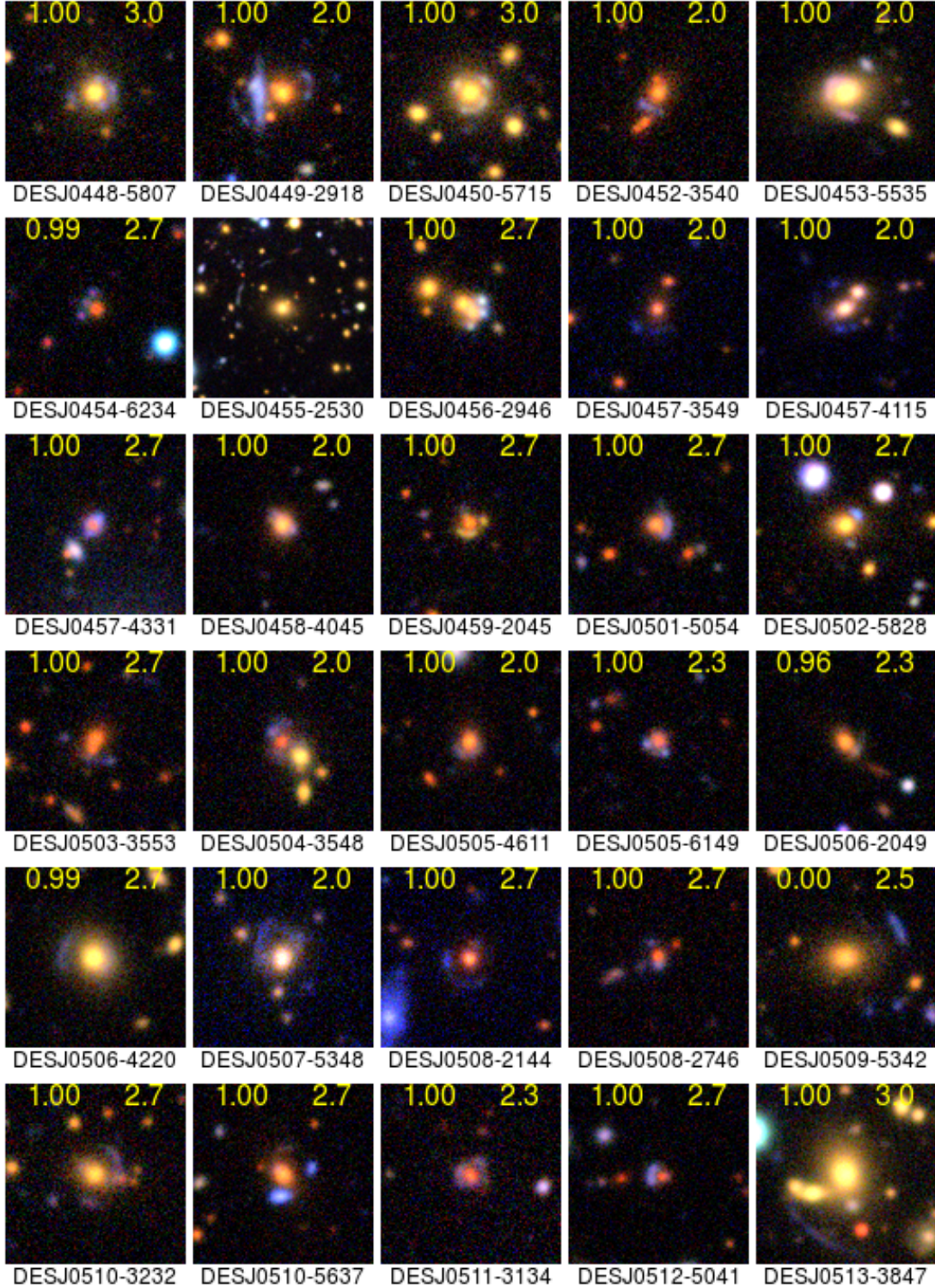


Figure 18. Candidate lenses found in DES using CNNs. In yellow, left: best CNN score, right: human grade.

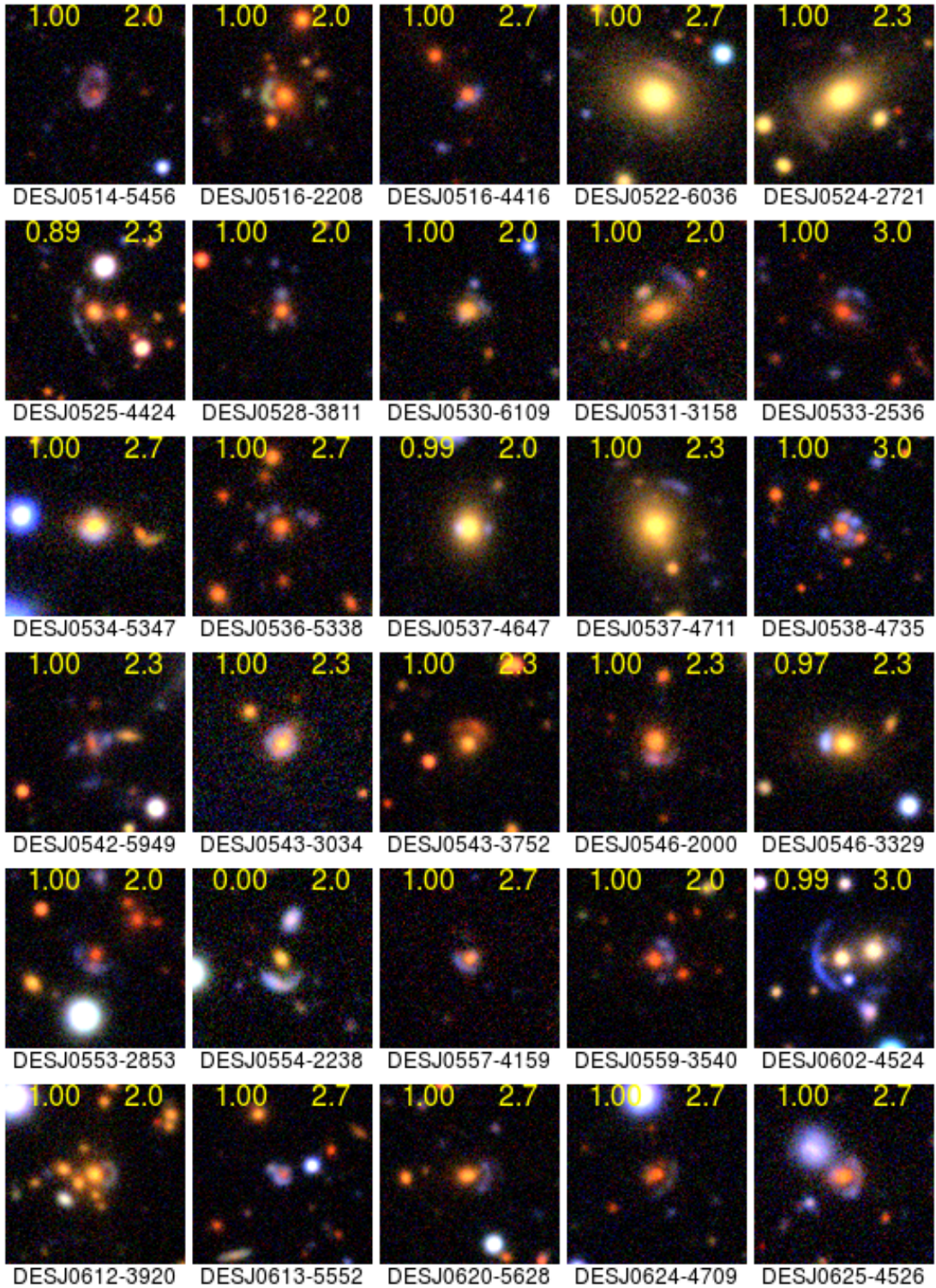


Figure 19. Candidate lenses found in DES using CNNs. In yellow, left: best CNN score, right: human grade.

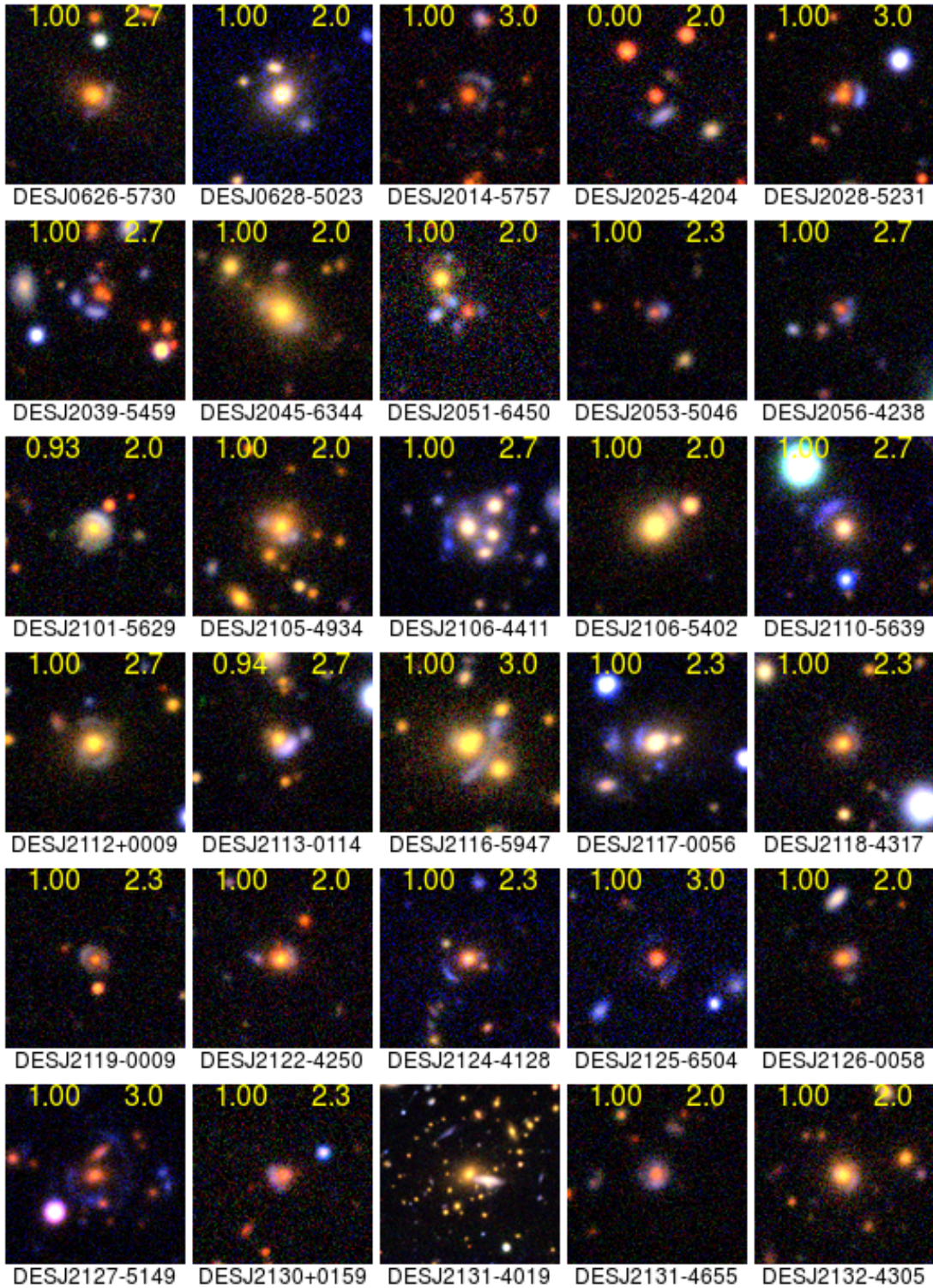


Figure 20. Candidate lenses found in DES using CNNs. In yellow, left: best CNN score, right: human grade.

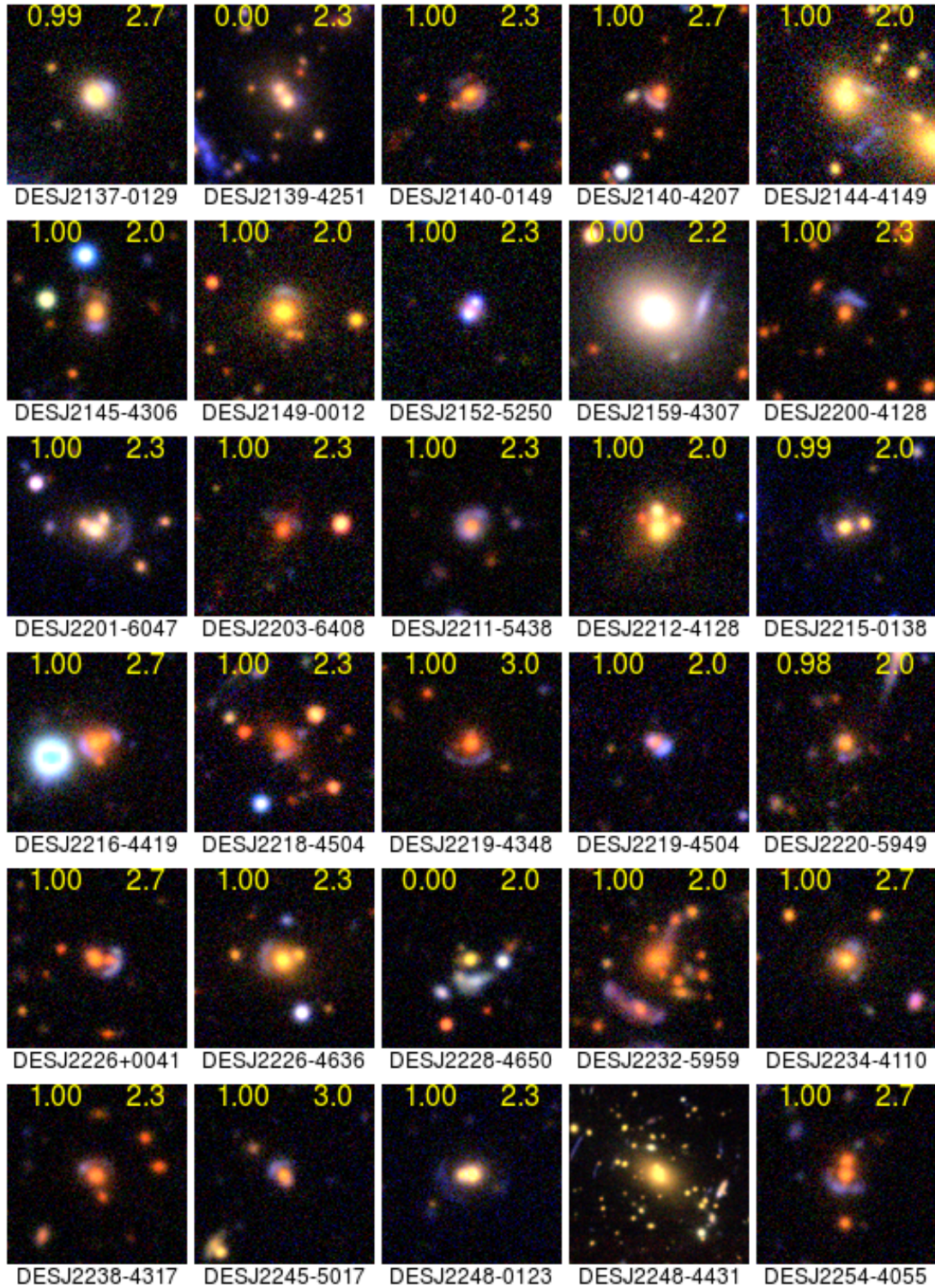


Figure 21. Candidate lenses found in DES using CNNs. In yellow, left: best CNN score, right: human grade.

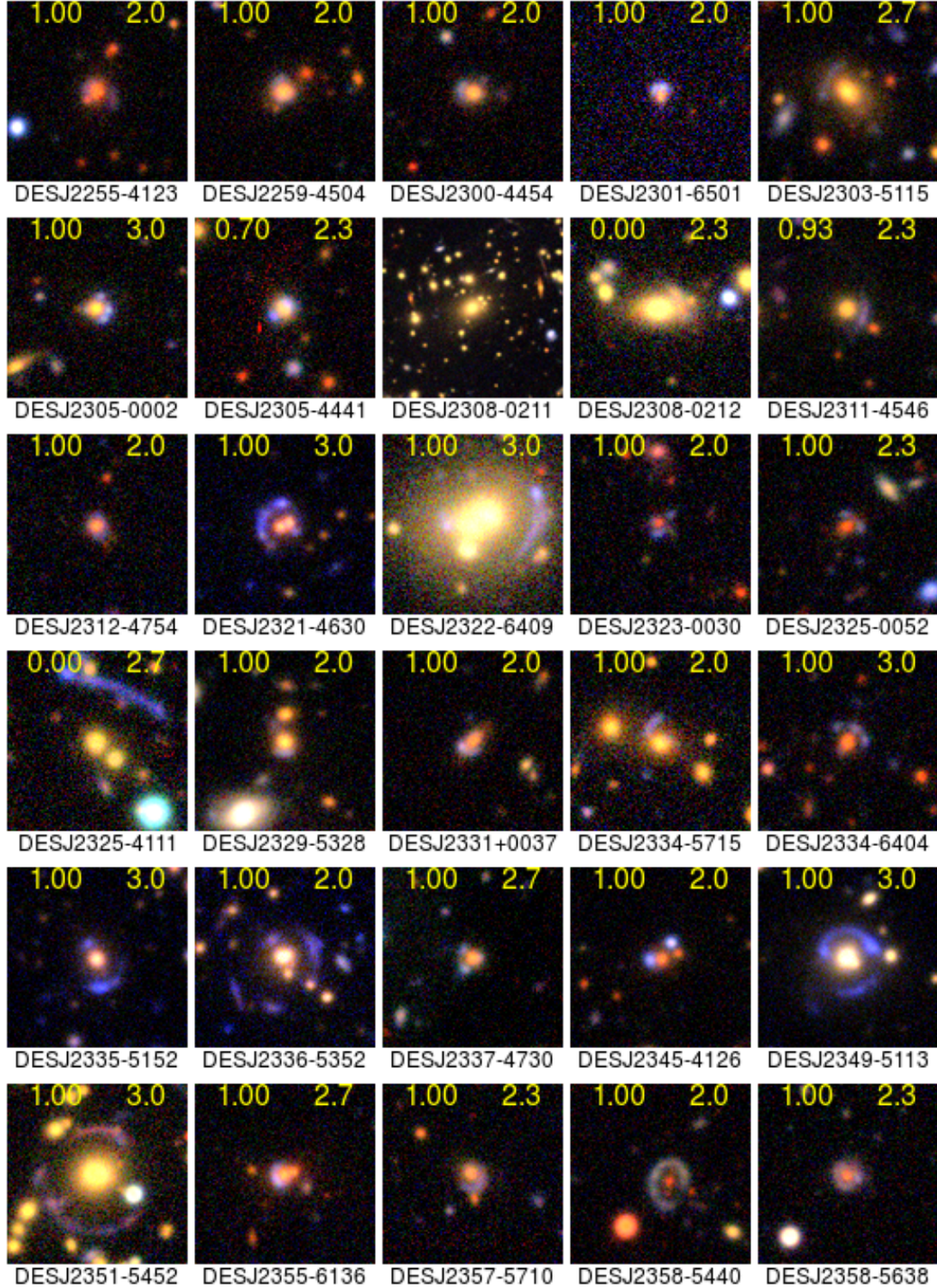


Figure 22. Candidate lenses found in DES using CNNs. In yellow, left: best CNN score, right: human grade.

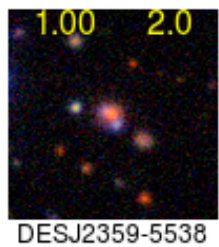


Figure 23. Candidate lenses found in DES using CNNs. In yellow, left: best CNN score, right: human grade.

APPENDIX

A. KERAS MODEL SUMMARY

Table 4. Output of the Keras model summary for the convolutional neural networks used in this lens search

Layer (type)	Output Shape	Param count
conv2d_13 (Conv2D)	(None, 96, 50, 50)	34944
max_pooling2d_10 (MaxPooling)	(None, 96, 24, 24)	0
conv2d_14 (Conv2D)	(None, 128, 24, 24)	307328
activation_19 (Activation)	(None, 128, 24, 24)	0
max_pooling2d_11 (MaxPooling)	(None, 128, 11, 11)	0
conv2d_15 (Conv2D)	(None, 256, 11, 11)	295168
activation_20 (Activation)	(None, 256, 11, 11)	0
conv2d_16 (Conv2D)	(None, 256, 11, 11)	590080
dropout_13 (Dropout)	(None, 256, 11, 11)	0
activation_21 (Activation)	(None, 256, 11, 11)	0
max_pooling2d_12 (MaxPooling)	(None, 256, 5, 5)	0
dropout_14 (Dropout)	(None, 256, 5, 5)	0
flatten_4 (Flatten)	(None, 6400)	0
dense_10 (Dense)	(None, 1024)	6554624
activation_22 (Activation)	(None, 1024)	0
dropout_15 (Dropout)	(None, 1024)	0
dense_11 (Dense)	(None, 1024)	1049600
activation_23 (Activation)	(None, 1024)	0
dropout_16 (Dropout)	(None, 1024)	0
dense_12 (Dense)	(None, 2)	2050
activation_24 (Activation)	(None, 2)	0
Total params:	8,833,794	
Trainable params:	8,833,794	
Non-trainable params:	0	

B. POSSIBLE STRONG LENS SYSTEMS

Table 5. Possible strong lens systems selected by CNN but with grades $0 < \text{grade} < 2$ indicating possible but not probable or definite lensing. The object ID is the identifier from the DES Y3A1 coadd object tables. Where the source has previously been flagged as a potential lens, this is noted. REFERENCES. ¹ Diehl et al. (2017), ² Petrillo et al. (2019), ³ Sonnenfeld et al. (2018), ⁴ Wong et al. (2018), ⁵ Sonnenfeld et al. (2013)

Object ID	RA	dec	notes
140003287	00 02 29.66	-52 29 19.90	
141268015	00 02 41.13	02 48 52.85	
142078524	00 03 38.47	-51 55 57.40	
142345819	00 04 28.14	-38 44 08.95	
182976851	00 06 10.34	-55 07 50.09	
182217410	00 06 25.41	-54 24 33.77	
182434686	00 08 35.18	-39 22 38.50	
182361791	00 09 47.88	-05 08 13.06	
182355539	00 09 53.66	-05 01 45.98	
180834563	00 12 05.46	-44 18 19.22	
143408267	00 13 30.65	-41 43 45.98	
143395314	00 15 16.14	-41 25 05.59	
192142855	00 15 54.63	-63 46 17.44	
192586066	00 16 26.21	-32 19 18.80	
142860768	00 16 51.66	-58 16 59.09	
188316185	00 18 47.89	04 36 28.58	
193187322	00 18 50.10	-30 37 59.99	
144318406	00 20 14.09	-26 16 18.84	
204041543	00 21 07.66	-49 34 51.35	
195632952	00 21 45.10	-46 21 02.48	
145359348	00 21 47.71	-04 58 23.02	
199806464	00 22 28.47	01 48 13.39	
196056924	00 22 31.20	-37 43 26.65	
200213917	00 22 55.29	-52 48 45.79	
196803706	00 22 55.97	-07 11 47.58	
282274727	00 23 26.20	-26 07 14.34	
198375031	00 23 42.53	-35 05 35.23	
202638525	00 24 09.40	-57 53 44.20	
145335798	00 24 47.19	-35 22 22.08	
146057194	00 24 58.32	-52 00 53.28	
201752581	00 25 23.04	-59 13 35.94	
203670392	00 25 59.71	03 28 33.13	
145678597	00 26 08.04	-27 41 36.46	
147394180	00 29 05.71	-33 01 23.48	
146792850	00 30 23.76	-23 41 31.20	
207264051	00 30 24.41	-04 26 52.26	
208835379	00 30 31.31	01 04 08.90	
212525588	00 30 50.60	-57 39 21.67	
145655334	00 31 01.23	-24 24 04.05	
208833887	00 31 15.37	01 03 55.44	
283274153	00 31 30.59	-39 29 55.25	
148390219	00 32 45.59	-54 16 44.94	

Table 5 continued

Table 5 (*continued*)

Object ID	RA	dec	notes
148780306	00 33 40.64	-46 33 08.03	
158227143	00 35 07.26	-35 25 19.99	
151130615	00 36 58.16	-51 12 31.14	
157735050	00 37 35.65	-59 04 13.22	
155609778	00 38 22.36	-25 50 32.07	
157163634	00 39 34.35	-39 27 47.38	
156544537	00 39 35.16	-52 44 37.64	
275297383	00 41 20.35	-62 13 04.19	
158340414	00 41 28.78	-39 35 02.26	
272271734	00 43 23.55	-38 12 58.68	
374259179	00 45 40.08	-25 20 08.70	
276795676	00 46 46.92	-58 25 25.10	
276362041	00 48 07.22	-18 17 10.21	
278411671	00 49 02.37	-35 48 10.62	
276950318	00 49 17.15	03 40 21.65	
277348367	00 49 36.96	-04 02 36.06	
278752575	00 51 30.78	-31 16 21.58	
278771567	00 51 35.76	-31 39 58.50	
351854338	00 52 09.25	-02 50 05.86	
281292916	00 53 33.61	-24 29 00.02	
281393993	00 54 00.69	-31 45 48.74	
282911553	00 54 33.87	-47 38 33.50	
281942609	00 54 44.70	-44 34 21.76	
281225347	00 55 14.16	-17 25 21.40	
282247069	00 55 20.15	-33 06 38.70	
283282583	00 56 05.90	-22 30 44.55	
284793807	00 56 25.71	-34 13 21.18	
286928697	00 57 22.08	-50 54 40.10	
286351501	00 57 22.52	-25 10 52.00	
283565866	00 57 33.23	-20 04 02.71	
282948823	00 57 57.66	01 32 50.64	
288288377	00 58 23.46	-41 01 07.72	
286737669	00 58 46.08	-22 35 09.10	
284398456	00 59 37.58	01 07 31.87	
288316801	00 59 50.50	-45 46 31.66	
290092556	01 01 27.67	-39 40 49.73	
288835913	01 01 30.70	-32 35 40.52	2
290111540	01 01 49.04	-40 04 03.29	
287745384	01 02 01.11	-61 23 04.38	
290469958	01 02 26.08	-24 57 44.57	
289951075	01 02 39.03	02 07 10.56	
293663539	01 03 51.90	-62 59 31.42	
291115723	01 04 41.03	-06 55 11.03	
290150173	01 04 47.68	-62 13 41.88	
293873535	01 04 57.46	-44 33 44.50	
294343525	01 04 59.68	-45 36 06.30	1
297475200	01 06 57.90	-15 41 34.12	
295418250	01 07 17.88	-30 15 20.02	
292872058	01 07 28.63	-55 32 48.97	
295239781	01 08 08.78	-22 47 57.16	
296206197	01 08 53.76	-50 17 47.90	
294538922	01 08 56.59	-23 15 11.81	
302694455	01 09 19.18	-55 45 00.76	
294832487	01 09 24.18	-57 50 33.29	

Table 5 continued

Table 5 (*continued*)

Object ID	RA	dec	notes
296922147	01 09 41.57	-26 19 03.68	
295739611	01 09 56.06	-53 50 26.97	
300525303	01 10 17.17	-26 52 06.25	
305053805	01 10 20.15	-59 22 03.76	
303259810	01 10 58.92	-56 18 09.36	
297541013	01 11 40.26	-04 56 57.08	
303157065	01 13 23.79	-35 18 18.79	
302447685	01 13 33.48	03 30 29.92	
304444921	01 13 38.56	-36 52 26.94	
299339305	01 14 01.08	-43 19 22.66	
305269879	01 14 07.26	-50 19 29.71	
352670072	01 17 08.77	-64 29 50.21	
355978757	01 17 09.87	-60 36 46.26	
304827407	01 17 31.46	-42 56 26.84	
354026053	01 17 42.46	-31 27 32.26	
353861298	01 18 10.25	-41 29 07.04	
355553922	01 19 35.22	-45 52 36.84	
218924751	01 20 32.40	-53 21 47.70	
353212496	01 21 04.95	-19 13 44.83	
357416437	01 21 06.28	-55 58 02.60	
221897791	01 22 15.18	-44 42 58.68	
217277819	01 22 46.52	-24 20 14.93	
219522076	01 23 20.45	-52 01 10.24	
221168892	01 23 45.54	-05 03 41.58	
222469495	01 24 14.04	-40 12 18.97	
220442763	01 24 19.31	-30 30 28.19	
224614142	01 24 32.23	-41 12 17.64	
224091535	01 24 45.46	-35 41 37.39	
221830512	01 26 41.83	-16 21 24.98	
226586041	01 26 52.43	-42 37 19.81	
219948218	01 27 31.97	-04 10 19.88	
225782129	01 28 34.84	-35 57 28.55	
226222518	01 28 37.02	-43 24 57.78	
227289864	01 28 38.65	-47 49 16.86	
223105070	01 29 07.91	-07 05 07.62	
228632469	01 29 51.84	-44 59 22.16	
228264363	01 30 26.53	-50 57 22.25	
229200952	01 31 07.39	-42 16 57.22	
227165154	01 31 26.86	-46 08 22.92	
229507345	01 32 45.55	-21 35 45.82	
229366536	01 32 49.98	-09 09 18.11	
231099447	01 33 22.00	-31 12 50.94	
267383311	01 33 29.29	-24 15 16.52	
230296790	01 33 42.11	-41 14 13.70	
231031870	01 34 23.95	-13 35 09.60	
232380298	01 34 38.40	-42 01 00.48	
230476510	01 35 05.87	01 19 11.42	
232831191	01 35 50.64	-08 50 34.87	
234088122	01 37 38.14	-37 05 23.21	
251080147	01 40 09.18	-43 47 09.92	
268852306	01 40 18.49	-47 13 03.83	
248793507	01 40 58.25	-15 49 12.54	
264803099	01 41 01.00	-13 03 03.22	
265384441	01 41 42.86	-14 52 29.39	

Table 5 continued

Table 5 (*continued*)

Object ID	RA	dec	notes
250048565	01 42 19.38	-05 28 27.26	
265695396	01 42 21.14	-52 09 48.92	
251275799	01 42 32.44	-13 18 39.53	
251287101	01 43 19.07	-13 30 30.35	
268506121	01 44 10.33	-28 54 24.30	
266210850	01 45 15.50	-14 23 18.96	
255373567	01 46 28.48	-60 37 08.04	
268642620	01 46 59.75	-22 40 55.09	
253600335	01 47 27.57	-28 10 31.76	
253021874	01 48 44.74	-08 47 45.74	
346268558	01 49 09.79	-04 40 10.02	
259136834	01 49 41.75	-44 14 18.38	
252904364	01 49 58.50	-20 52 02.03	
259200348	01 50 20.57	-21 35 45.64	
253428759	01 50 59.39	04 02 05.46	
256578545	01 51 21.00	-11 11 02.76	
258812971	01 52 04.42	-28 15 06.59	
264497461	01 53 03.22	-39 25 39.47	
261330008	01 53 30.13	-30 13 47.93	
256630673	01 53 33.60	-12 30 17.46	
264970534	01 53 54.56	-52 13 49.76	
262634959	01 53 59.51	-14 39 04.32	
263050656	01 54 17.29	-09 15 12.20	
263694516	01 55 28.35	-18 47 14.82	
260575550	01 55 44.06	-10 40 03.87	
65030639	01 57 03.49	-57 02 05.96	
61622068	01 57 33.20	05 15 07.60	
65187463	01 57 36.47	-39 51 09.62	
263292105	01 58 09.63	-41 33 39.17	
63273042	01 58 24.78	-25 09 13.75	
61683771	01 59 39.53	-31 08 54.92	
62648043	01 59 40.75	-24 01 10.85	
63681780	01 59 52.25	-19 31 12.32	
151757966	02 00 06.18	-30 48 01.62	
154129632	02 01 25.57	-42 36 32.22	
67549719	02 01 57.05	-21 27 54.72	
66217682	02 03 02.40	-06 36 08.50	
67739421	02 03 28.74	-06 59 52.45	
66052645	02 03 35.51	-63 22 09.63	
68882106	02 03 43.66	-40 46 18.12	
70449187	02 05 03.13	-11 05 46.56	5
78116056	02 05 05.73	-63 35 43.19	
68310205	02 05 41.78	-27 55 26.98	
68212451	02 05 42.05	-39 09 34.27	
77163505	02 06 36.84	-47 54 40.18	
78661878	02 08 03.08	-43 17 48.08	
81402026	02 08 29.46	-36 29 21.23	
85335019	02 11 09.33	-20 31 12.94	
83679335	02 11 19.41	-16 37 16.57	
83191374	02 11 26.13	-12 05 58.42	
90786519	02 13 09.27	-24 13 45.11	
89321653	02 14 03.11	-13 17 15.32	
93020846	02 14 15.06	-32 11 20.44	
91316604	02 14 35.35	00 04 30.11	

Table 5 continued

Table 5 (*continued*)

Object ID	RA	dec	notes
95402555	02 14 46.19	-36 49 19.06	
92149320	02 15 02.98	-22 41 37.93	
91138484	02 15 07.72	01 33 07.96	
93131225	02 15 09.26	-10 19 03.11	
92473640	02 15 09.54	-14 07 06.49	
153184779	02 15 52.44	-01 58 25.07	
95401317	02 16 53.95	-36 48 01.55	
93053169	02 17 40.24	-43 24 42.59	
102098924	02 17 42.13	-38 25 38.93	
101745197	02 18 03.78	-22 49 16.64	
94821348	02 18 20.08	-06 11 13.42	
104680046	02 18 23.59	-05 39 21.20	
100373905	02 18 34.70	-29 05 41.99	
101848037	02 18 40.23	-24 50 47.47	
104751185	02 18 48.38	00 21 25.60	
102679424	02 19 36.65	-44 19 47.75	
110478808	02 20 25.42	-04 48 16.92	
104019210	02 20 35.92	-32 37 07.03	2
103923619	02 20 45.48	-03 25 59.74	
115775009	02 21 58.76	-22 52 12.68	
109448882	02 22 20.80	-53 29 35.81	
104131647	02 22 27.68	-64 15 25.74	
112977988	02 22 33.10	-08 37 28.45	
111520117	02 22 42.08	-52 46 08.80	
108798307	02 23 00.47	-12 15 09.72	
115856590	02 23 38.55	-56 44 48.41	
115657345	02 24 11.04	-21 03 24.91	
117236225	02 24 16.23	-16 22 36.01	
116830209	02 24 56.01	01 27 07.34	
118284892	02 25 14.43	-39 18 16.81	
116699210	02 25 20.51	-20 25 29.42	
117472784	02 25 26.92	-04 21 17.75	
115862004	02 25 43.79	-56 51 37.58	
119249588	02 26 13.48	-26 29 12.55	
118076009	02 26 15.43	-32 31 34.67	
118530509	02 26 34.39	-21 22 42.89	
117613513	02 26 42.48	-23 46 48.83	
118085177	02 26 56.87	-32 43 55.67	
119511117	02 27 28.02	-62 59 51.11	
121840528	02 27 28.05	-57 18 11.20	
120653955	02 27 37.49	-10 39 04.83	
118506486	02 27 55.64	-53 02 26.41	
118607998	02 28 05.33	-14 40 11.42	
122209195	02 28 09.06	-12 52 52.14	
119289686	02 28 16.30	-29 23 45.60	
129756123	02 28 35.05	-44 07 37.78	
121098399	02 28 49.53	-01 12 56.52	
121828310	02 28 58.70	-57 11 27.67	
128638470	02 30 09.12	-18 45 40.57	
129822091	02 30 38.13	-01 52 49.04	
132723326	02 32 06.32	-35 29 23.42	
307406088	02 32 43.98	-28 24 37.15	
132450488	02 33 00.44	-33 08 20.08	2
130851287	02 33 28.60	-48 25 18.37	

Table 5 continued

Table 5 (*continued*)

Object ID	RA	dec	notes
131451316	02 33 30.13	-06 51 42.62	
307494523	02 34 01.78	-27 58 59.52	
310921570	02 34 54.70	-30 56 13.56	
307281753	02 34 56.72	03 47 36.53	
357239068	02 36 10.04	-51 05 04.06	
309904926	02 36 12.04	-19 25 08.47	
312747762	02 38 36.40	-13 51 28.98	
314860822	02 39 56.70	-27 07 14.66	
315450643	02 40 09.90	03 09 52.56	
313463058	02 40 23.96	-57 50 38.15	
316302408	02 41 01.50	-04 16 01.31	
316081456	02 42 01.68	-60 50 14.94	
314610666	02 42 05.93	-07 53 43.58	
317642734	02 43 23.81	-20 25 22.05	
316774735	02 44 49.80	-07 47 27.67	
323818232	02 47 41.04	-45 04 13.94	
323827638	02 48 09.84	-45 14 21.70	
321632698	02 48 49.53	-51 53 16.80	
323146667	02 48 57.75	-03 28 39.43	
323852889	02 49 14.43	-34 58 26.08	
324665212	02 50 28.51	-00 17 03.41	
324571256	02 50 29.00	-41 04 18.12	
325467144	02 51 04.52	-29 59 01.18	
334435700	02 51 05.00	-54 15 41.65	
327533167	02 51 05.08	-64 23 50.03	
325742111	02 52 14.69	-45 37 27.01	
331610601	02 53 58.88	-40 49 41.63	
330961586	02 54 48.03	-18 46 47.32	
335150929	02 57 02.79	-58 54 44.96	
338409152	03 00 14.88	-36 33 28.51	
335748575	03 00 52.99	-49 41 49.52	1
336671196	03 01 18.58	-21 40 53.22	
341151043	03 02 43.82	-38 56 13.42	
341540864	03 03 27.70	-34 11 40.41	
340216736	03 03 43.14	-46 48 51.34	
342983513	03 03 48.62	-15 27 13.03	
339077245	03 03 53.12	-51 26 33.90	
337846581	03 04 23.08	-16 34 49.01	
341385820	03 05 17.06	-38 02 15.90	
340244895	03 05 32.11	-47 19 24.13	
343225913	03 05 32.89	-28 22 13.84	
343235186	03 06 42.84	-28 32 18.24	
341072942	03 06 51.40	-62 08 17.09	
342189632	03 07 35.35	-34 44 28.95	
345482692	03 08 18.85	-49 02 53.88	
342675677	03 08 20.41	-10 02 06.04	
337333932	03 10 23.41	-54 59 32.46	
321165449	03 10 45.79	-35 47 54.28	
329253520	03 11 29.70	-37 44 30.41	
335256495	03 11 55.98	-38 41 42.14	
339562789	03 12 00.25	-14 12 22.14	
343880081	03 12 51.98	-44 07 37.09	
346707866	03 13 46.97	-31 31 07.14	
347476891	03 14 17.53	-56 06 49.32	

Table 5 continued

Table 5 (*continued*)

Object ID	RA	dec	notes
347086579	03 14 23.21	-51 21 15.70	
346534444	03 14 40.35	-25 23 13.17	
346517402	03 15 36.03	-26 32 35.92	
383718655	03 15 41.87	-59 23 23.39	
346529251	03 15 54.04	-26 44 39.51	
353492761	03 17 44.21	-22 52 47.71	
349129102	03 18 52.88	-34 20 56.76	2
355408920	03 19 24.00	-44 46 14.74	
352201976	03 19 46.52	-36 05 22.13	
348762861	03 20 06.29	-62 47 55.86	
355571868	03 20 28.14	-29 00 52.85	
351589215	03 21 21.56	-25 54 14.33	
360440131	03 22 40.80	-47 56 37.50	
354988980	03 22 50.22	-31 56 39.05	
352988851	03 22 55.54	-36 18 17.46	
359793341	03 24 00.49	-27 11 29.80	
360264529	03 25 02.34	-13 42 32.69	
360417001	03 25 40.36	-47 31 59.52	
360159895	03 26 13.34	-37 32 16.76	
361413073	03 27 17.10	-17 22 20.64	
364890268	03 27 45.60	-33 12 13.09	
360846867	03 27 59.47	-54 49 17.11	
363436205	03 28 21.98	-26 49 46.38	
364053751	03 28 28.80	-29 18 21.53	
361867694	03 28 50.04	-39 45 29.05	
364069244	03 29 33.65	-29 35 33.58	
430572426	03 30 36.29	-29 49 42.76	
366908608	03 30 36.86	-22 34 37.06	
365301340	03 30 48.55	-36 47 12.70	
367575834	03 32 02.82	-51 36 45.63	
366741209	03 33 48.47	-54 07 32.63	
368036984	03 34 04.35	-43 31 04.84	
368548459	03 34 40.23	-14 15 17.14	
367762586	03 35 20.92	-43 16 14.31	
369828048	03 35 45.40	-54 52 13.98	
368259364	03 36 13.27	-21 36 42.59	
368629802	03 37 42.38	-52 41 02.90	
373803496	03 39 25.91	-39 14 14.92	
371438007	03 40 02.52	-27 18 29.12	
374179387	03 40 41.98	-27 31 25.82	
374052775	03 40 54.94	-39 39 19.87	
376998704	03 41 35.94	-45 11 17.05	
372644331	03 42 33.82	-20 56 03.30	
375742960	03 42 58.14	-28 56 01.03	
378703554	03 45 00.83	-50 43 29.46	
377569602	03 45 47.61	-30 23 35.63	
378339907	03 45 58.72	-36 01 09.84	
379710385	03 46 37.28	-61 58 43.03	1
381738964	03 47 02.99	-65 36 59.94	
379320965	03 47 34.05	-27 25 10.60	
379570511	03 47 51.65	-54 50 39.41	
380892419	03 48 02.76	-28 39 10.84	
383260156	03 50 20.55	-26 36 46.98	
381339793	03 50 45.72	-42 17 53.66	

Table 5 continued

Table 5 (*continued*)

Object ID	RA	dec	notes
384084861	03 51 09.98	-42 35 19.93	
383379136	03 51 23.67	-25 59 13.85	
385510363	03 51 50.25	-22 14 30.59	
383764976	03 53 12.27	-66 49 21.83	
384435644	03 53 25.93	-18 33 48.67	
385911533	03 55 57.81	-34 06 12.24	
421573935	03 56 14.81	-42 51 07.70	
386201548	03 57 04.44	-22 39 59.76	
389206296	03 57 23.00	-42 07 55.34	
488419028	03 59 26.22	-53 56 23.42	
507569548	04 00 27.98	-22 26 42.61	
491271085	04 00 32.96	-55 46 13.66	
480144838	04 01 54.14	-49 59 40.27	
487213709	04 01 57.96	-48 45 01.19	
481908142	04 03 45.38	-40 26 37.50	
490891637	04 03 58.86	-26 02 05.42	
486785476	04 04 57.31	-49 22 21.54	
489531863	04 05 07.41	-44 08 51.71	
484444598	04 05 26.71	-25 40 24.71	
484302675	04 05 54.54	-28 54 00.40	
489186452	04 06 00.04	-55 04 26.36	
489584065	04 06 42.27	-33 06 26.60	
478836945	04 06 45.12	-15 02 53.48	
487375401	04 06 58.45	-30 44 25.94	
487457734	04 07 10.78	-32 07 13.44	
406696446	04 07 19.05	-61 10 14.41	
391106806	04 08 24.24	-20 56 12.45	
390200758	04 08 24.54	-39 56 26.38	
484398980	04 08 36.71	-26 56 56.36	
493679799	04 08 37.59	-39 24 50.83	
489927069	04 09 52.62	-65 10 51.20	1
393008323	04 10 44.87	-15 14 28.36	
401536284	04 13 24.79	-39 07 45.91	
400238380	04 13 32.15	-38 23 40.13	
399651358	04 14 28.04	-19 55 09.19	
401934514	04 14 28.42	-30 21 21.96	
403225250	04 14 54.95	-25 31 24.92	
399795578	04 14 58.93	-24 33 36.86	
402555505	04 15 46.45	-41 42 56.81	
400693969	04 16 12.95	-30 23 21.59	
403385829	04 16 48.67	-45 39 24.52	
405038616	04 18 33.29	-18 17 53.40	
496605641	04 19 02.74	-61 10 51.78	
405227648	04 19 07.93	-48 31 29.93	
401029558	04 19 57.36	-36 11 17.48	
498043683	04 20 15.00	-41 27 04.86	
496455775	04 21 01.64	-21 37 47.78	
413178342	04 21 40.35	-22 55 45.73	
503823880	04 24 51.24	-23 11 45.24	
497364738	04 25 15.75	-28 58 32.56	
470272133	04 27 31.80	-62 25 21.00	
504652711	04 28 03.51	-41 40 13.44	
502611089	04 28 10.27	-31 36 41.62	
502696285	04 28 10.85	-37 56 03.05	

Table 5 continued

Table 5 (*continued*)

Object ID	RA	dec	notes
506596864	04 29 00.21	-34 39 19.48	
507142703	04 29 03.10	-35 04 02.50	
469474840	04 30 44.57	-32 54 29.20	
470184935	04 32 53.97	-60 02 42.26	
470294183	04 33 14.60	-39 14 08.23	
471434596	04 34 17.98	-27 41 51.65	
508859888	04 35 12.59	-49 43 05.12	
472821007	04 35 15.03	-30 20 05.42	
507620996	04 35 33.13	-24 06 10.15	
471805340	04 35 41.83	-17 38 07.55	
473659680	04 36 00.44	-54 16 21.79	
473466587	04 36 32.98	-32 44 08.45	
473673328	04 36 37.30	-54 29 01.36	
474321149	04 37 07.63	-27 47 56.15	
489731693	04 37 09.54	-40 58 53.65	
490904922	04 37 10.67	-35 30 53.71	
474402376	04 38 15.38	-32 20 50.82	
508867520	04 38 50.87	-49 50 11.15	
490963495	04 38 54.38	-37 55 56.24	
491648560	04 39 07.63	-37 23 59.06	
494622114	04 39 29.97	-44 45 18.29	
500132356	04 40 58.85	-58 41 29.50	
491668672	04 41 00.69	-20 29 52.55	
507082094	04 41 47.67	-17 52 33.60	
505987847	04 42 07.60	-51 11 48.44	
504578003	04 43 04.23	-25 53 12.30	
496559159	04 43 25.82	-22 41 49.20	
500151981	04 44 12.59	-18 17 19.39	
503707314	04 44 53.04	-38 08 45.46	
502147040	04 46 34.55	-33 54 08.19	
502220340	04 46 48.82	-18 02 59.93	
483920327	04 47 34.70	-48 48 24.08	
479045859	04 48 02.53	-38 00 42.66	
502832489	04 48 24.20	-30 47 03.80	
505027360	04 48 36.29	-51 42 17.35	
485132805	04 48 52.52	-26 28 41.23	
481077966	04 49 13.11	-49 09 22.36	
485152379	04 49 55.99	-20 35 23.68	
483404421	04 50 21.07	-50 44 37.05	
481424822	04 51 10.80	-42 45 40.43	
481080414	04 51 30.21	-49 11 35.45	
482257515	04 51 43.40	-27 01 29.57	
482230835	04 51 53.57	-51 34 26.87	
480242623	04 52 30.91	-30 32 31.38	
482224238	04 52 47.76	-51 28 08.40	
399567679	04 54 16.50	-54 26 57.52	
493816383	04 55 01.87	-21 33 24.52	
396017579	04 55 05.62	-31 20 17.41	
395552394	04 56 26.62	-45 40 21.66	
396070142	04 57 04.83	-30 54 04.93	
397100948	04 57 08.31	-39 12 33.01	
396450593	04 58 26.24	-57 35 10.50	
400885398	05 00 38.64	-20 42 33.31	
403989879	05 00 55.20	-55 06 35.93	

Table 5 continued

Table 5 (*continued*)

Object ID	RA	dec	notes
395819989	05 01 25.62	-35 06 49.97	
408463311	05 01 58.14	-41 22 25.36	
395309449	05 02 18.29	-34 31 53.40	
395821232	05 02 23.19	-35 08 19.79	
407470599	05 03 16.41	-32 18 14.98	
410202908	05 03 19.96	-50 52 07.93	1
399501708	05 03 23.99	-46 12 05.72	
410085910	05 05 36.50	-27 38 28.54	
409482878	05 05 43.14	-18 30 38.12	
412752697	05 05 59.80	-30 39 17.46	
411499613	05 06 08.23	-51 59 54.49	
408582562	05 06 10.81	-31 19 43.25	
411431005	05 06 21.55	-48 17 55.54	
409918195	05 06 48.04	-25 03 58.14	
412200919	05 08 48.23	-40 48 52.52	
415443482	05 09 13.48	-35 43 40.15	
414168984	05 09 22.32	-54 27 10.37	
414348928	05 10 34.22	-23 17 56.08	
416958851	05 10 37.10	-44 57 24.73	
417324459	05 10 52.74	-36 36 26.04	
417854232	05 12 11.65	-51 11 34.12	
475508622	05 12 17.32	-37 40 30.14	
417459368	05 12 21.91	-55 43 25.03	
415746581	05 13 40.85	-28 14 06.47	
415177510	05 14 01.76	-57 23 45.06	
414751311	05 15 01.99	-57 49 49.98	
413967636	05 15 31.98	-35 34 50.63	
417408051	05 15 39.50	-41 42 15.95	
417616996	05 15 40.01	-33 24 07.24	
422562485	05 15 56.36	-58 26 32.82	
421105667	05 17 26.05	-39 59 26.84	
426691837	05 17 58.46	-33 10 34.90	
422759428	05 18 14.21	-22 51 33.26	
425857481	05 21 09.50	-52 52 27.96	
428264305	05 21 41.35	-29 59 37.97	
428916065	05 22 41.63	-43 47 15.25	
426787605	05 23 07.78	-32 44 18.24	
477772243	05 24 15.51	-61 31 07.39	
432381861	05 24 38.94	-25 22 26.80	
434191129	05 25 00.24	-26 16 40.65	
434674136	05 25 39.89	-19 18 37.22	
433418293	05 26 54.98	-25 05 31.88	
430780458	05 27 57.08	-18 10 05.12	
431943993	05 28 25.73	-51 09 37.22	
433904268	05 31 03.62	-52 21 21.78	
434395146	05 31 08.75	-59 01 24.17	
430881293	05 31 52.92	-18 03 00.68	
435655992	05 33 42.59	-37 44 32.35	
434516995	05 33 43.80	-28 18 35.92	
439483857	05 33 47.75	-22 15 56.70	
439704154	05 34 41.88	-38 18 51.37	
477630009	05 34 43.31	-54 46 22.08	1
434812274	05 34 50.43	-36 53 25.94	
477637342	05 34 52.05	-54 53 13.63	

Table 5 continued

Table 5 (*continued*)

Object ID	RA	dec	notes
441369380	05 35 00.20	-53 20 18.27	
438811319	05 35 19.20	-39 53 08.30	
439355396	05 35 22.91	-26 42 41.69	
440079366	05 35 45.98	-27 00 31.82	
440797367	05 36 17.83	-59 39 33.52	
443408206	05 37 28.21	-61 04 10.52	
477630222	05 37 40.58	-54 46 28.48	
441394915	05 38 15.23	-53 45 55.48	
442175861	05 38 38.47	-43 48 40.90	
441714547	05 39 15.02	-36 48 58.64	
444402602	05 39 26.02	-43 41 54.61	
445370749	05 40 16.66	-58 15 55.69	
441721427	05 41 12.30	-36 55 46.54	
446334014	05 41 27.10	-58 47 50.96	
441893575	05 42 17.99	-21 49 18.34	
446482433	05 42 49.14	-59 40 24.78	
446307824	05 43 04.01	-58 25 10.68	
446893996	05 43 42.66	-27 44 20.62	
446306406	05 44 27.41	-58 23 57.88	
447681916	05 45 04.15	-34 53 00.53	
445843787	05 45 15.56	-23 45 39.35	
444886603	05 45 23.76	-28 18 08.35	
446394573	05 46 17.80	-37 34 07.86	
449145933	05 46 24.29	-47 39 45.51	
454268545	05 50 39.36	-37 53 50.71	
452653199	05 51 06.29	-38 33 51.16	
454906407	05 51 53.83	-30 24 08.42	
459986855	05 53 48.17	-30 48 00.58	
465270006	05 54 06.74	-60 46 13.30	
449330410	05 56 38.37	-26 24 58.46	
450317573	05 57 29.21	-29 13 10.42	
450621903	05 57 44.62	-55 32 15.97	
449061667	05 58 25.72	-44 06 27.61	
449941872	05 58 27.92	-27 02 18.60	
450094954	05 58 33.85	-28 44 30.41	
451489421	05 59 08.33	-53 40 57.47	
452952414	06 00 25.77	-38 48 18.17	
459178468	06 03 51.70	-40 54 45.02	
455978070	06 03 56.50	-35 58 05.74	
455978863	06 03 58.76	-35 58 34.54	
456728016	06 04 31.95	-60 33 18.46	
459643327	06 06 28.78	-55 33 32.62	
457303869	06 06 30.53	-45 07 49.37	
456924183	06 07 30.72	-51 45 40.64	
455502718	06 07 48.10	-34 17 05.82	
460509633	06 09 34.12	-59 26 24.58	1
459743065	06 09 46.80	-51 12 45.94	
459003042	06 10 19.67	-36 46 50.09	
461495174	06 10 22.62	-45 25 54.73	
459007040	06 10 37.46	-36 51 41.62	
461781308	06 11 17.40	-48 56 03.16	
461471326	06 11 20.49	-47 58 42.38	
461500268	06 11 23.34	-37 41 32.17	
461663300	06 11 59.75	-46 01 01.49	

Table 5 continued

Table 5 (*continued*)

Object ID	RA	dec	notes
459221892	06 13 16.98	-53 46 55.78	
464432181	06 13 25.78	-45 09 09.97	
463101581	06 16 04.31	-57 11 16.84	
465306982	06 16 25.74	-51 12 49.00	
464569729	06 16 30.60	-56 24 28.84	
465182915	06 17 24.81	-60 01 14.92	
464681328	06 17 33.77	-40 33 32.38	
465773416	06 19 52.26	-55 15 21.67	
465321303	06 20 36.22	-51 27 59.26	
163109841	20 16 25.94	-63 26 12.73	
165170373	20 19 13.38	-51 56 17.20	
164262946	20 23 17.01	-44 07 10.63	
163065099	20 23 30.74	-64 57 55.03	
164558895	20 24 32.02	-43 07 21.43	
169392220	20 28 40.82	-43 16 55.67	
170827290	20 28 50.91	-48 21 49.39	
169415198	20 30 16.19	-43 36 43.96	
168236894	20 31 51.57	-54 07 13.33	
169021067	20 32 10.32	-41 35 40.38	
171336327	20 32 31.38	-56 58 13.26	
169928023	20 33 00.22	-44 48 43.78	
172652956	20 34 58.37	-57 51 12.71	
173537271	20 35 05.72	-52 57 03.82	
172408248	20 35 36.72	-56 14 42.18	
173376514	20 38 10.72	-46 49 54.42	
173104153	20 38 48.72	-61 02 22.38	
174436780	20 40 55.05	-42 42 29.74	
174590090	20 41 25.00	-55 14 45.16	
221013801	20 43 38.33	-45 30 01.08	
220339229	20 43 54.14	-61 31 35.80	
187465046	20 52 56.25	-48 58 48.83	
184474337	20 53 55.59	-63 22 31.98	
220375655	20 57 22.75	-46 38 24.86	
235718705	20 58 09.38	-55 03 45.61	
184626507	21 02 30.50	-56 21 52.67	
186070056	21 07 35.16	-48 48 09.72	
193684469	21 15 45.06	-58 43 49.80	
196631497	21 17 58.75	-00 44 48.37	
194791983	21 20 00.58	-53 37 24.71	
194325729	21 22 23.70	00 09 42.37	
197847566	21 23 48.68	-40 28 28.74	
200780623	21 27 52.43	-44 55 30.94	
197433332	21 29 49.70	-40 07 47.89	
197701273	21 30 58.90	-65 16 37.06	
210311376	21 36 08.16	-52 42 58.21	
244329206	21 39 06.05	-42 51 33.80	
212114409	21 39 37.58	-48 00 43.13	
210575399	21 40 25.82	-45 38 01.75	
242293712	21 47 18.15	-60 49 13.66	
215285904	21 48 08.44	-62 54 51.91	
245779138	21 54 13.98	-42 55 35.40	
246152159	21 55 26.36	-45 28 11.39	
246056162	21 55 46.76	-47 27 27.18	
246082708	21 56 18.11	-47 57 10.37	

Table 5 continued

Table 5 (*continued*)

Object ID	RA	dec	notes
244158030	21 56 28.17	-56 18 57.35	
246070576	21 57 25.61	-47 43 40.80	
219457653	21 58 04.00	-48 41 06.11	
247016257	21 58 47.86	-46 06 22.64	
246907314	22 02 51.17	-50 30 06.70	
72040968	22 06 29.28	-58 08 38.47	
73702229	22 11 54.87	-53 41 05.21	
73779919	22 12 33.09	-41 47 17.09	
76356149	22 12 58.75	-54 51 44.04	
75573608	22 13 20.67	-59 26 14.53	
75312079	22 14 00.77	-46 06 22.43	
75339515	22 15 34.12	-46 38 44.63	
76850425	22 15 58.78	-53 50 22.38	
75789565	22 16 23.23	-52 46 38.36	
75957728	22 17 53.78	-45 44 17.74	
76538867	22 18 11.00	-56 03 05.40	
75957081	22 18 23.22	-45 43 44.29	
80738122	22 21 31.69	-42 56 50.89	
81574849	22 22 31.91	-56 11 08.07	
80834421	22 23 09.36	-52 23 56.51	1
82452512	22 24 25.19	-49 54 13.50	
82531780	22 25 46.31	00 17 28.18	
83133438	22 25 58.49	-53 58 22.22	
84940744	22 26 44.55	-46 17 12.88	
84122044	22 27 09.19	-47 44 32.14	
85916632	22 29 47.49	-48 54 11.09	
84457134	22 30 40.32	-59 38 39.16	
85845936	22 31 59.25	-60 29 18.28	
86566557	22 34 10.88	-46 28 22.98	
88904957	22 35 26.13	-50 24 21.24	
88357719	22 37 18.33	-46 07 00.73	
98722821	22 40 41.33	-62 33 26.89	
95131747	22 41 31.50	01 15 01.98	
98849360	22 42 07.86	-56 40 27.98	
99097941	22 43 08.82	-55 08 29.62	
97173324	22 43 16.24	-59 04 35.54	
94354133	22 43 44.42	-65 14 55.18	
97171633	22 44 07.51	-59 03 03.50	
96210597	22 45 08.28	-40 06 36.86	
99179537	22 45 31.88	-40 42 35.38	
123187931	22 45 37.55	-62 01 43.32	
95944838	22 48 22.96	01 50 05.93	3
101317774	22 48 54.64	-49 55 24.32	
100860706	22 50 40.02	-53 11 42.18	1
100990808	22 51 23.39	-41 07 11.64	
106365995	22 54 60.00	-61 54 27.50	
106028685	22 56 08.73	-52 49 53.44	
106265460	22 56 28.97	-46 44 43.04	
105240820	22 57 35.59	-01 53 03.41	
109115033	23 01 08.94	-63 54 51.55	
111930650	23 02 15.87	-50 06 00.86	
110793226	23 02 48.37	-50 57 55.39	
111018859	23 03 29.10	-47 57 11.52	
114722072	23 07 10.33	-50 49 10.78	

Table 5 continued

Table 5 (*continued*)

Object ID	RA	dec	notes
114892905	23 07 24.57	-54 39 59.76	
115148237	23 07 58.53	-46 09 27.76	
112705964	23 08 47.10	01 12 58.32	
114948603	23 10 02.09	-51 06 22.07	
125452064	23 11 57.31	-52 17 30.95	
152309970	23 13 00.49	-42 40 08.54	
126025603	23 13 19.72	-54 46 48.54	
152418794	23 15 50.43	-56 42 41.90	
125639186	23 18 37.98	-51 56 33.68	
127137663	23 18 50.76	-53 34 08.47	
125312241	23 18 52.09	-01 41 12.16	
125203463	23 18 57.04	-61 15 08.57	
126893048	23 19 43.73	-56 44 25.66	
126703170	23 20 00.43	-56 27 40.77	
127435355	23 20 13.26	-59 12 02.81	
124440331	23 20 27.72	-00 35 44.95	
129496398	23 20 34.14	-54 27 15.14	
130306799	23 22 34.89	-61 14 14.96	
132547439	23 24 39.97	-49 21 50.00	
129984000	23 25 03.58	00 16 09.88	
133386091	23 26 09.29	-43 47 11.18	
132101000	23 26 20.87	-44 27 10.62	
131947563	23 27 22.00	-45 38 42.25	
130769524	23 28 15.99	-45 07 10.67	
132578371	23 29 47.94	-01 20 51.51	1
134721276	23 31 02.71	-57 10 31.15	
135138469	23 32 30.92	00 38 21.88	4
136378646	23 32 43.98	00 41 37.90	
134956820	23 33 00.76	-42 49 27.16	
135738695	23 35 10.91	-55 31 32.77	
135956402	23 37 07.06	-43 59 10.50	
136806695	23 37 59.41	00 40 40.04	
138566300	23 38 09.68	-51 01 14.89	
139494926	23 39 53.99	-56 15 02.95	
137993988	23 40 59.67	-39 48 50.76	
159678227	23 42 34.31	-47 52 36.59	
159158821	23 46 13.25	-51 24 49.61	
213426039	23 47 11.14	-45 29 00.88	
160163032	23 47 27.89	-46 24 51.05	
159852078	23 47 59.60	-57 13 52.32	
158794088	23 48 25.23	01 43 39.29	
158328414	23 48 35.56	-39 03 53.93	
215197482	23 48 59.71	-57 19 35.40	
215164863	23 49 06.24	-56 46 01.70	
215178100	23 49 16.95	-56 59 41.35	
161118112	23 52 11.70	00 06 14.56	
162518755	23 53 19.50	-60 21 19.76	
214772393	23 55 38.22	-56 33 04.75	
172759386	23 56 31.79	-38 45 09.90	
213007468	23 56 41.59	-41 42 56.84	
177095569	23 56 59.30	-41 18 58.14	
213772612	23 57 25.11	-39 22 27.95	
214207304	23 59 11.64	-63 43 03.11	